AD-A081 004 NAVAL RESEARCH LAB WASHINGTON DC F/G 18/10
STRUCTURAL INTEGRITY OF WATER REACTOR PRESSURE BOUNDARY COMPONE--ETC(U)
DEC 79 F J LOSS
UNCLASSIFIED NRL-MR-4122 NUREG-CR-1128 NRC-RES-79-103 NL

1 OF 2
AD A081004

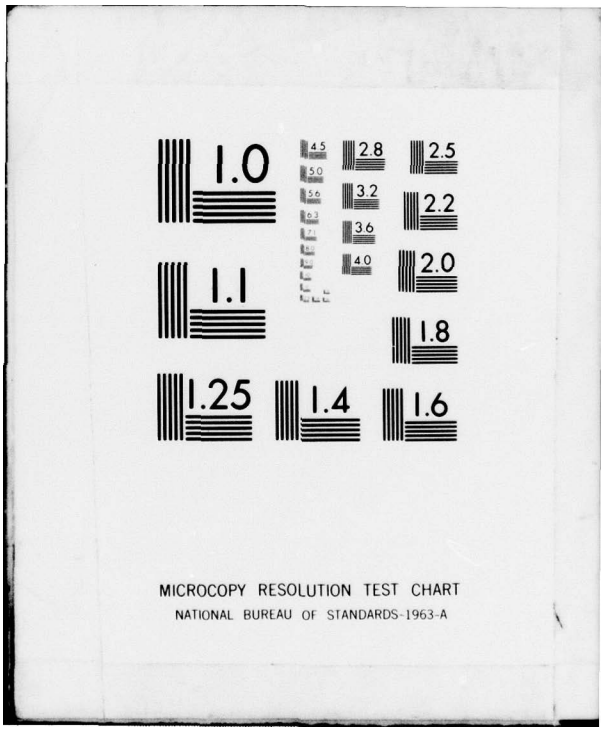
1.0
1.1
1.25
1.4
1.6
1.8
2.0
2.2
2.5
2.8
3.2
3.6
4.0
4.5
5.0
5.6
6.3
MICROCOPY RESOLUTION TEST CHART
NATIONAL BUREAU OF STANDARDS-1963-A

ade 000 366

LEVEL III (12)

B.S.

NUREG/CR-1128
NRL Memorandum Report 4122

ADA081004

DDC FILE COPY

Structural Integrity of Water Reactor Pressure Boundary Components

Annual Report, Fiscal Year 1979

F. J. Loss, Editor

Thermostructural Materials Branch
Material Science and Technology Division

DTIC

NOTICE

This report was prepared as an account of work sponsored by an agency of the United States Government. Neither the United States Government nor any agency thereof, or any of their employees, makes any warranty, expressed or implied, or assumes any legal liability or responsibility for any third party's use, or the results of such use, of any information, apparatus, product or process disclosed in this report, or represents that its use by such third party would not infringe privately owned rights.

The views expressed in this report are not necessarily those of the U. S. Nuclear Regulatory Commission.

Available from
U. S. Nuclear Regulatory Commission
Washington, D.C. 20555

and

(9) Annual rept. for FY 79,

SECURITY CLASSIFICATION OF THIS PAGE (When Data Entered)

REPORT DOCUMENTATION PAGE

READ INSTRUCTIONS BEFORE COMPLETING FORM

1. REPORT NUMBER
NUREG/CR-1128
NRL Memorandum Report 4122

2. GOVT ACCESSION NO.

3. RECIPIENT'S CATALOG NUMBER

(6) 4. TITLE (and Subtitle)
STRUCTURAL INTEGRITY OF WATER REACTOR PRESSURE BOUNDARY COMPONENTS ANNUAL REPORT, FISCAL YEAR 1979
A075349

5. TYPE OF REPORT & PERIOD COVERED
Interim report on a continuing NRL problem.

6. PERFORMING ORG. REPORT NUMBER

(16) 7. AUTHOR(s)
F. J. Loss, Editor

(15) 8. CONTRACT OR GRANT NUMBER(s)
NRC-RES-79-103
NRC FIN B5528

9. PERFORMING ORGANIZATION NAME AND ADDRESS
Naval Research Laboratory
Washington, DC 20375

10. PROGRAM ELEMENT, PROJECT, TASK AREA & WORK UNIT NUMBERS
NRL Problem 63-1065-0-0

11. CONTROLLING OFFICE NAME AND ADDRESS
U.S. Nuclear Regulatory Commission
Office of Nuclear Regulatory Research
Washington, DC 20555

(11) 31

12. REPORT DATE
December 31, 1979

13. NUMBER OF PAGES
128

14. MONITORING AGENCY NAME & ADDRESS (if different from Controlling Office)
(14) NRL-MR-4122

15. SECURITY CLASS. (of this report)
UNCLASSIFIED

15a. DECLASSIFICATION/DOWNGRADING SCHEDULE
(12) 130

16. DISTRIBUTION STATEMENT (of this Report)
Approved for public release; distribution unlimited.
(18) NUREG, SBIE
(19) CR-1128, AD-E000366

17. DISTRIBUTION STATEMENT (of the abstract entered in Block 20, if different from Report)

18. SUPPLEMENTARY NOTES
Prepared for the U.S. Nuclear Regulatory Commission, Office of Nuclear Regulatory Research, Reactor Safety Research Division under Interagency Agreement RES-79-103.
NRC Distribution Category R5 and AN

19. KEY WORDS (Continue on reverse side if necessary and identify by block number)

Charpy V-test	Low upper shelf	Single specimen compliance test
A533-B submerged arc weld	Microstructure	Radiation sensitivity
Dynamic fracture toughness	Nuclear pressure vessel steels	Corrosion fatigue
Fatigue crack propagation	Postirradiation recovery	Elastic-plastic fracture
J-integral, R curve		

20. ABSTRACT (Continue on reverse side if necessary and identify by block number)

This report describes research progress for Fiscal Year 1979 in a continuing program to characterize material properties performance with respect to structural integrity of light water reactor pressure boundary components. Progress under fracture mechanics investigations includes the first J-R curves from irradiated A533-B weld deposit. A dynamic finite element analysis was also performed to verify the NRL experimental procedure for dynamic fracture toughness, (K_{Id}). Work in corrosion fatigue has investigated the effects of waveform and temperature on cyclic
(Continues)

K sub Id.

DD FORM 1 JAN 73 1473 EDITION OF 1 NOV 65 IS OBSOLETE
S/N 0102-014-6601

SECURITY CLASSIFICATION OF THIS PAGE (When Data Entered)

251 950

JC

20. Abstract (Continued)

crack growth in reactor vessel steels; a hydrogen embrittlement model has been proposed. Research in radiation sensitivity has characterized the notch ductility of vessel steels at low fluence. Also investigated was the postirradiation notch ductility of vessel steels in a coordinated IAEA program. The effects of postirradiation annealing and reirradiation are described in terms of Charpy V-notch ductility and J-R curves. In addition, a survey of embrittlement recovery by postirradiation heat treatment has been prepared. Abstracts of reports prepared under this program in FY 79 are also included.

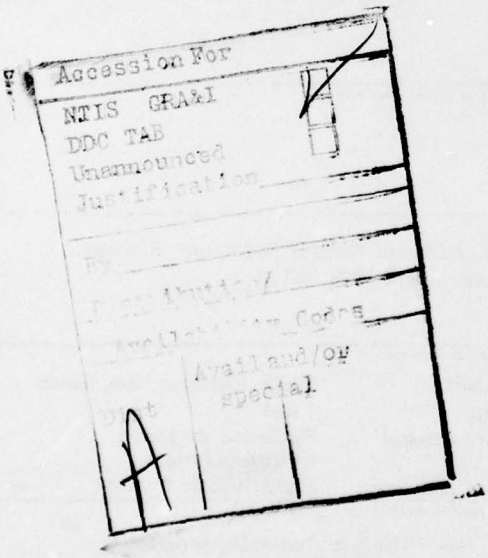

CONTENTS

PREFACE

The goal of this research program is to characterize materials behavior in relation to structural safety and reliability of pressure boundary components for light water reactors. Specific objectives include developing an understanding of elastic-plastic fracture and corrosion fatigue crack propagation phenomena in terms of continuum mechanics, metallurgical variables, and neutron irradiation. Emphasis is placed on identifying metallurgical factors responsible for radiation embrittlement of steels and on developing procedures for embrittlement relief, including guidelines for radiation resistant steels. The underlying objective is the interpretation of material properties performance to establish engineering criteria for structural reliability and long term operation. Current work is organized into three major tasks: (1) fracture mechanics investigations, (2) fatigue crack propagation in high-temperature, primary reactor water, and (3) radiation sensitivity and postirradiation properties recovery. In Fiscal Year 1980 a new task is being added. This task involves a subcontract with the Westinghouse Electric Corporation for the performance of research on corrosion fatigue. This task is being coordinated with on-going research of a similar nature at NRL to form a uniform program having common objectives.

This work is being performed at NRL by the Material Science and Technology Division, Thermostructural Materials Branch, F. J. Loss, program manager. NRC funding is provided by the Office of Nuclear Regulatory Research, Metallurgy and Materials Research Branch, Pedro Albrecht, project manager.

STRUCTURAL INTEGRITY OF WATER REACTOR PRESSURE BOUNDARY COMPONENTS ANNUAL REPORT, FISCAL YEAR 1979

SUMMARY

I. FRACTURE MECHANICS INVESTIGATIONS

A. J-R Curve Characterization of Irradiated and Annealed A533-B Weld Deposit

As part of the IAR program initial J-R curve toughness comparisons of A533-B submerged-arc weld deposit have been completed following irradiation and postirradiation annealing. The single specimen compliance technique has been developed for remote testing of irradiated 1T-CT specimens. This testing is now a routine operation and R curves of high precision have been produced. The results show that the R curve exhibits a power law behavior and is not straight as presumed earlier. This phenomenon, coupled with the need to define J_{Ic} in cases of brittle (cleavage) fracture where only a limited R curve is produced, has necessitated a new experimental procedure to be evolved for the calculation of J_{Ic} which permits a small amount of crack extension. Side grooving of specimens has resulted in a straight crack-front extension. This straight crack produces R curves of lower slope than those associated with curved crack fronts and is believed to result in a conservative characterization of the toughness trends.

Irradiation to a fluence of 1.2×10^{19} n/cm^2 >1 Mev reduced the upper shelf J_{Ic} level by one half. This is equivalent to a K_{Jc} of 117 MPa$\sqrt{m}$ for the irradiated material. On the other hand, the tearing modulus T appears to exhibit a greater reduction with irradiation than does J_{Ic}. Postirradiation T values of 25 were obtained for one weld deposit. Two subsequent postirradiation anneals at 399°C, each followed by reirradiation to a fluence of 0.7×10^{19} n/cm^2, produced no net embrittlement in addition to that which occurred with the initial irradiation. This trend suggests that postirradiation annealing can be a useful tool to control radiation embrittlement.

Postirradiation annealing has restored the tearing modulus by more than half of the amount which was lost with the first irradiation exposure. However, this behavior does not corroborate the full recovery in the upper shelf toughness which was predicted on the basis of C_v upper shelf energy. Nevertheless, both the C_v and tearing modulus trends confirm that annealing has arrested the progressive embrittlement which occurs with increasing neutron fluence. In addition, it was observed that the tearing modulus vis a vis C_v energy appears to be a more discriminating indicator of toughness changes with irradiation. However, the R curve, as defined by quasi-static tests, can terminate in brittle fracture within a portion of the upper shelf temperature regime. The possibility of cleavage fracture can be eliminated only within the upper shelf regime as defined by a dynamic test. Consequently, this phenomenon must be weighed carefully in structural applications of the tearing instability concept.

Note: Manuscript submitted November 2, 1979.

B. Dynamic Finite Element Analysis of Notched Beam Specimens

A dynamic finite element analysis was undertaken to validate the NRL experimental procedure for determining the dynamic initiation toughness K_{Id} from a three-point bend specimen under impact loading. The present investigation clearly demonstrates that Loss' procedure to compute K_{Id} from the measured dynamic bending moment at midspan (obtained from a strain gage located near the crack tip) along with a static K-calibration is an accurate and simple procedure which does not require a dynamic analysis. Furthermore, the success of Loss' procedure depends on the determination of a suitable location for the strain gage; this location was found to be independent of the range of loading rate ($\dot{K}$) employed in the experimental program.

II. FATIGUE CRACK PROPAGATION IN LWR MATERIALS

A. Results of Cyclic Crack Growth Rate Studies in Pressure Vessel and Piping Steels

An examination of all of the data sets produced under the guidelines of a preliminary test matrix involving a high temperature, PWR water environment, together with other tests run under similar environmental conditions but utilizing non-matrix waveforms, indicates that fatigue crack growth data sets fall into one of two rather clearly defined categories. One band of data lies close to, or essentially on, the ASME Section XI Code air environment default line. This class of data, exhibiting the lower of the two categories of crack growth rates, will be called "low." The other band of data, which resides a factor of three to five above the first, will be termed "high." This latter band of data resides approximately midway between the Section XI air and water environment default lines. The specific combinations of ramp and hold times, and temperature, which cause growth rates to reside in either of these two categories are described in detail.

Fractographic examination of the fatigue fracture surfaces indicates that cleavage-like features dominate the morphology of the "high" growth rate specimens, while striations and ductile, transgranular fatigue fracture characterize the "low" crack growth rate specimens. This fact, and the generalized kinetics of the crack growth behavior have led to the formation of a model for hydrogen-assisted fatigue crack growth which appears to adequately describe the data obtained in this study.

III. RADIATION SENSITIVITY AND POSTIRRADIATION RECOVERY

A. Notch Ductility Degradation by Low-to-Intermediate Neutron Fluence Exposure

The extent and trend of Charpy-V (C_v) notch ductility changes in reactor vessel materials with fluences of 1×10^{18} n/cm^2 to 10×10^{18} n/cm^2 >1 MeV were investigated with several thick section steel plates and submerged arc weld deposits irradiated at 288°C (550°F). The materials were fully representative of reactor vessels now in service and had copper contents ranging from

0.10 to 0.40% and phosphorus contents ranging from 0.008 to 0.020%. The C_v transition temperature elevations and upper shelf reduction with irradiation were compared to embrittlement projections by Nuclear Regulatory Commission Guide 1.99.

The steels with high radiation sensitivity indicated an onset of notch ductility change at fluences $\sim 1.5 \times 10^{18}$ n/cm^2 by an elevation in the ductile-to-brittle transition temperature. Reductions in upper shelf were not observed at this fluence level but were as high as 15% at $\sim 4 \times 10^{18}$ n/cm^2 and between 15 to 44% at $\sim 8 \times 10^{18}$ n/cm^2. The data trend suggests a power law relationship between upper shelf reduction and fluence at low-to-intermediate fluences.

B. Evaluation and Comparison of IAEA Coordinated Program Steels and Welds with 288°C Irradiation

Four steel materials supplied by Japan to the IAEA Program on "Analysis of the Behavior of Advanced Reactor Pressure Vessel Steels Under Neutron Irradiation," have been compared after 288°C irradiation against the IAEA reference steel plate (HSST Plate 03). Notch ductility and fracture toughness comparisons indicate the Japanese materials to be somewhat more resistant to radiation-induced embrittlement than the reference material. The observed difference is believed due to a copper content difference (0.04%Cu, max, Japanese-produced materials vs 0.12%Cu, IAEA reference plate).

C. Survey of Embrittlement Recovery by Postirradiation Heat Treatment

Postirradiation heat treatment (annealing) has been proposed as a method for the alleviation of radiation embrittlement in reactor vessel steels. Objectives of this study were to identify those service and metallurgical variables which can affect annealing response, to report data comparisons available for qualification of suspected influences, and to survey available experimental results.

Twelve factors are identified as having potential for affecting the postirradiation heat treatment response of low alloy pressure vessel steels. A tentative qualification of six factors as significant contributing variables is made on the basis of experimental comparisons

D. Irradiation-Anneal-Reirradiation (IAR) Program Investigation of Charpy-V Ductility Trends

The notch ductility behavior of two submerged arc weld deposits with irradiation to $\sim 1.2 \times 10^{19}$ n/cm^2 > 1 MeV followed by two full cycles of 399°C (750°F)-168 hr annealing and 288°C (550°F) reirradiation for $\sim 0.7 \times 10^{19}$ n/cm^2 has been determined. The total fluence received was $\sim 2.6 \times 10^{19}$ n/cm^2. The results demonstrate that the buildup of detrimental radiation effects can be reduced significantly by intermediate 399°C annealing and that the benefits can be retained through two cycles of reirradiation. The results also confirm an earlier observation with one cycle of reirradiation where the rate of embrittlement of annealed material was found to be higher than that of non-annealed material for the same increment of additional fluence.

RESEARCH PROGRESS

I. FRACTURE MECHANICS INVESTIGATIONS

A. J-R Curve Characterization of Irradiated and Annealed Weld Deposit

F. J. Loss, B. H. Menke, R. A. Gray, Jr., J. R. Hawthorne, and
H. E. Watson

BACKGROUND

The objective of the IAR Program is to characterize the Charpy-V notch ductility and fracture toughness trends of A533-B submerged arc (S/A) weld deposits with irradiation (I) followed by two full cycles of postirradiation annealing (A) and reirradiation (R). The intent of the program is to identify the merits and potential of postirradiation annealing as a means to control radiation-induced embrittlement in reactor pressure vessels. The fracture toughness characterization is discussed here; Ref. 1 provides a description of the C_v trends, chemical composition and irradiation conditions.

The fracture toughness is being characterized in terms of J-R curve trends developed from compact specimens of 25.4 mm (1 in.) thickness (1T-CT). The primary objective is to define the J_{Ic} and R curve behavior in the upper shelf temperature regime. Here, a correspondence is being developed between changes in the J-R curve and in C_v upper shelf energy as a function of irradiation and annealing. If successful, this relationship will provide added quantitativeness to data from surveillance programs which may involve only C_v specimens. As a secondary objective, an estimate of the temperature elevation of the brittle/ductile transition region with irradiation is being developed from the results of only a few J_{Ic} tests. This temperature elevation, based on static tests, will be compared with a similar change based upon the (dynamic) C_v tests.

The J-R curves are measured by means of the single specimen compliance (SSC) technique. A large part of the program has centered on the development of procedures to assure adequate definition of crack extension, Δa, using this technique as well as to develop methods for the hot cell testing of irradiated specimens. In addition, a related study on specimen side groove depth was undertaken to characterize the influence of this variable on crack front straightness and the resulting effect on R-curve slope.

Progress to date has included the successful implementation of the SSC technique for irradiated specimen testing. R-curve trends have been developed from the two weld deposits (Codes V84 and V86) in both the

irradiated and annealed conditions. Both welds have a high impurity copper level (0.35) which increases the sensitivity to irradiation embrittlement. In the unirradiated condition, one weld, Code V84, has a high C_v upper shelf level (145 J, 107 ft-lb) while the other, Code V86, exhibited a lower preirradiation value (108 J, 80 ft-lb). The program is sufficiently advanced so as to permit initial conclusions to be drawn concerning the toughness recovery following annealing in terms of crack initiation (J_{Ic}) and tearing modulus (T) criteria. Likewise, initial comparisons between C_v and R-curve trends can now be made.

EXPERIMENTAL AND COMPUTATIONAL PROCEDURES

The experimental procedure utilizes a CT specimen of ASTM E-399 proportions with a modified notch geometry to permit the mounting of razor knife edges for the measurement of load line displacement with a clip gage (Fig. 1). The notch modification has required a small increase in the distance between hole centers of the E-399 specimen. In addition, specimens were side grooved using a C_v notch cutter (45° angle, 0.25 mm root radius). A crack length, a, to width, W, ratio of 0.6 has been used in this study.

With the SSC technique the crack extension is inferred through changes in specimen compliance ($EB\,\delta/P$, (Fig. 2) where E is Young's modulus, P is load, δ is load-line displacement and B is the specimen thickness. To compute absolute crack length from compliance, it is necessary to know the modulus as well as the δ/P slope. The former is a function of temperature and is generally not known exactly. To avoid this problem, agreement is forced between the length of the fatigue precrack, a_o, as predicted by the SSC method and as measured optically. This agreement defines an effective modulus which is then used for subsequent crack length predictions.

To produce accurate crack length predictions it is important that the correct compliance relationship be employed. Most investigators have used the theoretical compliance of Hudak and others [2] based on a plane stress assumption. To verify this theoretical relationship we have measured the compliance experimentally using the specimen of Fig. 1 with machined notches of different depths. As illustrated in Fig. 2, the difference between these two compliance curves is not significant and both will predict nearly identical crack lengths when normalized to a common initial crack length.

Since a theoretical compliance relation does not exist for side grooved specimens, it was necessary to establish an experimental relationship for this type of specimen. As shown in Fig. 2, the experimental compliance of a 25% side grooved specimen differs from that of a smooth specimen by a small factor. Because of the similar shape of the compliance curves associated with smooth and side grooved specimens, either relationship will predict approximately the same value for small crack extension. For side grooved specimens exhibiting long crack extensions, however, the experimental compliance should be employed.

Successful application of the SSC technique depends upon accurate crack length predictions. This, in turn, requires the minimization of both friction and electronic noise so that the specimen compliance can be established with

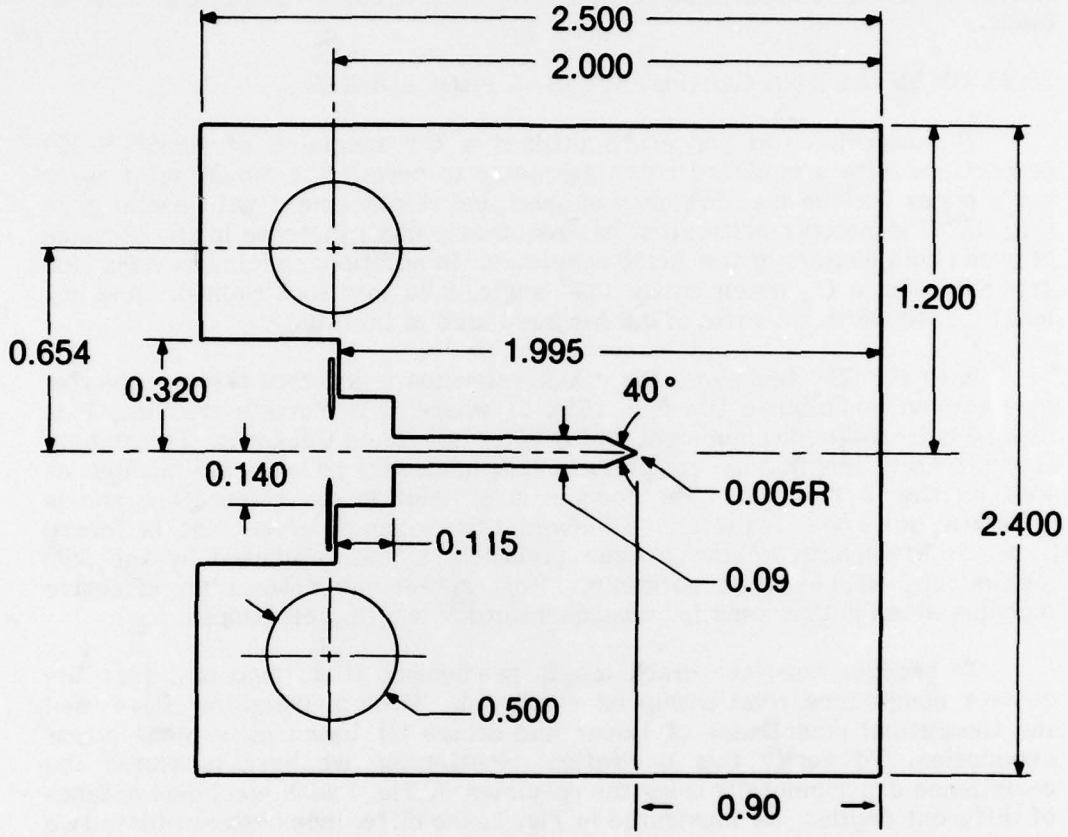

Fig. 1 — 1T compact specimen geometry for an a/W of 0.6. A precrack of 2.5 mm (0.100 in.) is added prior to testing. All dimensions are in inches (in. x 25.4 = mm).

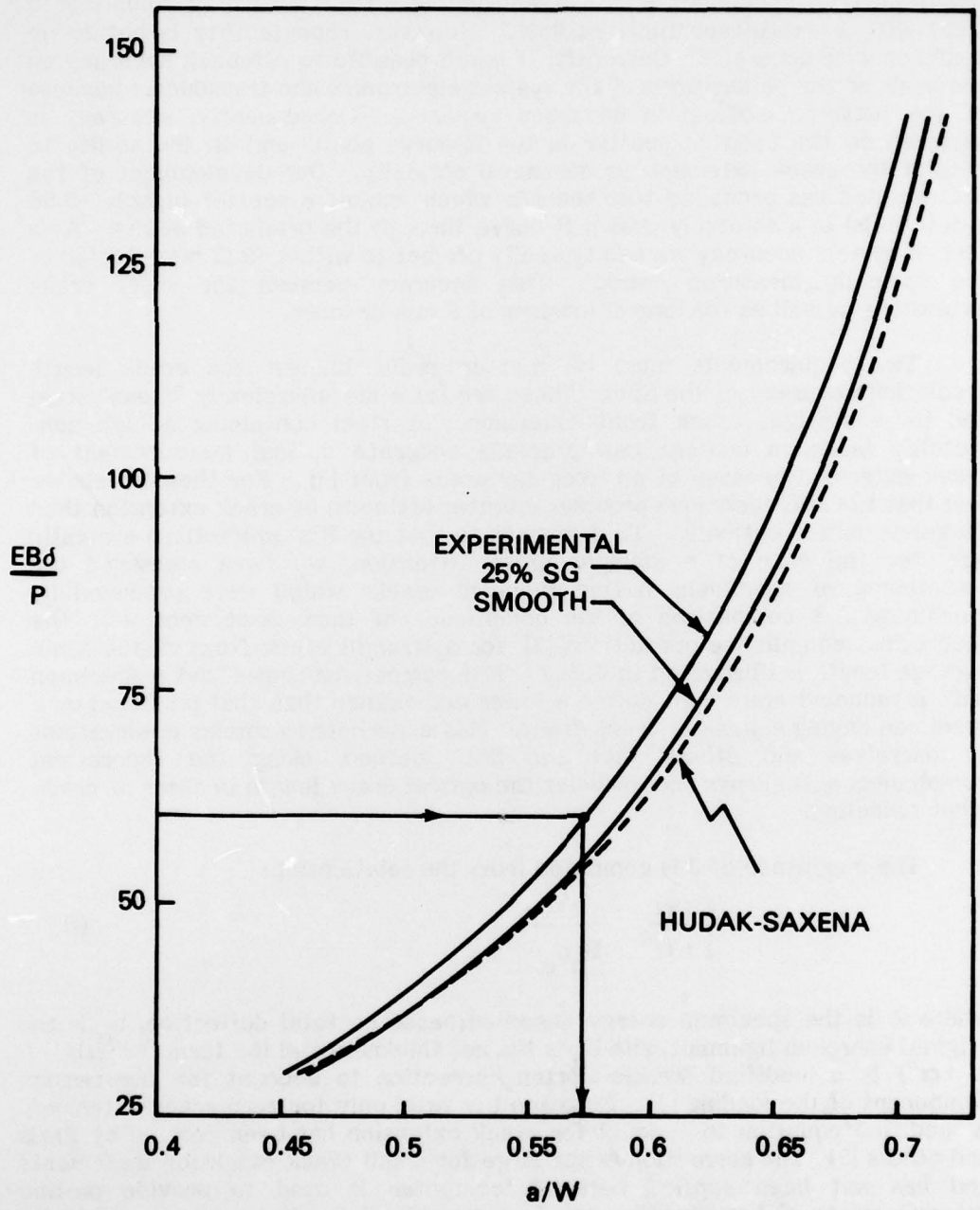

Fig. 2 — Comparison of the CT specimen compliance derived analytically using a plane stress assumption (Hudak-Saxena) with that measured experimentally with blunt-notch specimens (smooth). The two curves have been "matched" at an a/W of 0.5. Also illustrated is the experimental compliance for specimens having 25% side grooves (25% SG).

precision. Our system has been developed to a point where a given crack length in 1T-CT specimens can be established to a repeatability of ±0.05 mm (2 mils) with a confidence limit of 95%. However, repeatability is not to be confused with accuracy. Currently, it is not possible to establish accuracy on the basis of the calibrations of the system electronics and transducers because of the extreme calibration accuracy required. Consequently, accuracy is assessed on the basis of scatter in the R-curve points and on the ability to predict the crack extension as measured optically. Our development of the SSC method has produced test records which exhibit a scatter of only ±0.08 mm (3 mils) in a smoothly drawn R curve through the predicted points. As a test of system accuracy we can typically predict to within ±0.13 mm (5 mils) of the optically measured crack. This accuracy persists for short crack extensions as well as for long extensions of 9 mm or more.

Two requirements must be met in order to test the crack length prediction accuracy of the SSC. These are (a) a metallurgically "clean" steel and (b) a straight crack front extension. A steel containing a high non-metallic inclusion content can preclude accurate optical measurement of crack extension because of an irregular crack front [3]. For these steels we feel that the SSC technique provides a better estimate of crack extension than that determined optically. To demonstrate that the SSC predictions are valid only for the case of a straight crack extension, we have measured the compliance of specimens having tunneled cracks which were produced by machining. A comparison of the compliance of these specimens with the theoretical compliance predictions [2] for a straight crack front of the same average length is illustrated in Fig. 3. This comparison shows that a specimen with a tunneled crack will define a lower compliance than that produced by a specimen having a straight crack front. This experiment explains observations by ourselves and others that the SSC method, using the theoretical compliance, will always underpredict the optical crack length in cases of crack front tunneling.

The magnitude of J is computed from the relationship:

$$J = \frac{1+\alpha}{1+\alpha^2}\,\frac{2A}{B_n b_o} \qquad (1)$$

where A is the specimen energy absorbed based on total deflection, b_o is the original unbroken ligament, and B_n is the net thickness and the term $(1+\alpha)/(1+\alpha^2)$ is a modified Merkle-Corten correction to account for the tension component of the loading [4]. Equation 1 is valid only for zero crack extension. A modified equation to account for crack extension has been derived by Paris and others [5]. The correction is not large for small crack extension increments and has not been applied here. A computer is used to provide on-line determinations of J and crack extension, Δa. The computer code was originally developed by Joyce and Gudas [6].

A correction [7] is applied to the compliance, δ/P, to account for the specimen rotation which occurs during the loading. This rotation reduces the moment arm of the load and also results in a deviation of the clip gage loading points from the true load line. An example of this correction, illustrated in Fig. 4, has produced a 10% reduction in J. The magnitude of the correction for

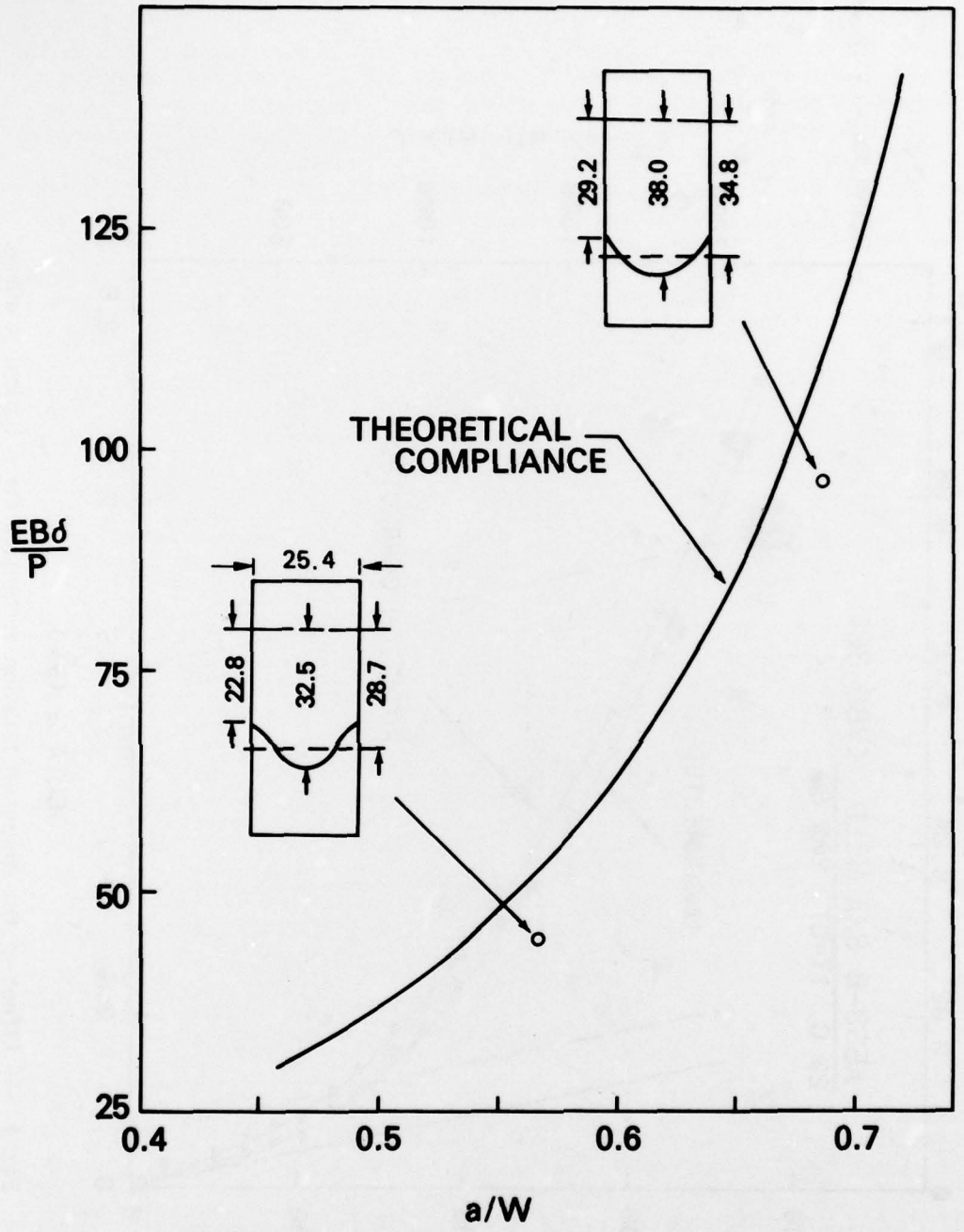

Fig. 3 — Comparison of theoretical compliance [2] with that measured from two specimens having machined-tunneled crack fronts. For the same average crack length, the tunneled crack front produces a lower compliance than a straight crack front. (Specimen dimensions are in mm).

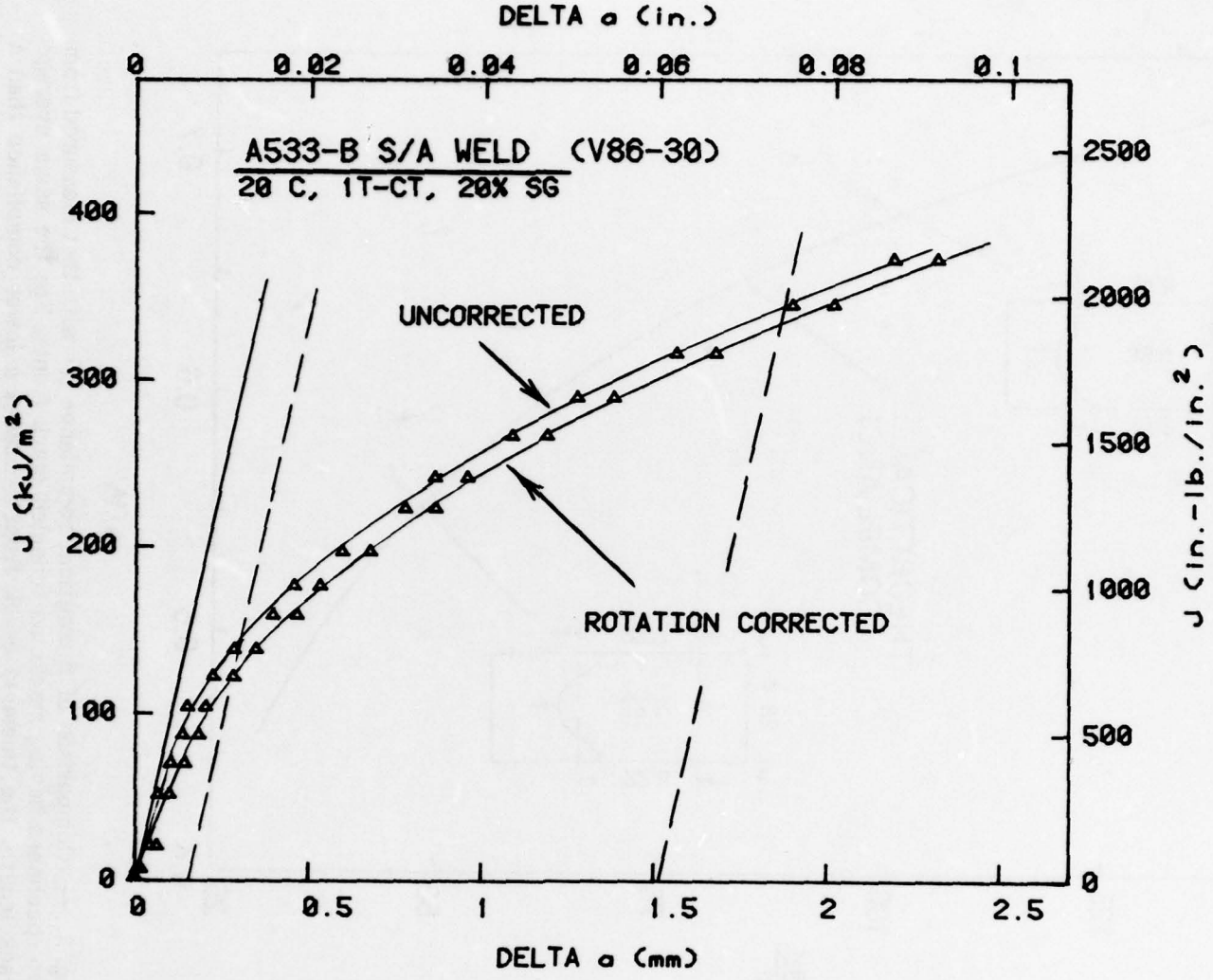

Fig. 4 — Effect of the specimen rotation correction for a typical R curve. The corrected J values have dropped by 10%.

different steels can be greater or less than this amount depending on the toughness which, in turn, affects the amount of rotation prior to crack extension.

J_{Ic} MEASUREMENT PROCEDURE

A standard procedure does not currently exist for the measurement of crack initiation toughness, J_{Ic}, with a single specimen. However, a J_{Ic} measurement procedure based upon multiple specimen testing is being developed by ASTM [8]. With the latter, J_{Ic} is given by the intersection of the blunting line ($\Delta a = J/2\,\sigma_f$ where σ_f is the flow stress) with the least squares fit of the R curve points for specimens having a crack extension between 0.15 and 1.5 mm (Fig. 5).

As illustrated in Fig. 5, the R curve for A533-B S/A weld metal is curved and not straight as presumed by the ASTM procedure. Consequently, we feel that it is more appropriate to represent the R curve as a smooth curve through the data points. When this is done it becomes apparent that J_{Ic} can no longer be defined by the intersection of the R curve with the blunting line. In other words, J_{Ic} would always be near zero as seen in Fig. 5. Therefore, we have evolved an alternative definition of J_{Ic} to be used with SSC testing. The essence of this definition is (a) to permit a small amount of real crack extension in terms of the crack opening displacement (COD) and (b) to require a minimum (fixed) crack extension to account for experimental scatter in the R-curve data points.

The alternative J_{Ic} definition is illustrated in Fig. 5. J_{Ic} is taken as the value of J which corresponds to the intersection of the smoothly drawn R curve with either the crack extension or exclusion lines, whichever produces the higher value. We have found that both the alternative procedure and the proposed ASTM multispecimen procedure (when applied to SSC testing) can yield comparable values of J_{Ic} (see Fig. 5 and Tables 1 and 2). In fact, differences of less than 3% have been determined for A533-B plate and weld deposit for cases where R curves of at least 1.5 mm crack extension were developed. Consequently, both procedures are comparable.

The logic behind the alternative procedure is that J_{Ic} should be determined at a small (non-zero) crack extension to preclude the difficult task of defining an absolute quantity which denotes the beginning of crack extension. This approach is analogous to the definition of yield stress vis a vis the proportional limit. The permissible crack extension is defined in terms of COD so as to be physically reasonable for materials of different toughness level. For this purpose, Tada [9] has suggested a crack extension of $3\,J/4\,\sigma_f$ and this value will be employed here for the crack extension line shown in Fig. 5. If one considers the COD $\approx J/\sigma_f$ then this value of real crack extension amounts to approximately one half of that used to define the blunting line.

In practice, a small, but fixed, crack extension must be required to account for scatter in the experimental points. A crack extension of 0.15 mm, parallel to the blunting line, has been chosen to be consistent with that value used by the proposed ASTM multispecimen J_{Ic} standard. This crack extension

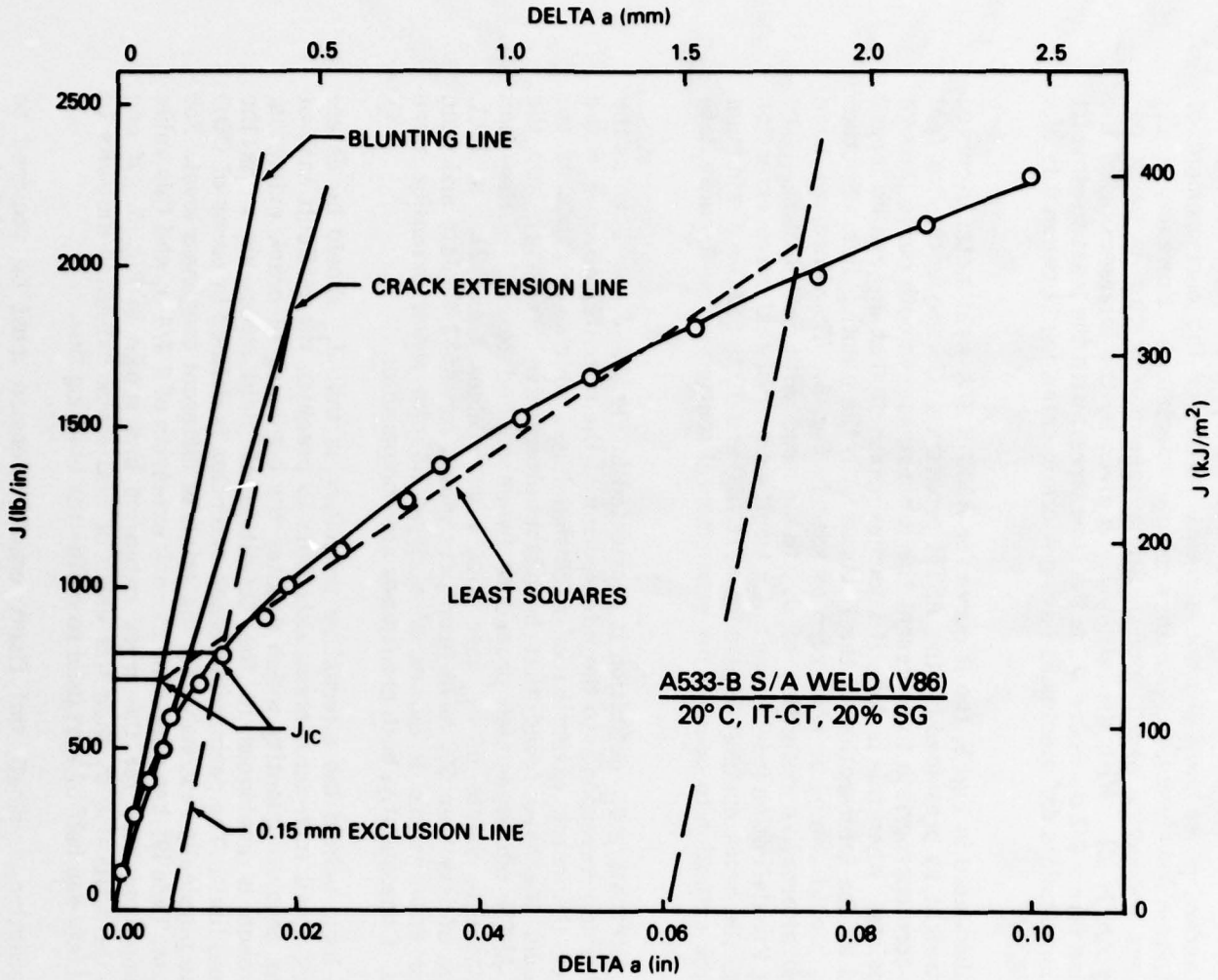

Fig. 5 — Illustration of the typical power law behavior of the R curve. An alternative definition of J_{Ic} is indicated by the intersection of the smoothly drawn R curve with the 0.15 mm exclusion line. For higher toughness levels, J_{Ic} would be taken as the intersection of the R curve with the crack extension line. Also shown is the proposed ASTM definition of J_{Ic} (least squares).

Table 1 — Fracture Toughness Properties of Weld V86

Specimen Number	% Side Grooves	Irrad. Condition	Fluence[a]	Test Temp °C	J_{Ic}[b] kJ/m²	J_{Ic}[c] kJ/m²	25 J_{Ic}/σ_f mm	25 J/σ_f[d] mm	b_o[e]	$T^{f,g}$	$T^{f,h}$	$T^{f,d}$	$\omega^{i,g}$	$\omega^{i,h}$	$\omega^{i,d}$
24	20	U	0	-100	23	-	1.1	-	19.3	-	-	-	-	-	-
28	↓	↓	↓	- 72	38	-	1.8	-	19.8	-	-	-	-	-	-
31				- 60	62	-	3.0	-	19.3	-	-	-	-	-	-
29				- 50	89	-	4.3	-	19.3	-	-	-	-	-	-
17				- 40	119	-	5.7	-	19.8	-	-	-	-	-	-
1				- 11	119	-	5.8	-	18.3	-	-	-	-	-	-
30				20	124	119	6.1	15.9	19.3	202	103	68	42	25	4.8
32				26	83	84	4.1	14.2	19.5	163	101	90	50	32	7.1
3				200	123	118	6.4	13.0	19.3	128	70	49	23	14	3.1
26	0				132	120	6.8	18.3	19.8	196	116	87	36	23	5.1
15	10				144	138	7.4	17.6	19.8	174	102	81	29	17	5.3
18	0	I	1.2		79	76	3.2	8.2	20.1	91	43	31	47	21	5.6
21	10	↓	↓		80	92	3.3	5.2	19.7	74	21	15	35	8	3.4
27	20				66	77	2.7	6.4	19.6	89	28	15	53	14	3.4
13	↓				65	63	2.7	5.4	19.6	54	24	15	31	14	3.9
7		IA		38	92	90	4.5	11.8	19.8	198	90	59	55	25	5.7
19		↓		200	88	90	4.6	10.3	19.6	145	60	39	40	16	4.3
25				-18	47	-	2.3	-	19.7	-	-	-	-	-	-
4		IAR	1.9	200	77	74	3.2	6.8	19.8	66	34	20	32	17	4.1
5				200	72	72	3.0	6.3	19.5	76	30	18	42	15	4.0
10				100	53	49	2.1	6.7	19.9	88	41	26	73	33	5.5
22				38	62	-	2.3	-	19.6	-	-	-	-	-	-
9		IARA		38	78	-	3.7	-	19.5	-	-	-	-	-	-
11		↓		200	92	92	4.7	9.9	19.6	117	57	39	30	15	4.2
23				-18	47	-	2.1	-	19.9	-	-	-	-	-	-
2		IARAR	2.6	200	71	74	2.9	6.7	19.9	76	32	23	40	17	4.9
8		↓	↓	38	44	-	1.6	-	19.8	-	-	-	-	-	-
14				120	90	-	3.6	-	19.7	93	44	-	40	20	-
20	↓	↓	↓	100	63	-	2.5	-	19.2	-	-	-	-	-	-

[a] E x 10^{19} n/cm² > 1 MeV

[b] Alternative definition

[c] Proposed ASTM definition

[d] Evaluated at Δa = 1.5 mm plus blunting

[e] Original unbroken ligament

[f] $T = E/\sigma_f^2 \times dJ/da$

[g] Evaluated at J_{Ic}

[h] dJ/da by ASTM least squares fit

[i] $\omega = b/J \times dJ/da$

[j] Uses J_{Ic} and dJ/da by ASTM least squares fit

Table 2 — Fracture Toughness Properties of Weld V84

Specimen Number	% Side Grooves	Irrad. Condition	Fluence[a]	Test Temp °C	J_{Ic}[b] kJ/m^2	J_{Ic}[c] kJ/m^2	25 J_{Ic}/σ_f mm	25 J/σ_f[d] mm	b_o[e]	$T^{f,g}$	$T^{f,h}$	$T^{f,d}$	$\omega^{i,g}$	$\omega^{i,h}$	$\omega^{i,d}$
12	20	U	0	200	107	109	5.5	17.8	19.9	252	120	83	59	26	5
22				60	58	46	0.9	28.2	19.7	135	227	93	59	129	3
24				150	163	164	8.3	21.2	19.8	218	127	95	33	19	5
25				200	116	108	6.0	16.6	19.6	181	108	74	36	24	5
26				-90	174	-	8.4	-	19.7	-	-	-	-	-	-
27				-62	52	-	2.5	-	19.8	-	-	-	-	-	-
29				-40	158	-	7.6	-	19.9	-	-	-	-	-	-
30				60	105	53	5.1	26.9	19.6	88	235	157	21	113	7
5		I	1.2	200	112	117	4.6	9.7	19.6	116	41	29	41	13	4
6		I		140	25	-	2.9	-	19.6	-	-	-	-	-	-
1		IA		200	105	106	4.3	12.1	19.5	175	72	48	39	16	4
7		IA		150	137	134	5.5	16.3	19.7	198	98	71	36	18	5
3		IAR	1.9	200	116	117	4.8	10.8	19.6	111	51	32	37	16	4
9		IAR		125	139	-	5.6	-	20.0	-	-	-	-	-	-
2		IARA		200	128	128	5.2	15.7	20.0	198	95	68	37	18	5
8		IARA		150	145	142	5.8	17.2	19.8	196	104	77	33	18	5
4		IARAR	2.6	200	107	109	4.4	10.1	19.7	100	46	37	36	16	5
10		IARAR	2.6	150	126	120	5.1	11.6	19.7	115	57	39	36	18	5

[a] E x 10^{19} n/cm^2 > 1 MeV

[b] Alternative definition

[c] Proposed ASTM definition

[d] Evaluated at Δa = 1.5 mm plus blunting

[e] Original unbroken ligament

[f] $T = E/\sigma_f^2 \times dJ/da$

[g] Evaluated at J_{Ic}

[h] dJ/da by ASTM least squares fit

[i] ω = b/J x dJ/da

[j] Uses J_{Ic} and dJ/da by ASTM least squares fit

defines an "exclusion line" and is used to distinguish crack tip blunting from actual extension. This point is illustrated in Fig. 6. Due to data scatter, it is not possible to define a unique J_{Ic} value simply by the intersection of the R curve with the crack extension line. Instead it is required to first demonstrate a physical crack extension such as stipulated by the exclusion line.

For reactor vessel steels, the J_{Ic} point will often be governed by the exclusion line for toughness values below approximately 300 kJ/m^2 (1713 in.lb/in.^{2}); for irradiated steels this value increases to 400 kJ/m^2 (2284 in.lb/in.^{2}). Since the initiation toughness for the steels reported here is always less than the above values, the crack extension line has been omitted from the graphs for the sake of clarity.

An advantage of the alternative definition of J_{Ic} is that it will define the same value of J_{Ic} irrespective of how much or how little crack extension is developed prior to failure in a brittle or cleavage mode. Figure 7 illustrates the R curve for an A533-B steel specimen which exhibited a small crack extension beyond the 0.15 mm exclusion line before failure in the cleavage mode. This expanded plot highlights the $\pm$ 0.08 mm ($\pm$ 3 mil) scatter which can be produced with 1T-CT specimens. (This figure is typical of the largest scatter which has been observed with the current experimental technique). For this case, J_{Ic} is given as 214 kJ/m^2 (1225 lb/in.) by the alternative procedure. Since the crack extension is less than twice the extension to the blunting line, the proposed ASTM procedure would define J_{Ic} at the level of fracture. The latter corresponds to a value of 308 kJ/m^2 (1765 lb/in.) which is 44% greater than that given by the alternative definition.

Note that the R curve of Fig. 7 exhibits a sharp change in slope prior to cleavage. This is not a result of data scatter and a similar trend has been observed with other specimens cut from A533-B steel plate [7]. Possibly this is a new phenomenon associated with a "hardening" of the steel prior to cleavage fracture; this behavior is illustrated by the flattening of the load versus deflection trace just prior to failure. For a similar-type behavior but at a somewhat greater crack extension, the proposed ASTM procedures requires a least squares fit of the data in order to define J_{Ic}. The hardening phenomenon observed for cleavage failure would appear to make such a least squares fit inappropriate.

EFFFECT OF SIDE GROOVES

In order to characterize the significance of side grooves in promoting crack front straightness, a comparison was made between specimens having a 0, 10, and 20% total groove depth. Fracture surfaces from these specimens in the unirradiated and irradiated conditions are illustrated in Figs. 8 and 9, respectively. From these figures, it can be observed that a 20% side groove depth is sufficient to produce a straight crack front. Note, however, that side grooving tends to produce some reverse tunneling near the edges. It was also observed that 10% side grooves produced a straight crack in the irradiated weld whereas the same groove depth in the unirradiated material was insufficient to eliminate tunneling. In a related program [7] 10% side grooves in an irradiated A533-B plate still did not eliminate the tunneling. From this we conclude that the optimum side groove depth is still an art and apparently depends upon flow stress as well as product form.

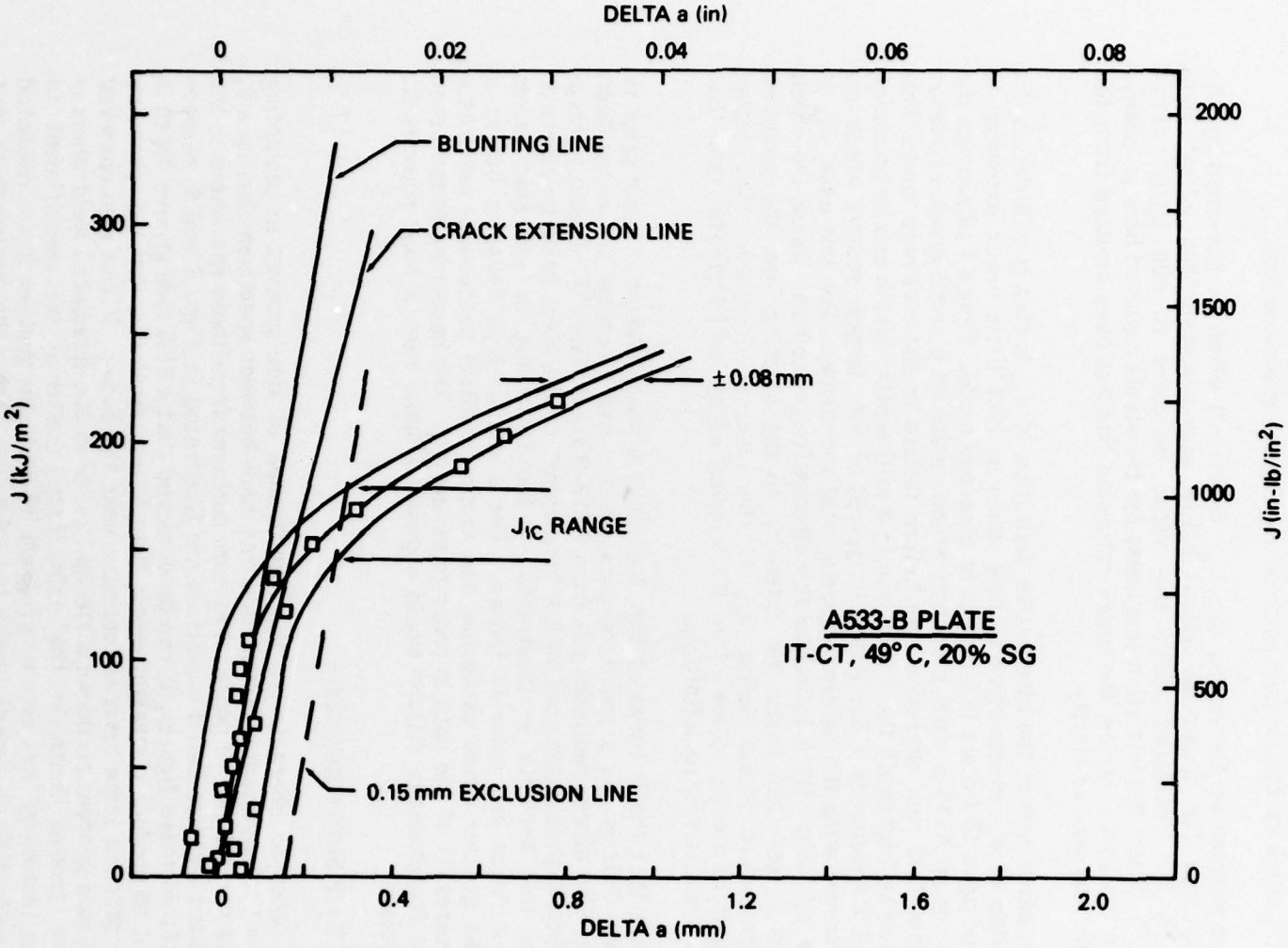

Fig. 6 — J_{Ic} definition illustrating the interaction between the data scatter and the crack extension line and the exclusion line. Because of this scatter the crack extension line cannot be used to measure J_{Ic} until a fixed crack extension has occurred.

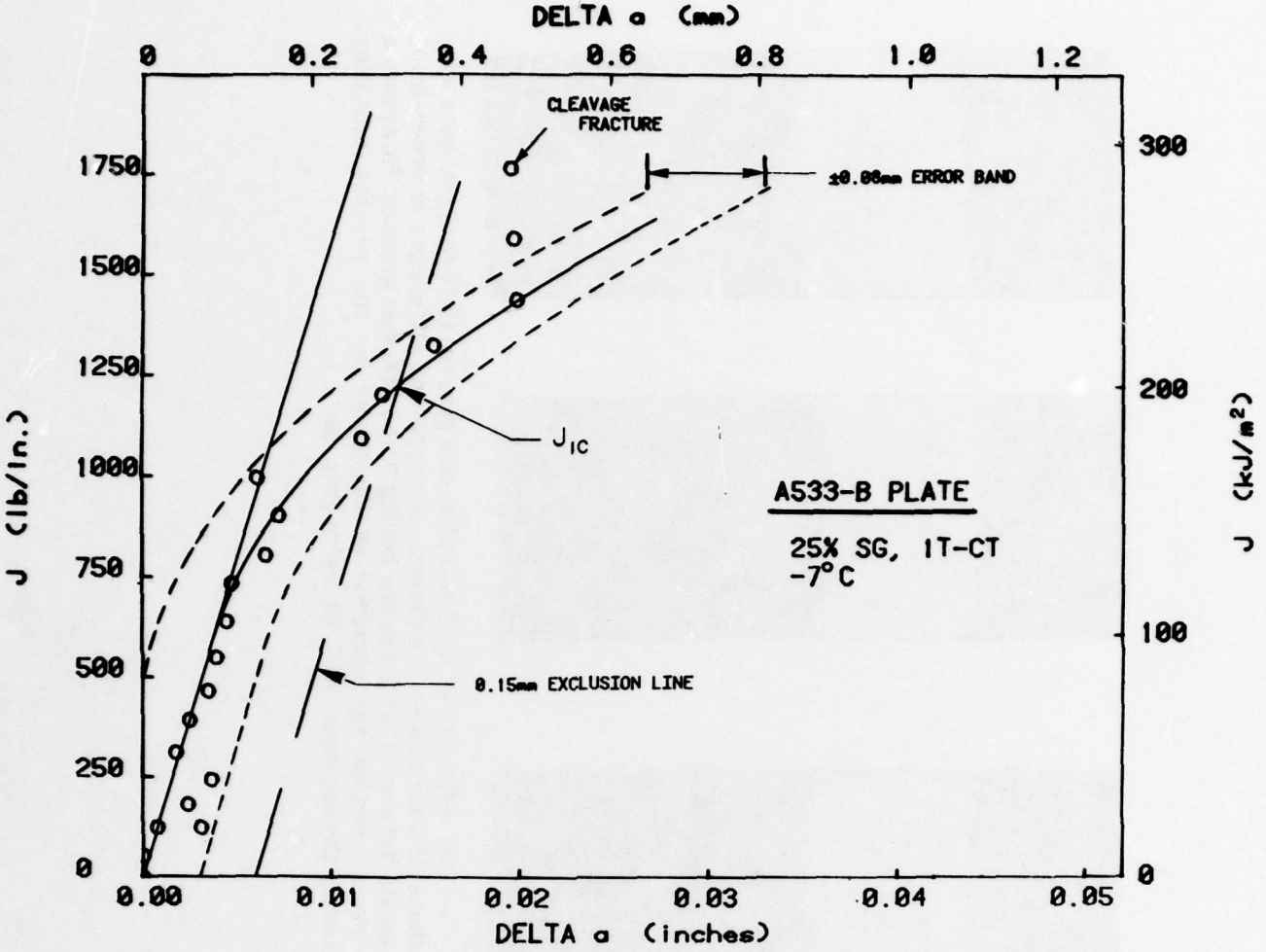

Fig. 7 — R curve for an A533-B steel plate which exhibits cleavage fracture at a crack extension slightly in excess of the 0.15 mm exclusion line. The scales have been expanded to highlight the data scatter which represents the extremes using current experimental techniques.

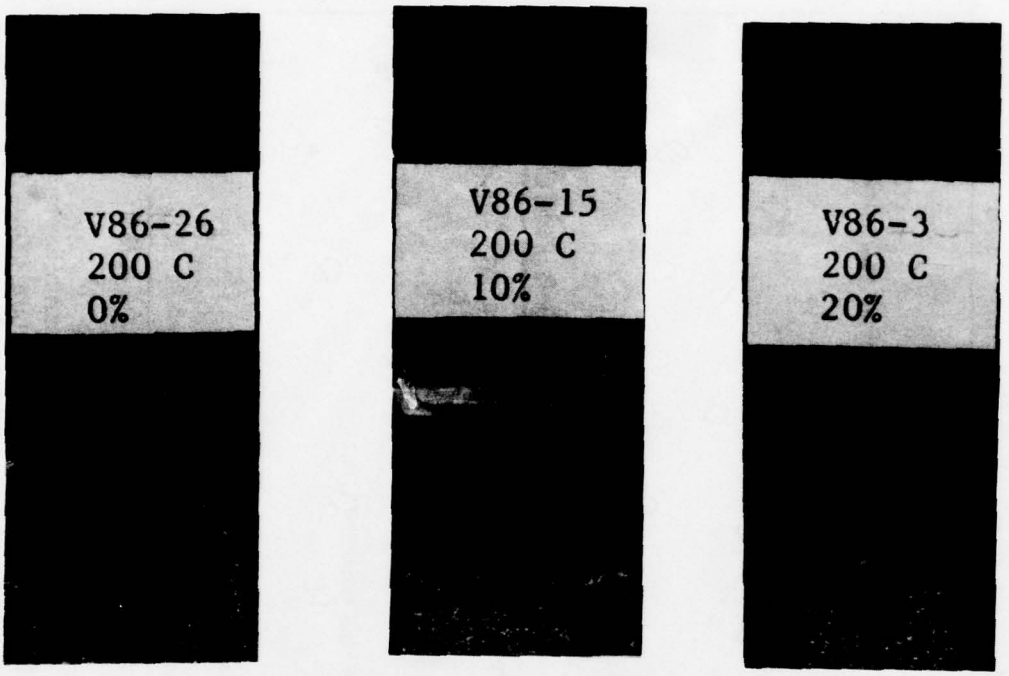

Fig. 8 — The influence of 0, 10 and 20% side grooves (left to right) on crack-front shape of unirradiated specimens. No apparent difference in crack-front shape exists between the specimens having 0 and 10% side grooves. However, a slight overcorrection has occurred as illustrated by the reverse tunneling exhibited by the specimen with 20% side grooves.

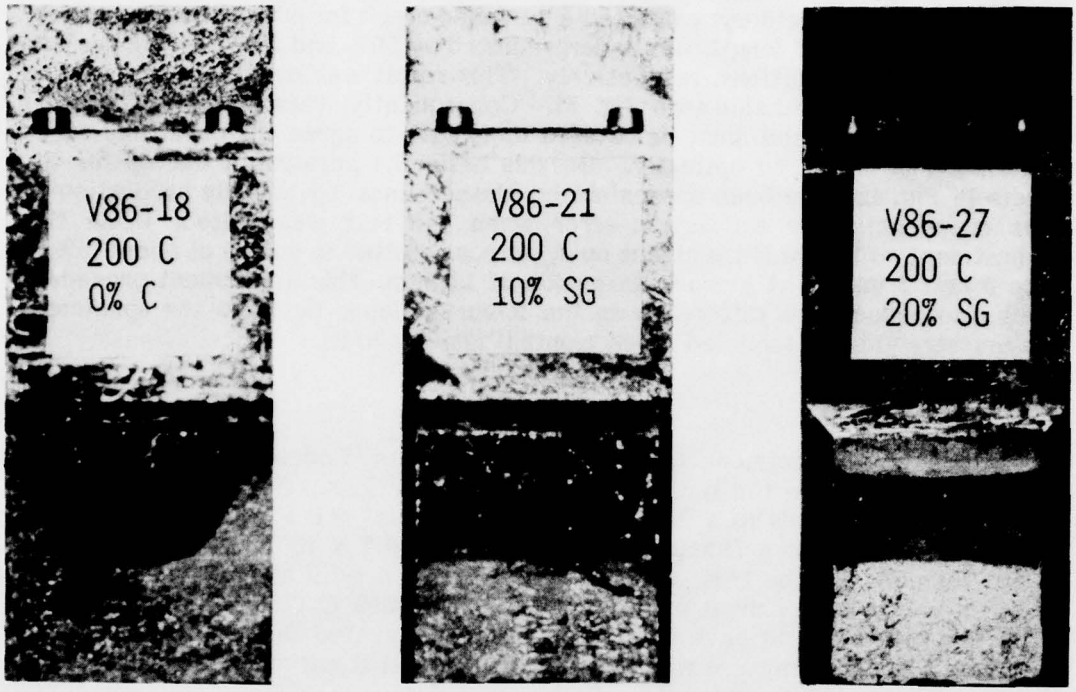

Fig. 9 — Influence of 0, 10 and 20% side grooves (left to right) on the crack front shape of irradiated specimens. A 10% side groove depth was sufficient to produce a straight crack front. However, this depth was insufficient to straighten the crack front in unirradiated material (Fig. 8).

The R curves for the above specimens are illustrated in Figs. 10 and 11. It can be seen that for both irradiated and unirradiated material the specimens with straight cracks have produced R curves with the lowest slopes. For this reason the balance of the specimens in this program were tested with 20% side grooves.

A comparison of R curves from one weld deposit (Code V86) in the pre- and postirradiation conditions is presented in Fig. 12 for specimens without side grooves. These specimens exhibited a tunneled crack for which the final crack-extension increment length was underpredicted by 20% and 30% for the pre-and postirradiation conditions, respectively. This result was expected on the basis of the previous discussion (see Fig. 3). Consequently, these R curves are not physically correct and must be rotated clockwise to agree with the final crack extension as measured optically. On this basis the physical R curves for the tests in Fig. 12 have been approximated (dashed lines) by linearly proportioning the crack extension estimation error when the test was halted. While this adjustment will have little effect on J_{Ic} it has resulted in a drop of about 15% in the J and T values at a crack extension of 1.5 mm. This adjustment procedure will also reduce the difference in the R-curve slopes between the specimens having straight and tunneled crack fronts (Figs. 10 and 11).

R-CURVE COMPARISONS

Irradiated specimens from two weld deposits (Codes V84 and V86) have been investigated in the I, IAR, and IARAR conditions. For both welds the I condition corresponds to a fluence of 1.2×10^{19} n/cm^2 >1 MeV; each subsequent reirradiation was to a fluence of approximately 0.7×10^{19} n/cm^2. Thus, the total fluences for the IAR and IARAR conditions are 1.9 and 2.6×10^{19} n/cm^2, respectively. Each anneal (IA and IARA) was at 399°C (750°F) for 168 hours. The majority of tests have been conducted at elevated temperatures so as to produce a ductile fracture which would result in an R curve. The results of all tests are listed in Tables 1 and 2.

Figure 13 compares the R curves for weld V86 in the unirradiated, irradiated and annealed conditions. The test temperature chosen for the comparison (200°C) is within the upper shelf regime of the C_v test [1]. A more detailed comparison of the I, IAR and IARAR conditions is provided in Fig. 14. J_{Ic} for the irradiated material (I) is approximately 65 kJ/m^2. This value is one-half of that from the unirradiated condition (see Table 1). Figure 14 shows that there is a slight improvement in the J_{Ic} values for the IAR and IARAR conditions in comparison to the I condition even though the former represent higher fluence levels. This behavior is consistent with the C_v upper shelf trends [1].

In terms of both J_{Ic} and the level of the R curve slope, Fig. 13 shows that approximately half of the toughness which was lost as a result of irradiation (I) has been recovered by annealing (IA). After reirradiation, a second anneal (IARA) has resulted in a recovery to the level of the first anneal. This trend suggests that it is possible to "cycle" the material with successive reirradiation and reanneals so as not to decrease the toughness below the level of the I condition. While this annealing recovery trend is encouraging, it is not as

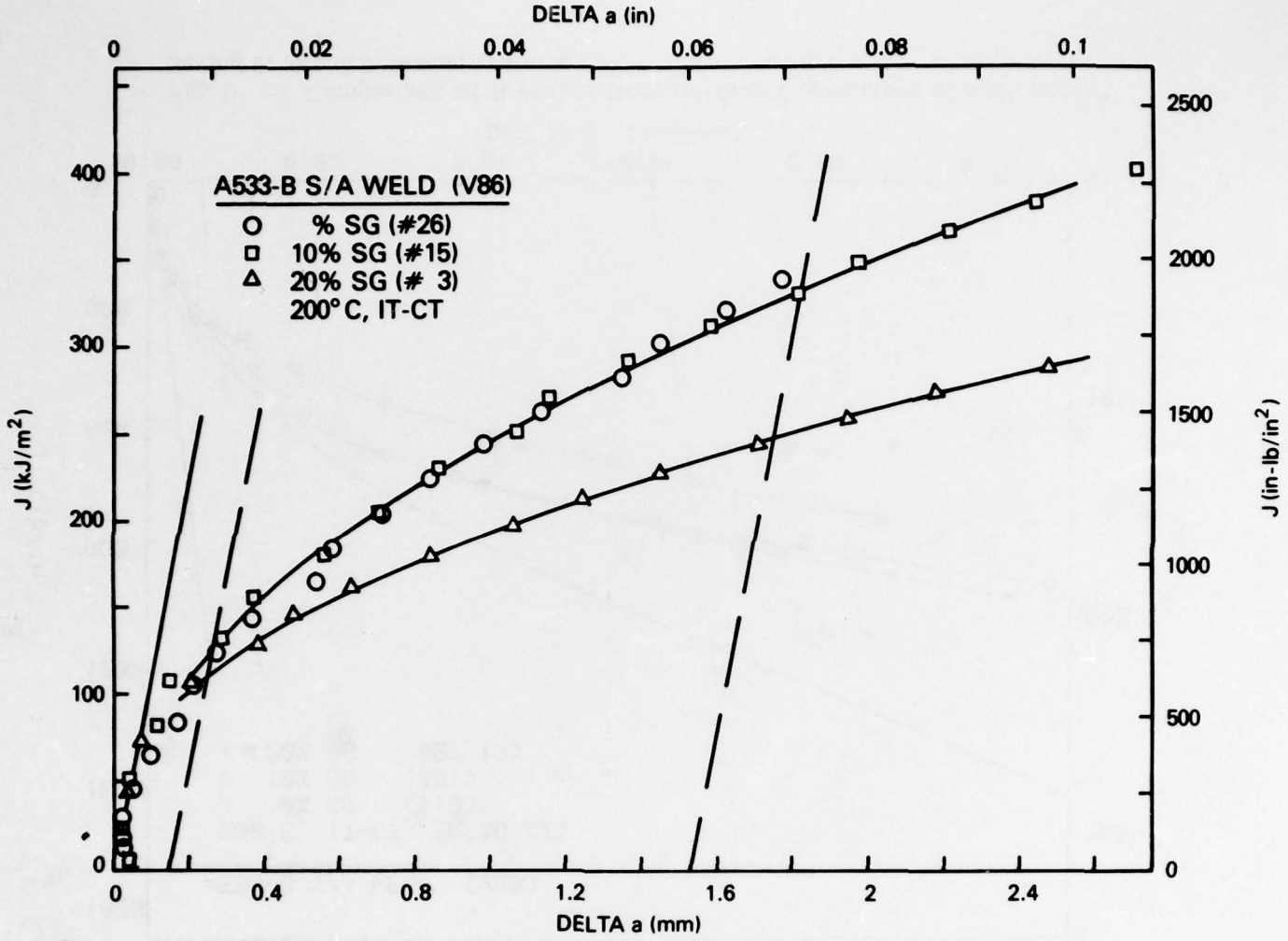

Fig. 10 — Comparison of R curves for unirradiated specimens having 0, 10 and 20% side grooves.

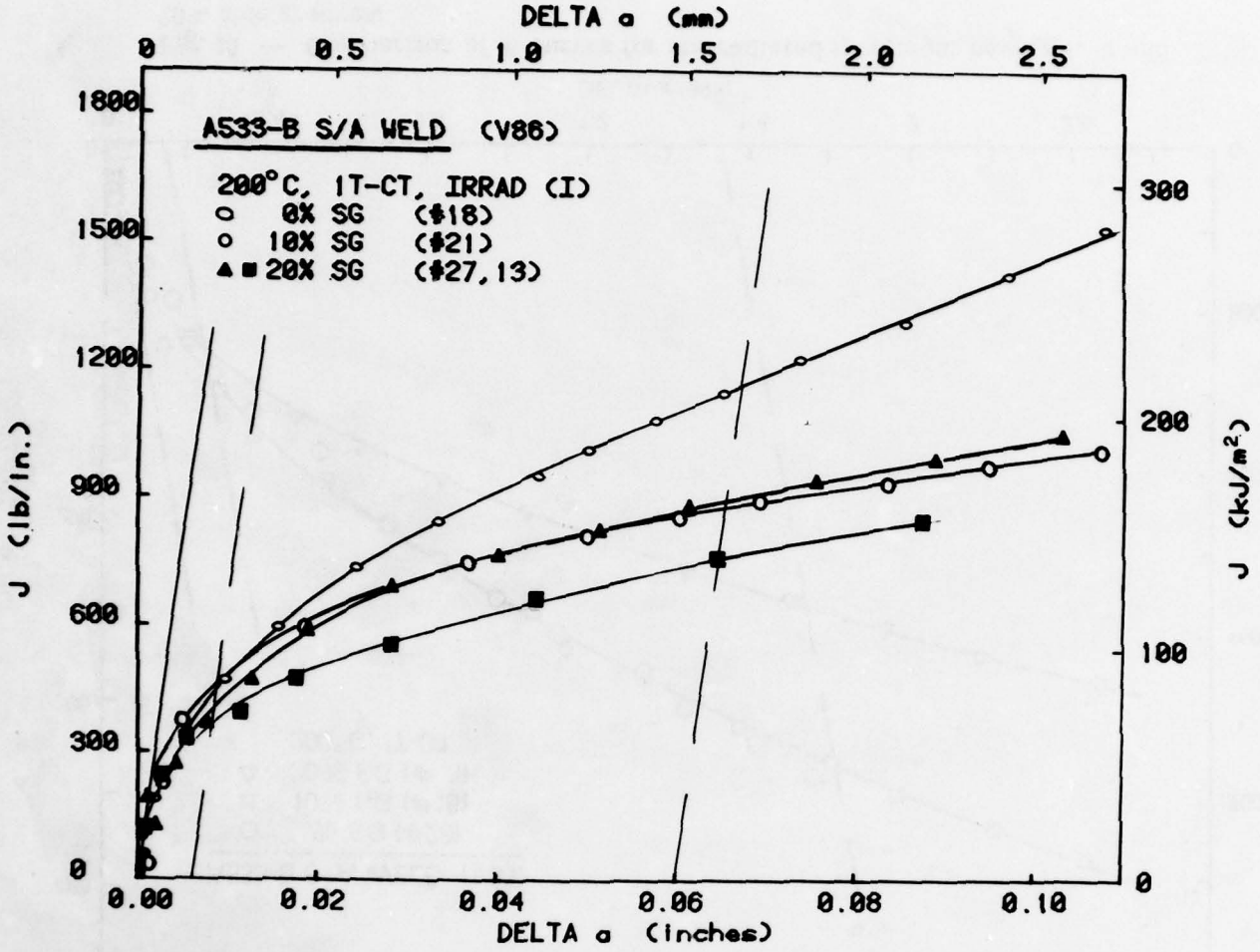

Fig. 11 — Comparison of R curves from irradiated specimens of weld deposit having 0, 10 and 20% side grooves.

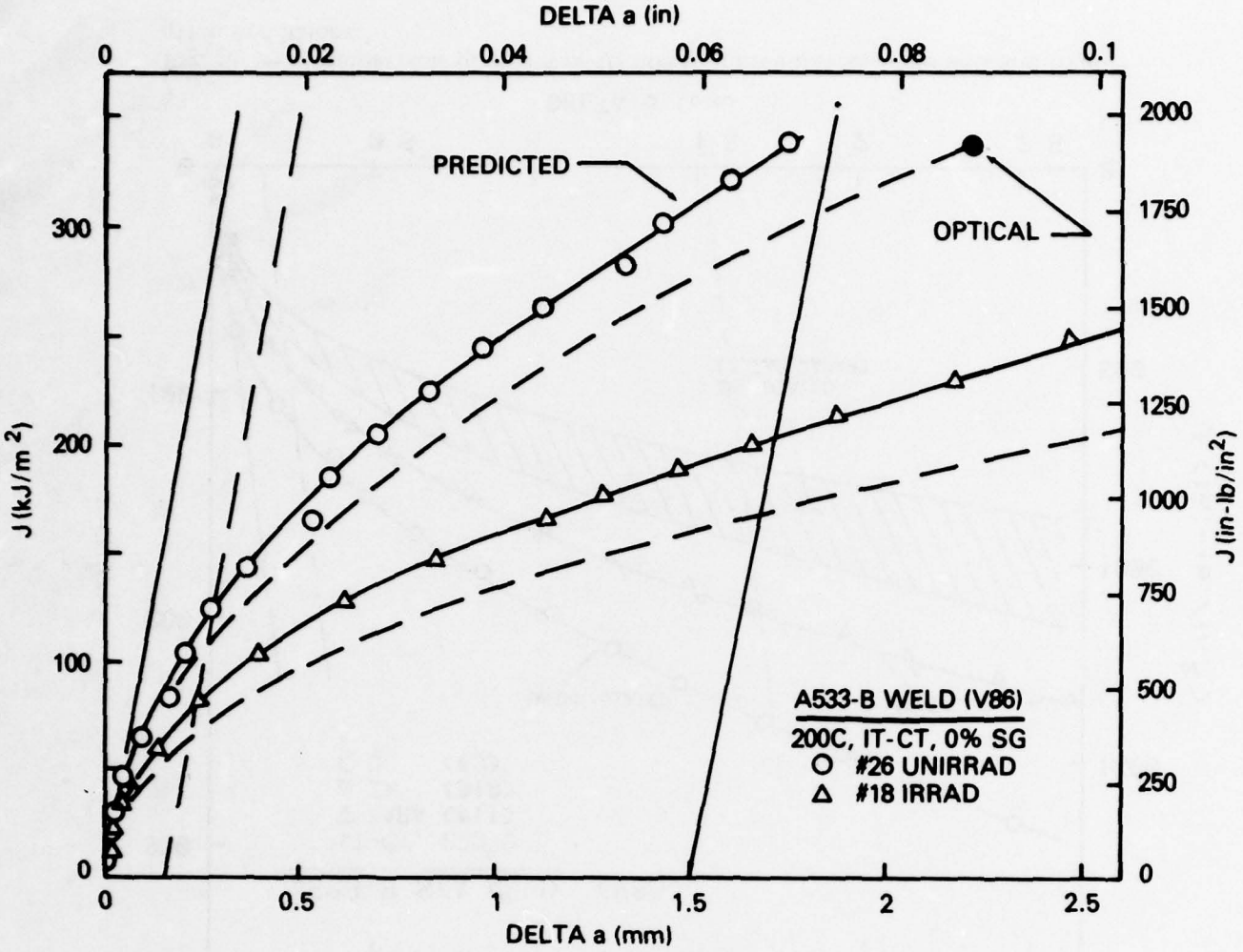

Fig. 12 — Comparison of R curves from weld metal in the pre- and postirradiated conditions for specimens without side grooves. The dashed lines approximate the R curves so as to account for the crack-length prediction error associated with a tunneled crack front.

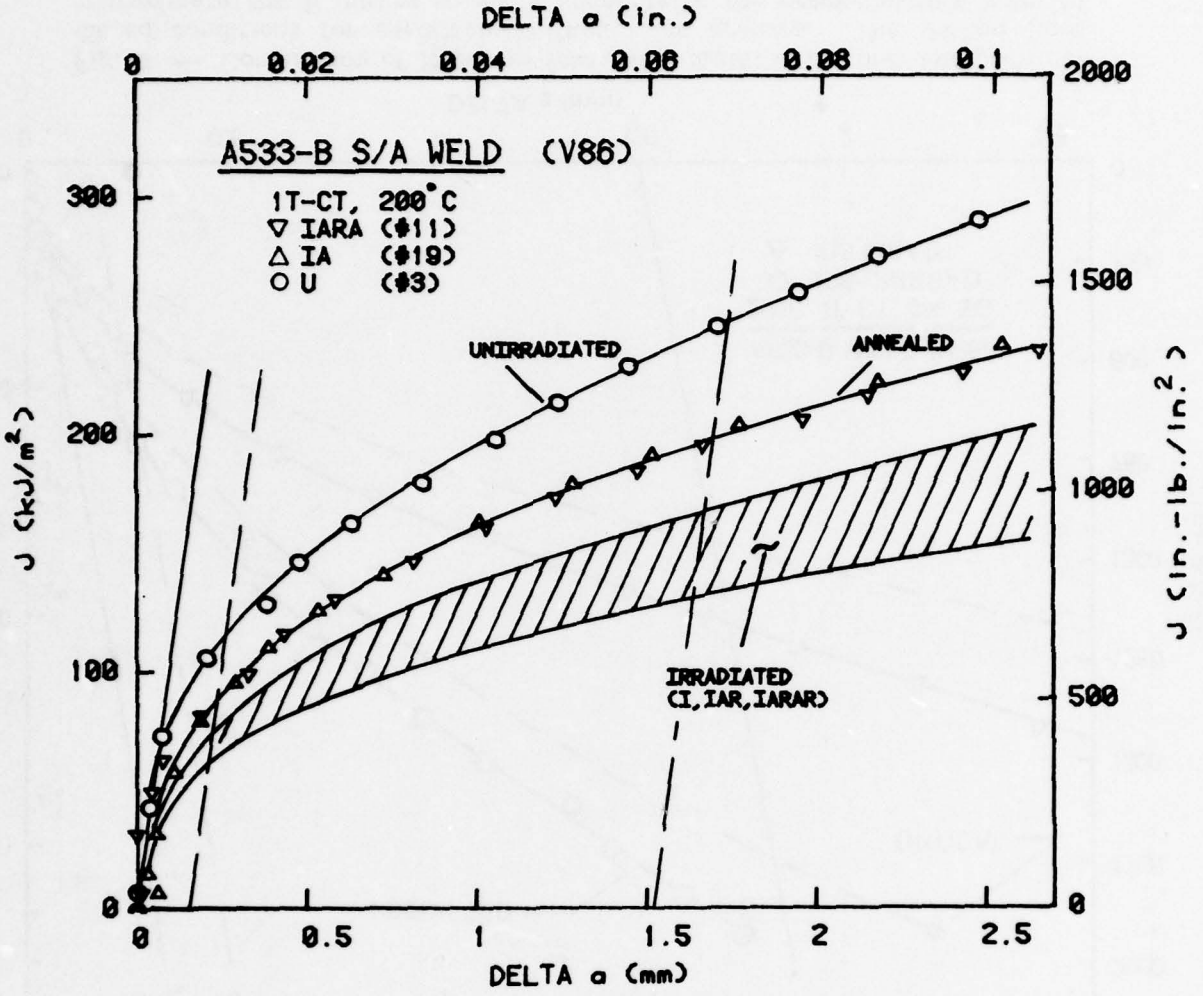

Fig. 13 — Comparison of R curve trends in unirradiated, annealed and irradiation conditions.

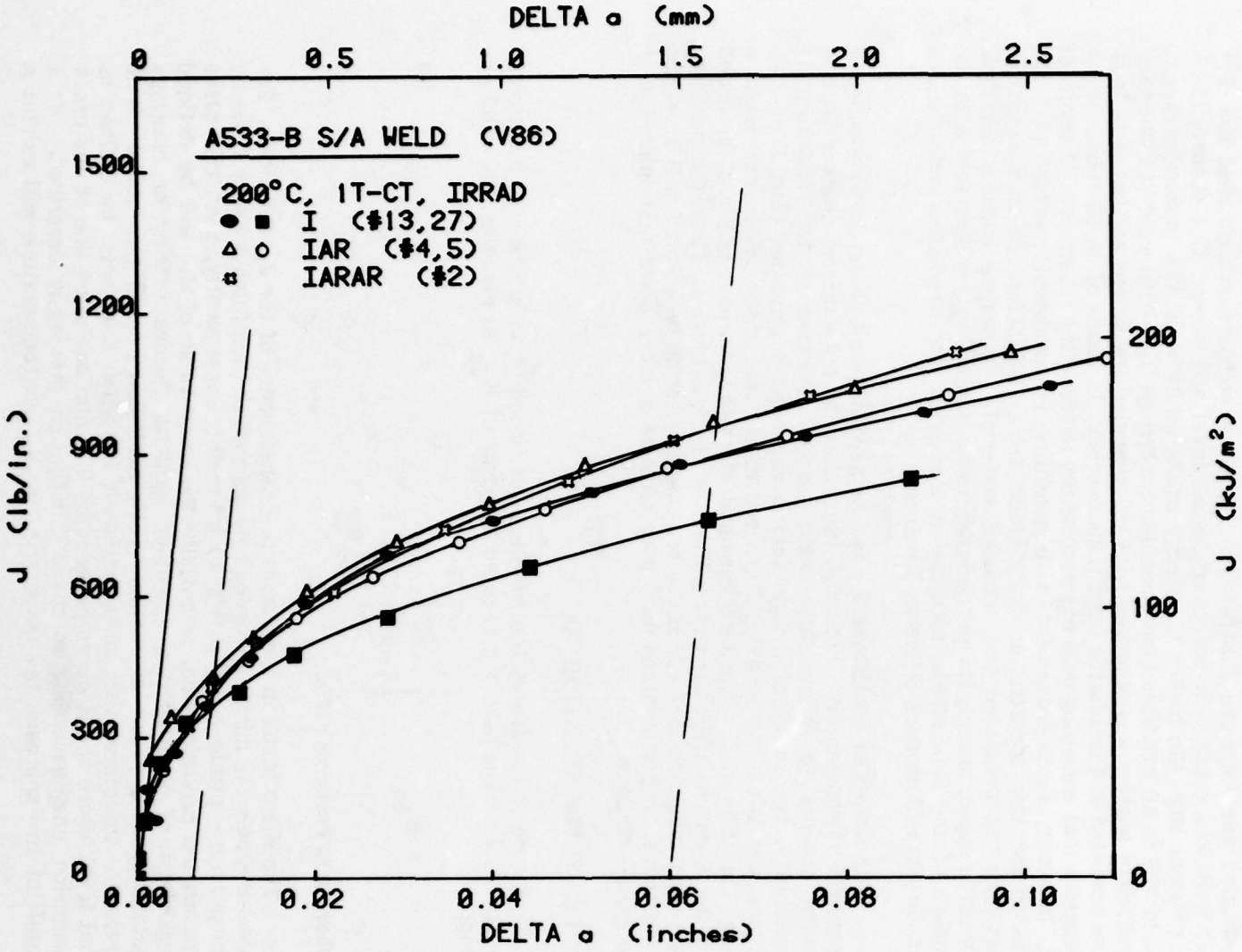

Fig. 14 — Comparison of R curves for irradiated weld deposit (I) with those for material which has been reirradiated with intermediate annealing (IAR, IARAR).

optimistic as that projected by C_v tests. The latter has shown a full recovery of the upper shelf energy level [1].

The R curve trends for weld V84 in the unirradiated, irradiated and annealed conditions are illustrated in Fig. 15. In comparison with weld V86 (Fig. 13) weld V84 exhibits R curves of higher level and slope. This observation is consistent with the higher C_v energy exhibited by weld V84 in comparison to weld V86 in all irradiated and annealed conditions [1]. With weld V84 however, sufficient scatter was observed with the annealed specimens so that data from the annealed and irradiated conditions overlap. In terms of dJ/da this behavior suggests that annealing does not necessarily improve the toughness. In terms of T, however, an improvement with annealing is consistently exhibited. The reason for this apparent anomaly stems from the difference in flow stress between the irradiated and annealed material. Annealing reduces the flow stress to approximately its unirradiated level. Since T varies inversely with the square of the flow stress, identical R curves for the irradiated and annealed conditions will produce different T values.

For weld V84 consistent J_{Ic} values were difficult to establish because of material inhomogeneity. Figure 16 illustrates the non-uniform crack extension which appears to follow three weld passes. Because of the metallurgical variability, two cases of a sigmoidal R curve were produced (Fig. 17). This figure highlights the initial differences in R-curve shape which can cause a large variation in J_{Ic}. On the other hand, the two specimens in Fig. 17 produced similar R curves after the first 0.5 mm of crack extension. From this behavior one could conclude that a fracture toughness criterion based on T will be easier to establish experimentally and may produce a more consistent indicator of toughness changes.

UPPER SHELF BEHAVIOR

Figure 18 illustrates the toughness variation of weld V86 as a function of temperature. The plot is presented in terms of K_{Jc} as given by the relationship:

$$K_{Jc} = \left[\frac{E\,J_{Ic}}{1-\nu^2}\right]^{1/2} \qquad (2)$$

where ν is Poisson's ratio.

The sharp break in the curves is a consequence of the J_{Ic} definition. For A533-B steels the initial R-curve slope appears to be influenced very little by temperature within a 100°C (180°F) interval. Consequently, once this curve crosses the exclusion line, essentially the same value of J_{Ic} will be defined regardless of whether the specimen exhibits fibrous tearing or cleavage instability as a result of further crack extension beyond this point. It is proposed, therefore, that an upper "shelf initiation toughness" be defined as that level where the R curve crosses the 0.15 mm exclusion line or the crack extension line, according to the J_{Ic} definition previously described. As a result of this approach the trend in J_{Ic} or K_{Jc} vs temperature will exhibit a

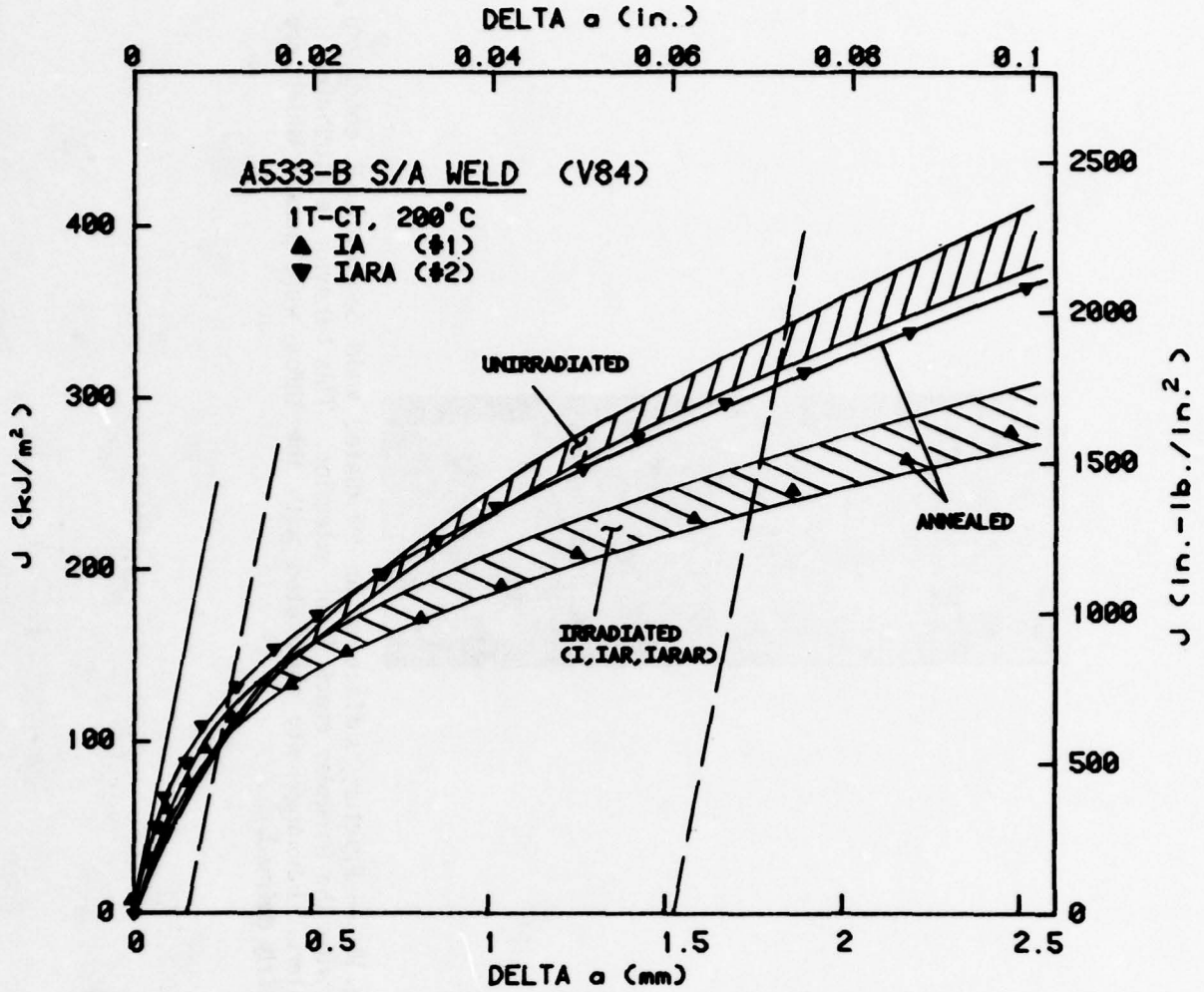

Fig. 15 — Comparison of R curve trends in unirradiated, annealed and irradiated conditions.

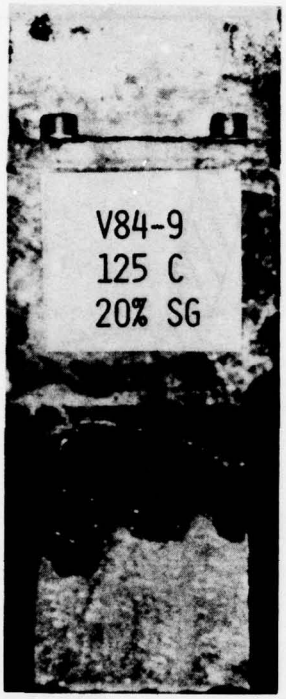

Fig. 16 — Fracture surface of an irradiated weld deposit (IAR condition) showing the irregular crack front extension. This behavior is attributed to material inhomogeneity associated with the three weld passes which are clearly defined.

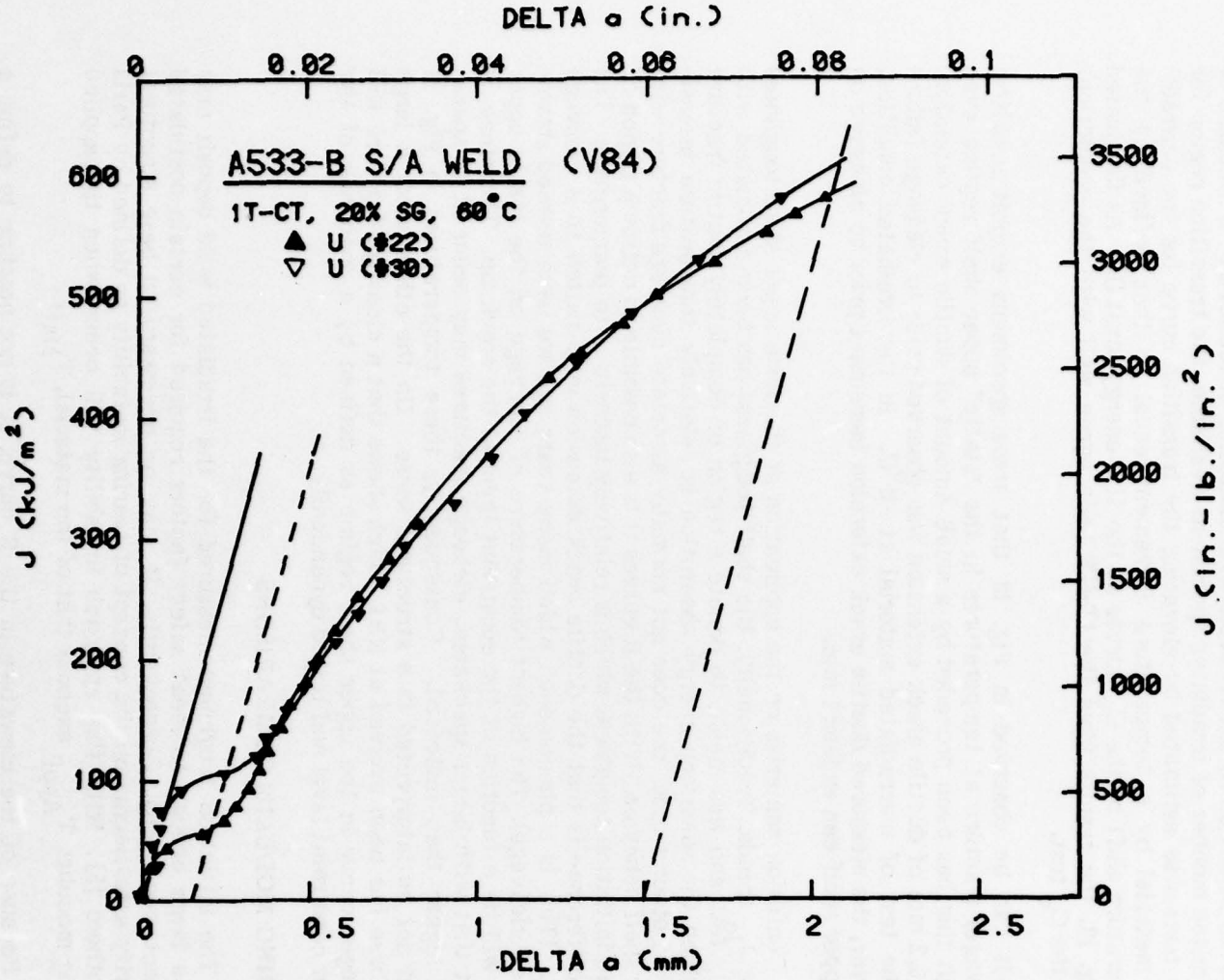

Fig. 17 — Sigmoidal-shaped R curves which are believed to result from material inhomogeneity as illustrated in Fig. 16. This behavior explains the observed scatter in crack initiation (J_{Ic}) trends for this weld. However, the slope of the R curve, as used for T, appears to be well behaved.

sharp break when the upper shelf temperature is reached as illustrated in Fig. 18.

In the unirradiated condition, weld V86 exhibits an upper shelf toughness of 170 MPa$\sqrt{m}$ (155 ksi$\sqrt{in.}$). This toughness drops to 117 MPa$\sqrt{m}$ for the irradiated condition (I) but recovers with annealing to 138 MPa$\sqrt{m}$. Because of the limited number of irradiated specimens available, the transition region for these tests was estimated by elevating the transition curve for the unirradiated material by a temperature increment equal to that defined by the temperature shift of the C_v curves at the 41 J energy level [1]. As illustrated in Fig. 18, the results from the 1T-CT tests agree well with the predictions from the C_v test.

It can be observed in Fig. 18 that some specimens exhibit a brittle (cleavage) fracture at temperatures in the "static" upper shelf regime even though this has been preceded by a small amount of ductile crack extension. Only 0.2 mm of ductile crack extension was observed prior to cleavage failure for the test of unirradiated material at -11°C. In the irradiated condition, however, the measured ductile crack extension increment prior to cleavage on the upper shelf can exceed 1 mm.

Confusion can arise on the application of the term upper shelf toughness to the J_{Ic} trends. Traditionally, the shelf toughness has been associated with the C_v test and was meant to denote a region of completely ductile fracture for which the specimen energy absorption is relatively temperature insensitive. In other words, one does not normally associate cleavage fracture with upper shelf behavior. With the R curves it is also possible to define a region of ductile initiation toughness which is relatively insensitive to temperature. The only difference is that the ductile crack extension may switch to a cleavage mode. (This is a phenomenon which many years ago we have termed strain-induced cleavage). The highest temperature of cleavage on the static upper shelf will be a function of the constraint level at the crack tip. Therefore, it is felt that with larger specimens, cleavage fractures may occur at temperatures higher than indicated. Consequently, these temperatures in Fig. 18 should not be interpreted in a structural sense. On the other hand, a large data base has been evolved at NRL which shows that a cleavage fracture will no longer occur in the upper shelf regime as defined by a specimen of the proper constraint level and tested dynamically.

TEARING MODULUS COMPARISONS

The initiation toughness measured for the irradiated weld deposit may not be large enough to meet safety factors required for certain postulated accident conditions. Consequently, it may be necessary to base structural integrity assessments on the concept of tearing instability as defined by Paris and others [5]. With this approach instability will occur when the applied tearing modulus, T_{Appl}, exceeds that of the material, T_{Mat}.

Because of the curvature in the R curve, it is not possible to define a unique value of T. For purposes of discussion, we have chosen to compute T

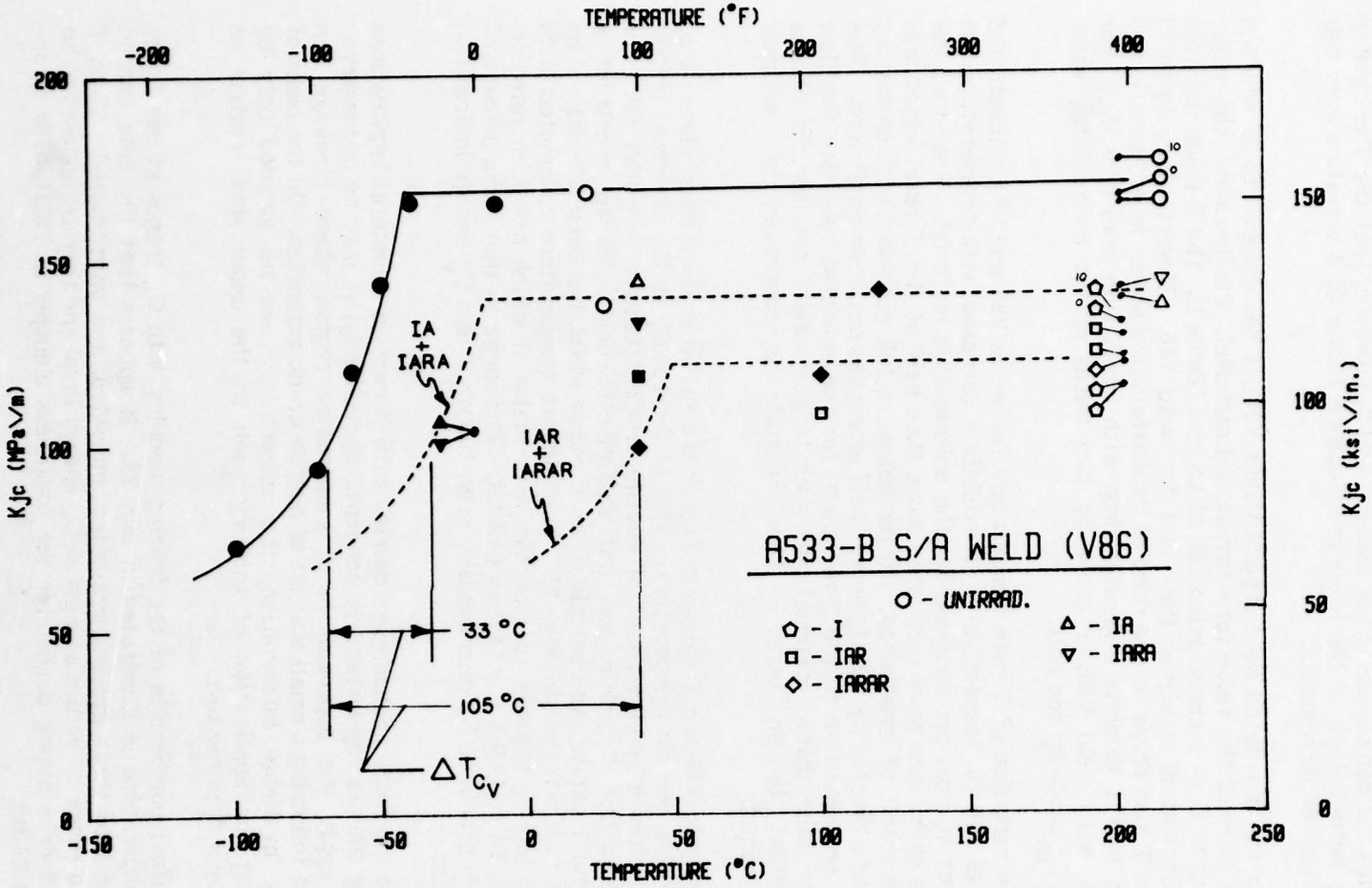

Fig. 18 — Comparison of pre- and postirradiation fracture toughness initiation (K_{Jc}) trends. The transition regime for this material in the irradiated conditions were estimated by the temperature elevation of the C_v curves at the 41 J energy level.

using the least squares fit to the R curve between a crack extension of 0.15 and 1.5 mm. It can be seen from Tables 1 and 2, however, that the T computed with the actual slope of the R curve exhibits a factor of 3 variation over this crack extension increment.

For the irradiated weld deposit (Code V86), T has dropped to 25 which is only one third of the value for unirradiated material. Furthermore, this value decreases to 15 at a crack extension of 1.5 mm (Table 1). The T value for weld V84 (unirradiated) is higher than that for weld V86. Nevertheless, in the I condition T also drops to one third of its unirradiated level. In addition, it was observed that T exhibits a greater drop with irradiation than does J_{Ic}. For example, with weld V86, T drops by two thirds of the unirradiated value whereas J_{Ic} drops by one half.

The variation of T with temperature for welds V86 and V84 is illustrated in Figs. 19 and 20, respectively. T exhibits a decrease with temperature but the effect is most prounounced for the unirradiated material. Note that the annealed specimens have recovered more than half of the T level which was lost as a result of irradiation. Nevertheless, a full recovery with annealing, which was indicated by the C_v upper shelf levels, has not been confirmed. (The T levels are sensitive to the flow stress; for the annealed condition the flow stress for unirradiated material was used to compute T pending the results from actual tensile tests. This estimate is supported by hardness measurements).

For weld V86 the T values in Fig. 19 are shown as decreasing abruptly to zero below a certain temperature. This is the result of the observed brittle fracture after a small amount of ductile crack extension (see Fig. 18). For these tests the R curve was not sufficiently developed to construct a meaningful T value. An example of an R curve which has been interrupted by cleavage is illustrated in Fig. 21. The highest temperature associated with cleavage failure appears to increase with material which has been reirradiated, i.e., IA vs IARA and IAR vs IARAR. This suggests that some amount of damage is produced by reirradiation even though T and C_v energy indicate no differences.

The cleavage phenomenon carries with it certain structural implications regarding the tearing instability concept. Specifically, it may be unconservative to apply the approach in a temperature region where cleavage can intercede following a small amount of ductile crack extension. On the basis of currently available information, this uncertainty can be avoided only by restricting the application of this approach to the upper shelf regime as defined by a dynamic test.

A final comparison of the tearing modulus with C_v trends at one upper shelf temperature is illustrated in Fig. 22. It appears that the data can be separated into three groups: irradiated, annealed, and unirradiated. Thus, T exhibits a range of values at a given C_v energy level and thereby appears to be a more discriminating parameter for toughness changes as related to structural instability.

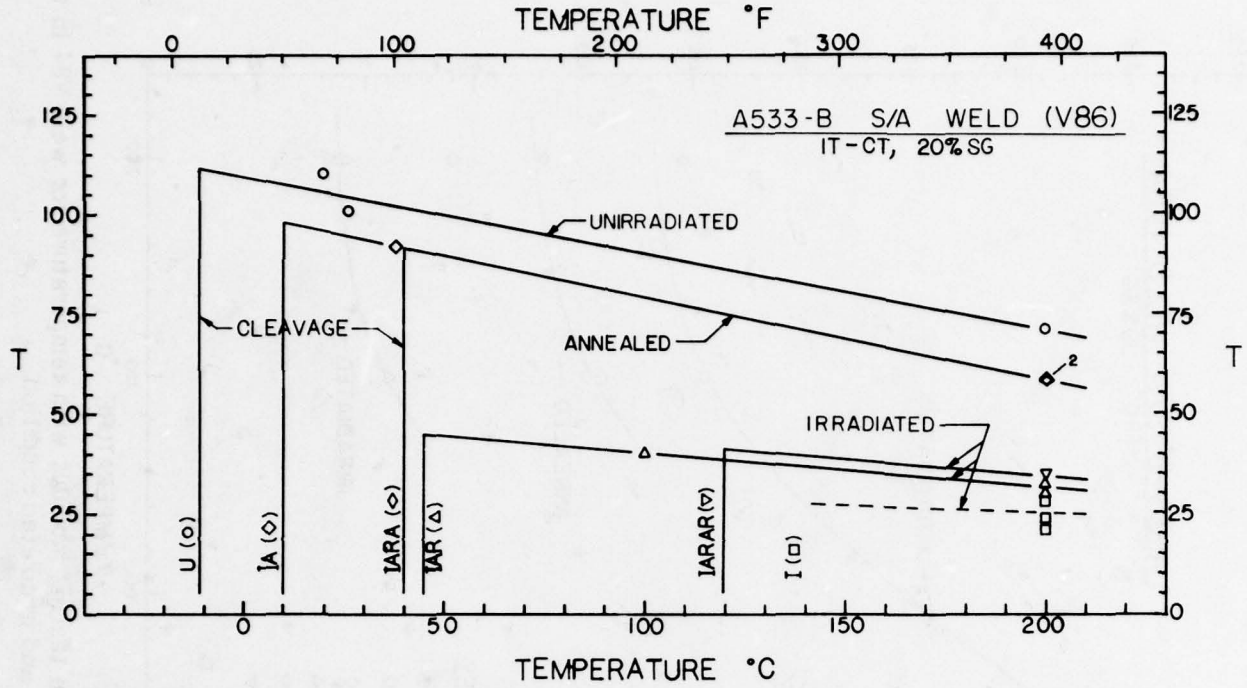

Fig. 19 — Variation in tearing modulus with temperature for weld V86 in the unirradiated, annealed and irradiated conditions. The abrupt drop in the curves denoted by "cleavage" corresponds with the observed brittle fracture after a small amount of stable tearing (Fig. 18).

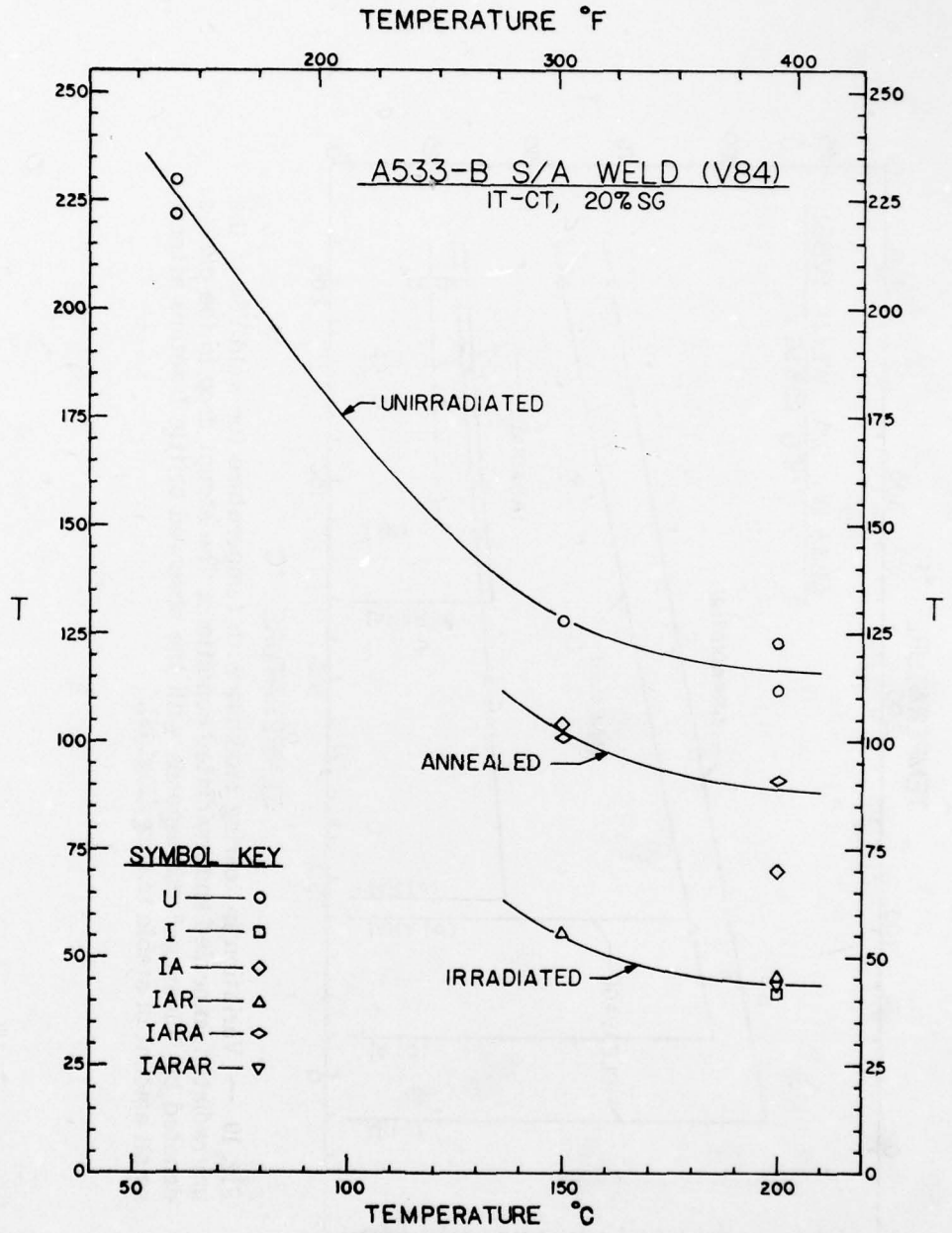

Fig. 20 — Variation in tearing modulus with temperature for weld V84 in the unirradiated, annealed and irradiated condition.

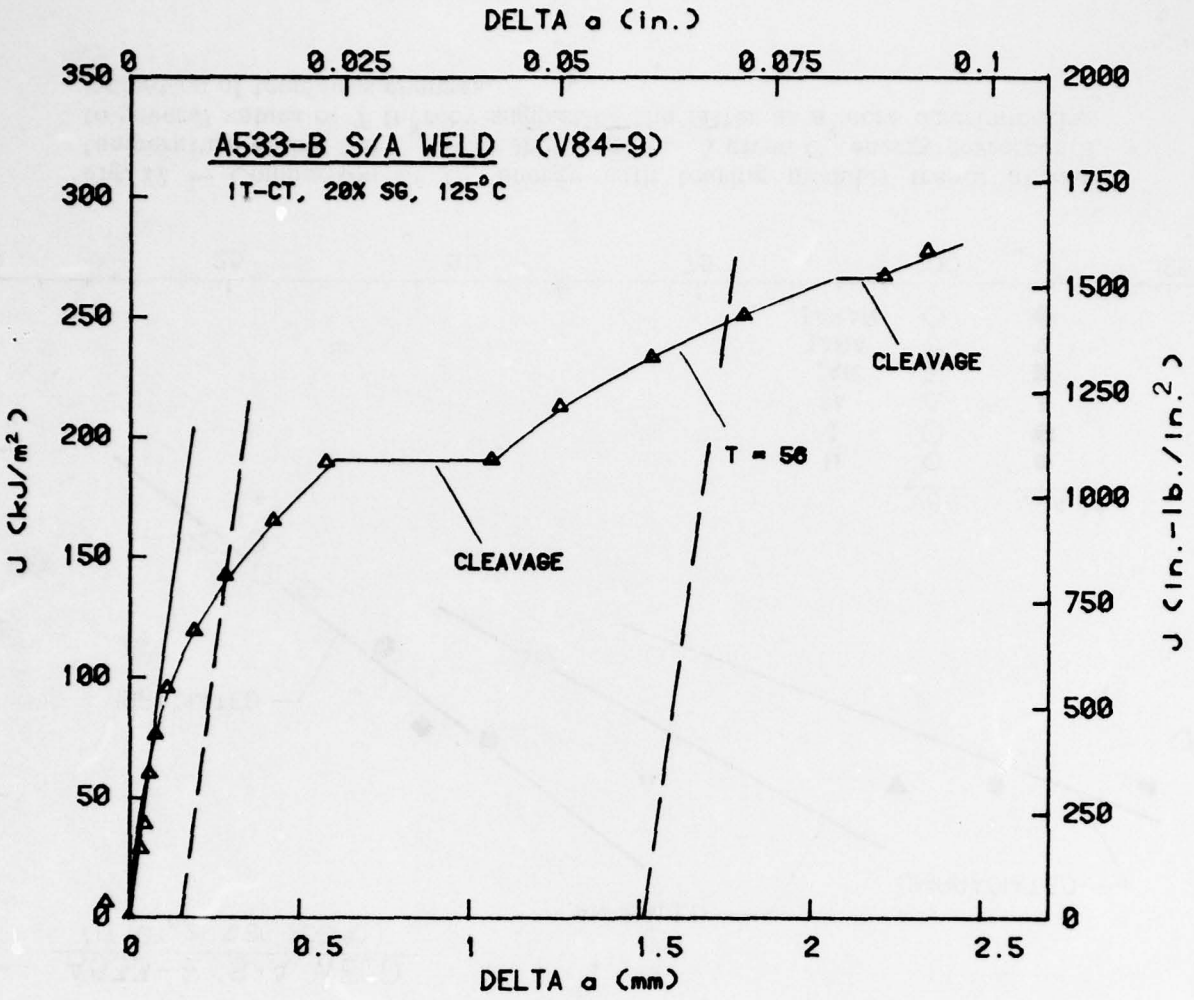

Fig. 21 — R curve showing two regions of cleavage instability followed by arrest and stable crack extension.

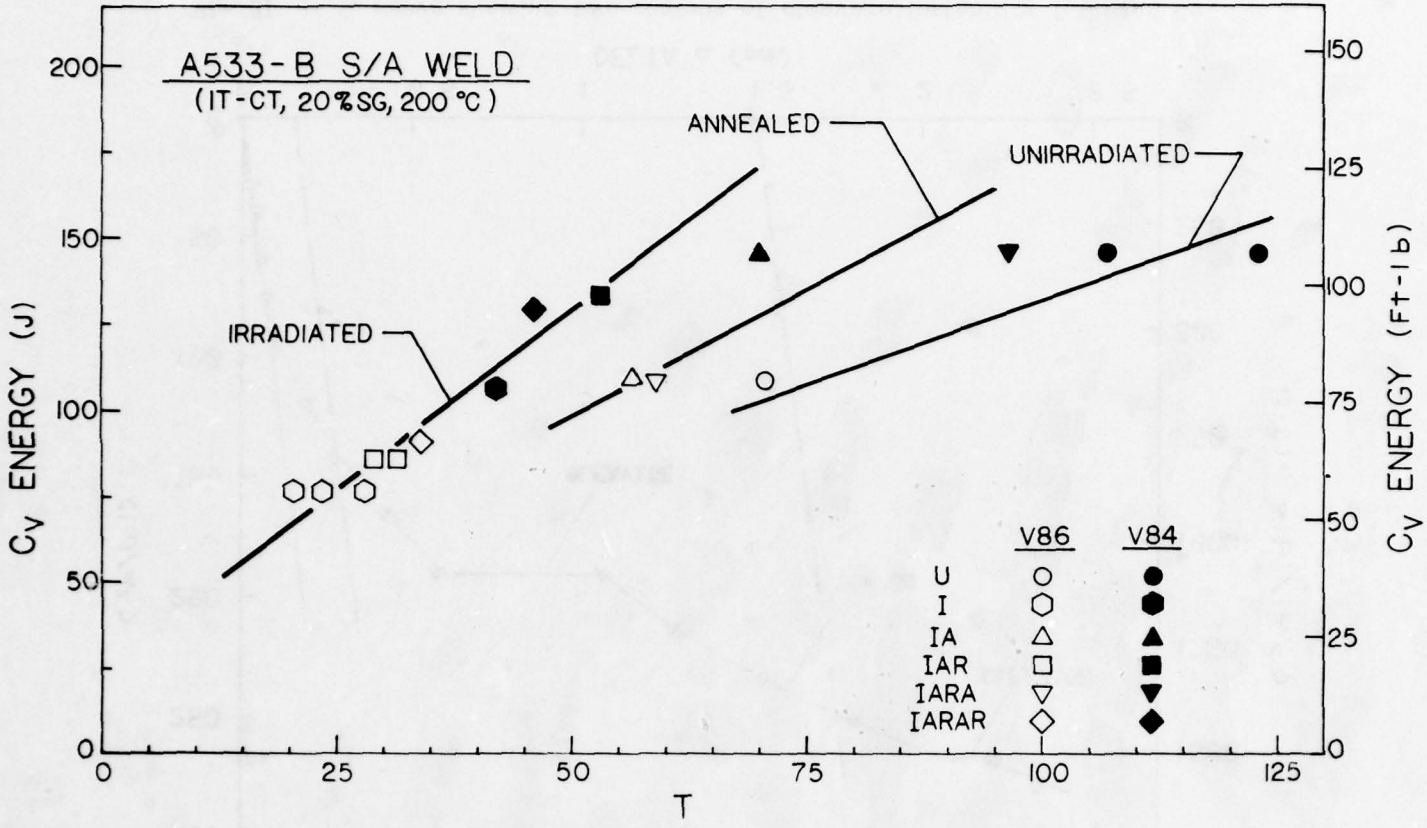

Fig. 22 — Comparison of C_v energy with tearing modulus trends at one temperature within the C_v upper shelf regime. A given C_v energy corresponds to several values of T thereby suggesting the latter as a more discriminating indication of toughness changes.

B. Dynamic Finite Element Analysis of Notched Beam Specimens

S. Mall[a]

INTRODUCTION

Loss [10] has conducted a series of drop-weight impact tests of three-point bend specimens in a previous program involving an investigation of the dynamic initiation fracture toughness, K_{Id}, of nuclear pressure vessel steels. These specimens, machined from A533-B steel, of dimensions 228.6 mm long x 50.8 mm thick, support length of 203 mm with nominal crack length of 25.4 mm were fatigue precracked. It is known that the hammer (tup) force vs time relation during impact loading cannot be employed directly without rigorous dynamic analysis to compute K_{Id} without restrictions on the maximum loading rate ($\dot{K}$) and on the system electronics [11]. For this reason, these specimens were instrumented with a 3.2 x 3.2 mm strain gage near the crack tip as indicated in Figs. 23 and 24. Prior to impact testing, a static calibration was established between this strain gage output and tup load. During the actual impact test, the dynamic strain gage was recorded. The recorded dynamic strain in conjunction with static calibration was used to compute the dynamic bending moment at midspan. The dynamic K_{Id} was, then, determined from this dynamic bending moment at fracture in conjunction with the equation for static K_{Ic} given in ASTM E-399 [12].

The above procedure was empirical and was based on the following assumptions and uncertainties:

1. The dynamic bending moment measured from the strain gage near the crack tip is proportional to the instantaneous stress intensity factor as computed under static loading.

2. Was the strain gage near the crack tip located properly to compute K_{Id} from the above procedure?

3. Is the strain gage location sensitive to loading rate ($\dot{K}$)?

The present study was, therefore, undertaken to assess Loss' procedure in the above context with the help of dynamic finite element analysis.

DYNAMIC FINITE ELEMENT ANALYSIS

Out of the numerous test results available, two specimens were analyzed due to the fact that they had typical impact load-time histories (i.e., different fracture load and crack initiation time) which represented the two extremes of all tests. These two specimens were tested at two different temperatures (10 and -18°C). The two-dimensional finite element code , HONDO, was employed in the present investigation. The material properties of A533-B steel were: Young's modulus = 207 GPa, Poisson's ratio = 0.3 and density = 7.9 g/cm^3. The

[a]University of Maine, Orono, Maine 04473.

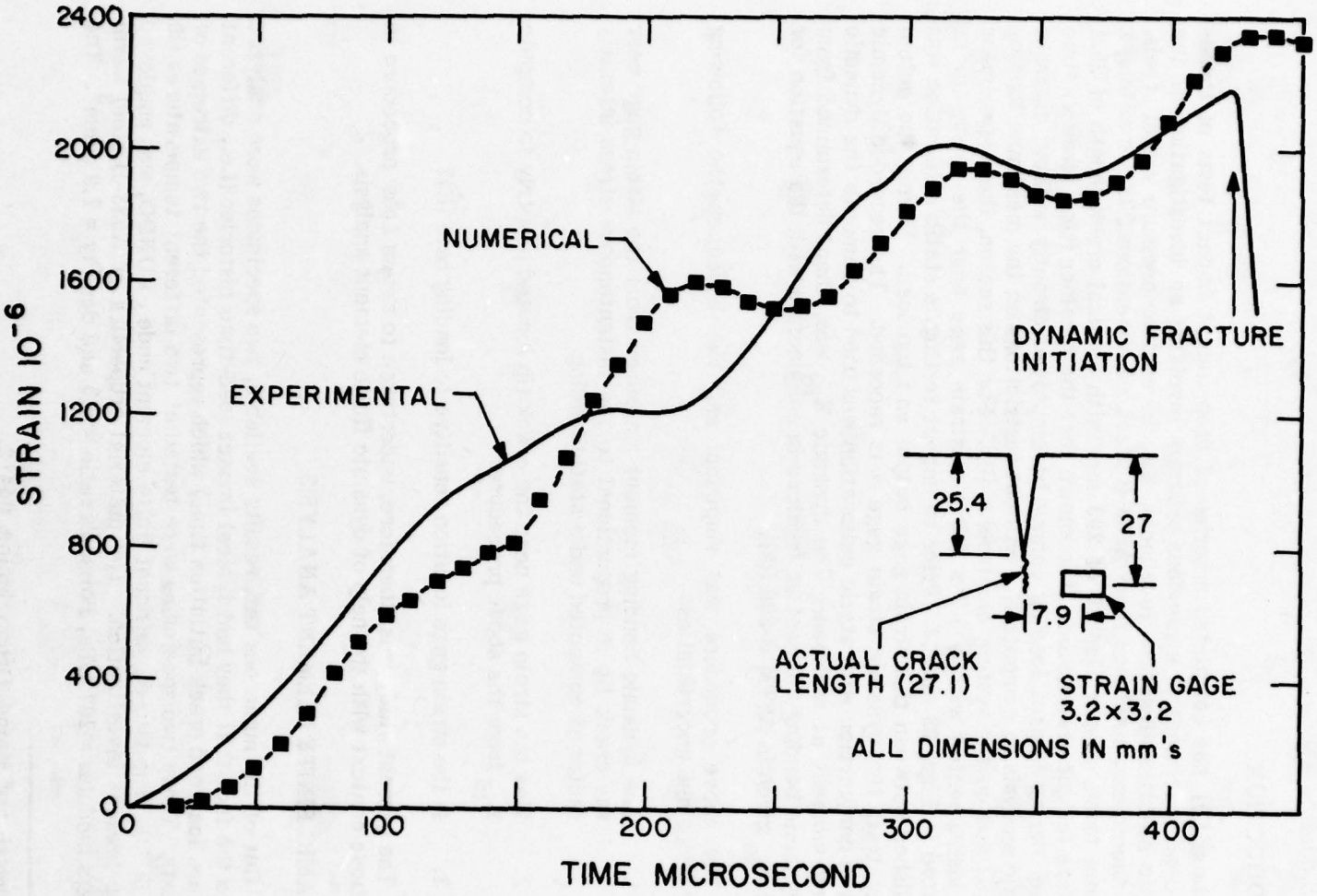

Fig. 23 — Dynamic strain at location 1, A533-B steel bend specimen No. 1.

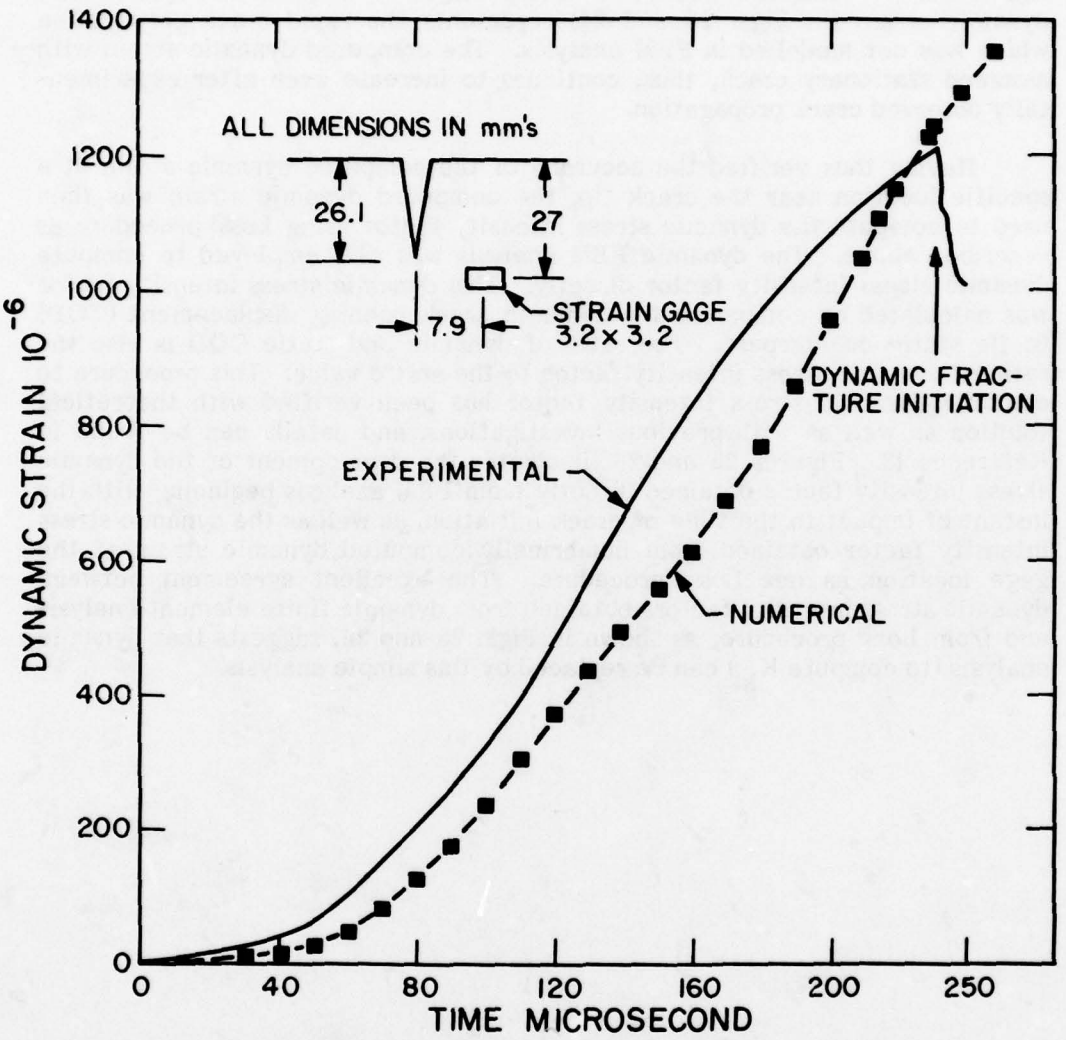

Fig. 24 — Dynamic strain at location 1, A533-B bend specimen No. 2.

dynamic finite element analysis was conducted under a plane strain condition. The experimental impact load-time history, which was obtained from strain gages located on the tup, was used as input in the dynamic finite element analysis. Figures 23 and 24 show reasonable agreement between the experimental and numerically computed dynamic strain at the location shown in figures for two analyzed specimens. The precipitious drop in the experimental dynamic strain (in Figs. 23 and 24) represents the rapid crack propagation which was not modelled in FEM analysis. The computed dynamic strain with assumed stationary crack, thus, continues to increase even after experimentally observed crack propagation.

Having thus verified the accuracy of the computed dynamic strain at a specific location near the crack tip, the computed dynamic strain was then used to compute the dynamic stress intensity factor using Loss' procedure as described above. The dynamic FEM analysis was also employed to compute dynamic stress intensity factor directly. This dynamic stress intensity factor was calculated by comparing the dynamic crack opening displacement (COD) to its static counterpart. The ratio of dynamic and static COD is also the ratio of dynamic stress intensity factor to the static value. This procedure to compute dynamic stress intensity factor has been verified with theoretical solution as well as with previous investigations, and details can be found in Reference 13. Figures 25 and 26 illustrates the development of the dynamic stress intensity factor obtained directly from FEM analysis beginning with the instant of impact to the time of crack initiation, as well as the dynamic stress intensity factor obtained from numerically computed dynamic strain at the gage location as per Loss' procedure. The excellent agreement between dynamic stress intensity factors obtained from dynamic finite element analysis and from Loss' procedure, as shown in Figs. 25 and 26, suggests that dynamic analysis (to compute K_{Id}) can be replaced by this simple analysis.

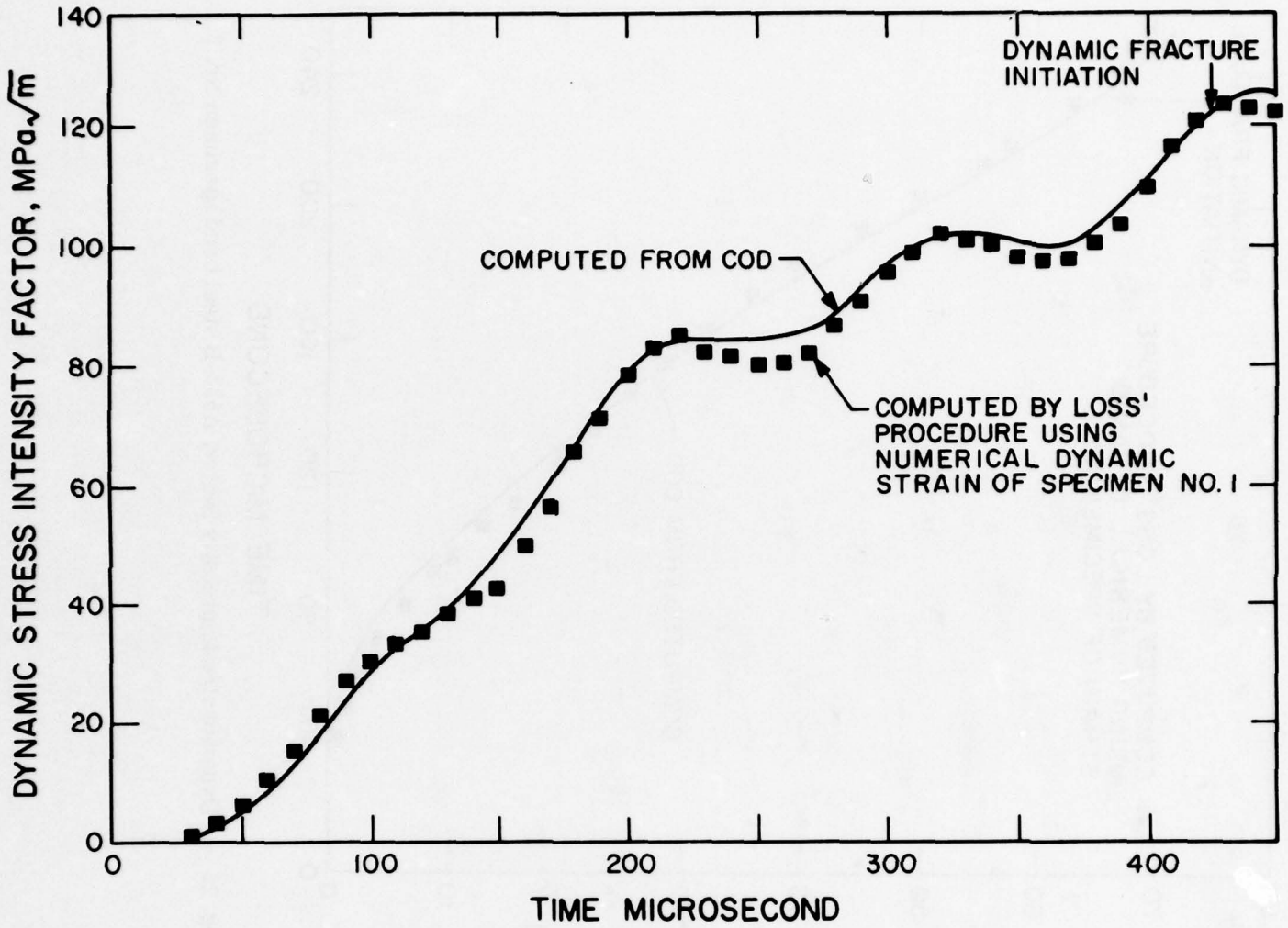

Fig. 25 — Dynamic stress intensity factor, A533-B steel specimen No. 1.

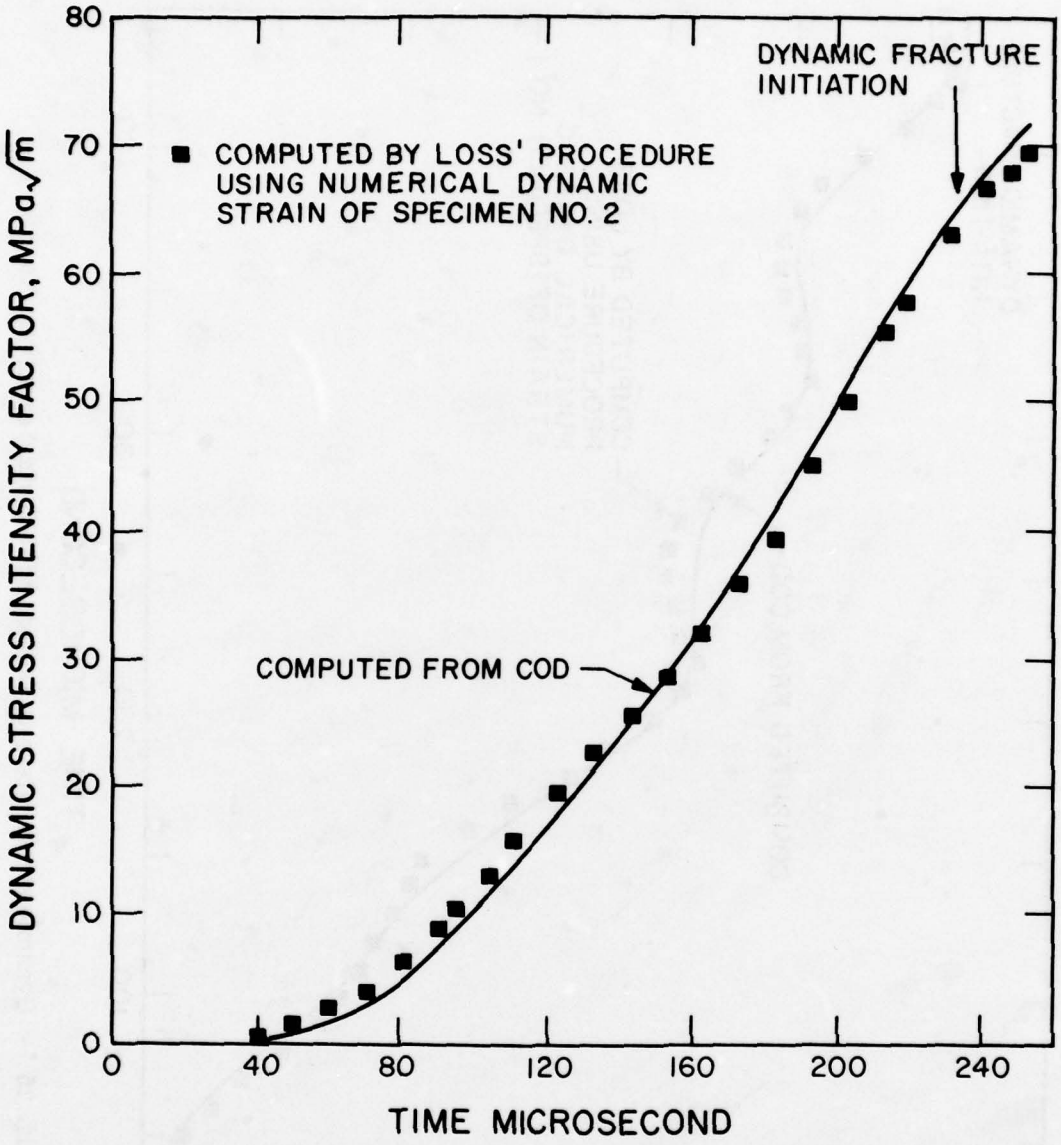

Fig. 26 — Dynamic stress intensity factor, A533-B steel bend specimen No. 2.

II. FATIGUE CRACK PROPAGATION IN LWR MATERIALS

A. Results of Cyclic Crack Growth Rate Studies in Pressure Vessel and Piping Steels

W. H. Cullen, H. E. Watson, V. Provenzano

BACKGROUND

In consideration of the fluctuating water pressures, thermal stresses, and mechanical vibrations which take place in a typical light water reactor, the possibility of fatigue crack growth exists. Thus the determination of fatigue growth rates in pressure vessel and piping materials becomes an especially important component of reactor safety studies. Computations based on these measured growth rates become an indication of the total useful life of pressure vessel and piping components. Calculation of the in-service growth of some defect requires, as input, confident knowledge of the fatigue crack growth rates.

At the present time, the use of fatigue crack growth rates during in-service, reactor inspection is only necessary for application of procedures of ASME Code Section XI Nonmandatory Appendix A. However, there is currently some discussion of the possibility of incorporating a similar procedure in Section III of the ASME Code. In either case, nuclear design and operations engineers should have access to accurate and comprehensive data with which to carry out their computations. The data which are being generated are used then, to both sustain and improve the Code, as well as to prepare for its extension into new areas of application.

Especially, programs directed at evaluation of fatigue crack growth rates for use in light water reactor lifetime computations must address the following relevant areas:

a. Materials. Plates, forgings and welds of reactor pressure vessel materials, hot and cold leg piping materials and welds, and safe-end materials are all susceptible to fatigue failures. The effect of heat input during welding, and continued operation at 288°C (550°F), as well as thermal changes during annealing cycles must be acknowledged, and irradiation effects on reactor beltline materials must be accounted for.

b. Stresses. The loads, and the rates and waveforms associated with the application of those loads, should approximate or easily extrapolate to those of an operating power reactor. While in reality this is obviously a variable amplitude load sequence, the understanding of crack growth mechanisms is more easily attained through data from constant amplitude load (ΔP), or constant stress intensity factor (ΔK) types of tests. Once this understanding is attained, variable amplitude and random sequence loading tests can be carried out.

c. Environment. The tests must be carried out in high-temperature, pressurized reactor-grade water which simulates the operating reactor

conditions. The water is either deoxygenated, to simulate pressurized water reactor (PWR) conditions, or a low, but constant concentration of oxygen (~200 ppb) is maintained to simulate boiling water reactor (BWR) conditions. In addition, a neutron moderator, boric acid, together with a small amount of lithium hydroxide, is added to the PWR coolant. Electrochemical corrosion effects, which result from having different metallic species immersed in an electrolyte, are also a potential problem, although the intrinsically low conductivity of reactor grade water serves to minimize these concerns.

On a laboratory scale, these tests are carried out in autoclaves, really small pressure vessels, which are implemented so as to pressurize and heat the reactor-grade water. The NRL specimens are either compact tension (CT) or wedge-open-loaded (WOL) types. Each specimen is instrumented with a displacement gage for measuring crack mouth opening and gripped in clevises mounted on load rods which pass through water-cooled sliding seals to the load cells and actuators which are external to the autoclaves. The current crack length (a) in each specimen is inferred by measuring the crack mouth opening (δ) as a function of increasing load (P), and relating this ratio (often called the compliance) to an experimentally pre-determined relationship between δ/P and crack length. Our tests are run under load control, and with these types of specimens (CT, WOL), the ΔK values increase slowly with crack length. Details of this equipment and these procedures can be found in Reference 14.

The NRL autoclave facility features six test stands - five autoclaves for use at 288°C (550°F), and up to ~15 MPa (~2250 psi), and one (the "waterpot") for tests at 93°C (200°F) and near ambient pressure. All are completely equipped with on-line water chemistry monitors for dissolved oxygen content, pH and specific conductance. Three of the autoclaves are for multiple specimen testing, and will hold up to four 25 or 50 mm (1T or 2T) specimens, or two 100 mm (4T) specimens. Thus, at full numeric capacity, up to fifteen specimens may be under test at one time. One of the single specimen autoclaves is located in a "hot" cell and is currently being remodeled for a test of an irradiated 1T specimen. A second single specimen autoclave is slated for relocation into a hot cell in 1980, but is currently used for testing of unirradiated specimens. Currently, all NRL autoclaves and the waterpot operate with the PWR chemistry, including dissolved oxygen contents of less than 3 ppb at all times.

All six test stands are wired for fully automated computerized data acquisition. A Hewlett-Packard System 45 controller, together with two Measurement Processors, assumes all of the data acquisition responsibilities for this facility. Crack mouth opening and load readings are converted to slopes, related to the crack length and stored on floppy disk files for each particular specimen. All associated simultaneous readings of water chemistry, from the above-mentioned monitors, are also stored on the same file. At any convenient time, the data may be differentiated, or otherwise processed, and plotted in a variety of ways: da/dN vs ΔK, da/dN vs a, a vs N, as examples. More details of the data acquisition architecture and software can be found in Reference 15.

PROGRAM OVERVIEW

The multi-faceted NRL approach to this problem centers on the requirement for the establishment of a broad and accurate data base on which to verify, revise or extend the existing ASME Code. For this reason, test matrices have been established with the goal of providing a large volume of fatigue crack growth data on both pressure vessel and piping steels. In addition to this experimental effort, concurrent research on the fractographic and mechanistic aspects of fatigue crack growth is also on-going. Substantial progress in all three of the areas - fatigue data generation, fractography and micromechanism development - has been achieved during this fiscal year.

Between Westinghouse Nuclear Energy Systems Division and NRL, cooperative efforts, in the form of coordinated research, and exchange of results and program planning information, have been underway for several years. This cooperation was formed to mutually resolve the effects of loading waveform (rise time/hold time), cycling rate, temperature, and reactor-grade water on the cyclic crack growth rate in a forging material. During this time, the Westinghouse cyclic crack growth program was managed and funded by the Oak Ridge National Laboratory (ORNL) as part of the Heavy Section Steel Technology (HSST) program. The agreement between Westinghouse and ORNL has been in existence since 1 June 1969. In 1977 NRL took delivery of a multi-specimen autoclave fatigue test system containing three test chambers and capable of testing up to twelve 50 mm thick specimens at one time. This increased the simultaneous specimen test capacity to fifteen and gave NRL the capability to assume a lead role in the NRC cyclic crack growth program. As a result, NRC has directed NRL to assume project management of the part of the Westinghouse cyclic crack growth program that is funded by the NRC.

As a result of the unification of the NRL and Westinghouse efforts, an integrated fatigue crack growth research program is planned by NRL for 1980. The main thrust of this program will be the resolution of the effects of the materials and waveform variables detailed by the main matrix test scheme described in a later section. A purchase order has been prepared and approved by Westinghouse research personnel which calls for the procurement of services to assist NRL with the main matrix test program. The contract will run for one year beginning 1 October 1979 and may be extended. The contract requires Westinghouse to operate three single specimen test devices on a continuous basis. As an initial assignment, Westinghouse has accepted the task of FCGR studies on Mn-Mo welds deposited with Linde 124 flux.

Because the concern for adequate knowledge and understanding of fatigue crack growth rate (FCGR) phenomena is international in scope, and because the many aspects of the problems are too numerous for any one laboratory to address, various other cooperative research programs, both formal and informal, have been established. Primary among these is the International Cyclic Crack Growth Rate (ICCGR) cooperative, an association of about twenty-five laboratories and sponsoring organizations from about twelve countries, all of which are involved or interested in determination of FGCR in high-temperature, pressurized water. Besides serving as a forum for the exchange of the most recent results of the member laboratories, the co-op group has devised

numerical and experimental round robin tests and is attempting to foster small inter- and intra-laboratory programs addressing select topics, such as on the effects of dissolved oxygen levels on FCGR, electrochemical effects, and fractographic interpretation exercises. NRL is an active member of the coop, taking part in the round robin experiments, to be discussed in a later section, and in several informal programs with other laboratories.

Over the past two years, four scientists from foreign laboratories (two from West Germany, one each from Finland and Italy) have assumed extended residencies in the NRL group, both to observe the NRL FCGR operation, and to share with us their own expertise and experience in this area. The NRL research effort has been measurably enriched through this program. On a smaller scale, some interlaboratory programs have been directed at specific topics of concern. One, a fractographic study of ambient condition FCGR specimens of A302 steel, with personnel from Centro Informazione Studi Esperienze (CISE) of Italy has been published [16]. A second study, with the Technical Research Centre of Finland (VTT) will evaluate electrochemical transients during the ramp and hold time components of trapezoidal waveforms and is scheduled to begin in FY-1980.

Lastly, besides NRL and Westinghouse, several other laboratories in the United States are engaged in high-temperature, pressurized water fatigue crack growth research on pressure vessel and piping materials. The Electric Power Research Institute (EPRI) sponsors fatigue crack growth and/or stress corrosion research at Babcock and Wilcox (B&W), Alliance, Ohio, and at General Electric Corporation, San Jose, California. EPRI-sponsored research on FCGR in irradiated specimens, a subtask of the B&W program, will begin at Westinghouse in 1981. NRL maintains a close awareness of the progress and developments of these programs, and both NRL and these other laboratories benefit from the exchange of data, results and test method information.

From late 1976 to December 1978, the NRL fatigue program was carried out in accordance with the "preliminary" matrix - a test schedule drafted by NRC, Westinghouse and NRL personnel with the general aim of delineating dependence of the fatigue crack growth rates of a single material (A508 steel) on temperature and waveforms. The test responsibilities for this program were divided between NRL and Westinghouse, and specifically involved tests of a variety of ramp and hold time combinations at two different temperatures (93 and 288^{o}C, or 200 and 550^{o}F). Both NRL and Westinghouse have published their findings through a series of quarterly and interim reports. Reference 14 gives the NRL conclusions as well as a listing of the Westinghouse references and overall findings.

Having terminated the preliminary matrix test series, a main matrix for pressure vessel steels, and a piping matrix addressing piping materials were drafted. These test matrices will be carried out using two different waveforms, and the autoclave test temperature of 288^{o}C. Work on selected items from this main matrix set, shown in Tables 3 and 4, began in early 1979 and results to date are described in a later section.

Table 3 - Main Test Matrix (Unirradiated Materials)

	R = 0.2		R = 0.5		R = 0.7	
	1 cpm Sinewave	1 min Ramp	1 cpm Sinewave	1 min Ramp	1 cpm Sinewave	1 min Ramp
A508	4C+S	2C+U	D	D	1C+S	S+U
Linde 80	2S	2S	D	D	2S	2S
Linde 80 - HAZ	2S	2S	D	D	2S	2S
Linde 0091	2S	S+U	D	D	2S	S+U
Linde 0091 - HAZ	S	2S	D	D	2S	2S
Linde 124	S+U	2S	D	D	2S	2S
Linde 124 - HAZ	D	S	D	D	S	S
A533-B	2S	S+U	D	D	2S	S+U

Entries reflect combined Westinghouse and NRL effort.

S - Test scheduled
C - Test completed
D - Test deferred
U - Test underway

Table 4 - Main Test Matrix (Irradiated Materials)

	R = 0.2		R = 0.5		R = 0.7	
	1 cpm Sinewave	1 min Ramp	1 cpm Sinewave	1 min Ramp	1 cpm Sinewave	1 min Ramp
A508	S	S	D	D	S	S
Linde 80	2T	2T	D	D	2T	2T
Linde 80 - HAZ						
Linde 0091	2S	S	D	D	S+T	S+T
Linde 0091 - HAZ						
Linde 124	2S					
Linde 124 - HAZ	S					
A533-B	2S	S	D	D		2T

Entries reflect combined Westinghouse and NRL effort

- Blank - No test or irradiation scheduled at present
- S - Test scheduled
- T - Test tentative, pending other test results
- D - Test deferred

In addition to the data generation, which is the primary objective of the main matrix, several research tasks are coordinated with or conducted in addition to these items of Tables 3 and 4. The results help to substantiate the observed behavior and the specimens provide additional material for fractographic examinations and surface analysis of the oxide formed during the tests. Fatigue crack growth rate tests are also being conducted at other temperatures (specifically 93°C [200°F]) and a variable amplitude, randomly sequenced loading test was initiated at NRL in September 1979. Other tests are aimed at refinements of the hydrogen-assisted model, or address the influence of starting ΔK, or other mechanical or environmental phenomena.

While the main matrix addresses the subject of reactor pressure vessel materials, a separate test matrix is directed toward identical testing of piping materials. Table 5 lists the materials which are currently included in the scope of the piping matrix, and it is expected that there may be some further additions to this list. The tests will be conducted using the same waveform and load ratio combinations as the main matrix, until evidence to suggest improved alternatives becomes available.

RESULTS TO DATE

Results of Preliminary Test Matrix

The results of tests selected from the preliminary matrix plan, together with supporting tests, are shown in Figs. 27 through 30. Figures 27 through 29 are paired according to certain characteristics of the waveforms and the lower temperature (93°C) results are on the left and the higher temperature (288°C) results are on the right. There are three factors which strongly influence the crack growth rates in A508-2 in the reactor grade water environment; these were the prime variables of the preliminary matrix scheme: rise time, hold time and temperature. An interrelationship among the three determines the particular crack growth rate; it is impossible to isolate one variable without fixing the other two.

An evaluation of all of the data sets produced under the guidelines of the preliminary matrix, together with other tests run under similar environmental conditions but utilizing non-matrix waveforms, indicates that each data set falls into one of two rather clearly defined categories. One band of data lies close to, or essentially on, the ASME Section XI Code air environment default line. This class of data, exhibiting the lower of the two crack growth rates, will be called "low." The other band of data, which resides a factor of three to five above the first, will be termed "high." This latter band of data resides approximately midway between the Section XI air and water environment default lines.

Figure 27, showing data from tests with a fast (1 sec) ramp time, and Fig. 28, showing data from tests with a longer ($\geq$1 min) ramp time, indicate that combinations of long ramp times and low temperature (93°C) result in growth rates belonging in the high category. Regarding the high temperature (288°C), it is impossible to determine, from Figs. 27 and 28, whether the longer ramp or

Table 5 - Materials Included in the Piping Test Matrix

Materials	Approximate Number of Specimens Available
A106	26
A516	36
A515	6
A351 (stainless)	12
Welds:	
A351-to-A351	6
A351-to-A515	6
A515-to-A106	6
A516-to-A351	6

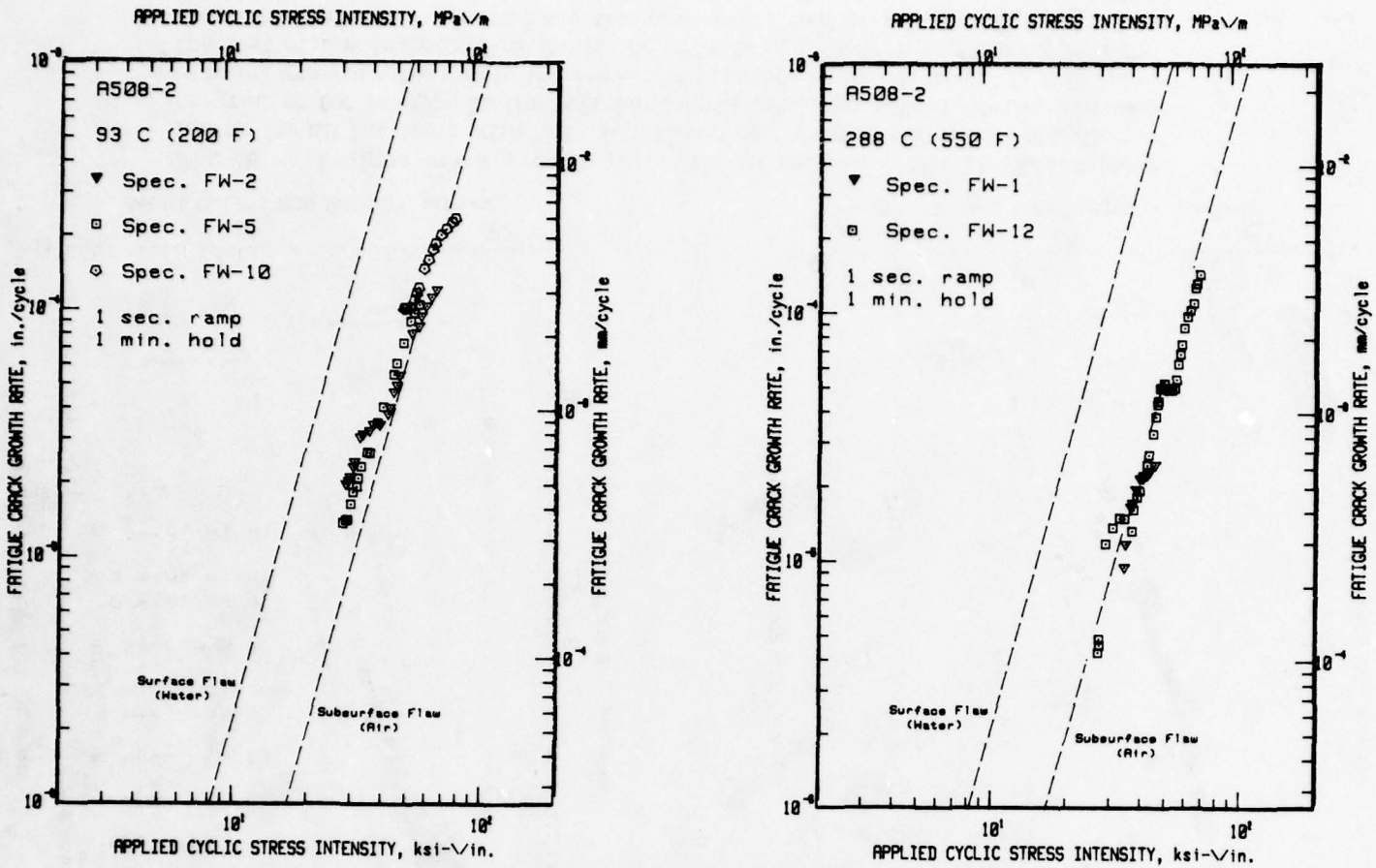

Fig. 27 — Fatigue crack growth rate data vs applied cyclic stress intensity factor for all the tests with a very short (1 sec) rise time. In this and the two following figures, the lower temperature test results are on the left. Both these temperatures yield growth rates close to the ASME Section XI air default line. It is believed that this ramp time is too fast to allow significant hydrogen admission and the crack growth rate is thus unassisted by any hydrogen mechanism.

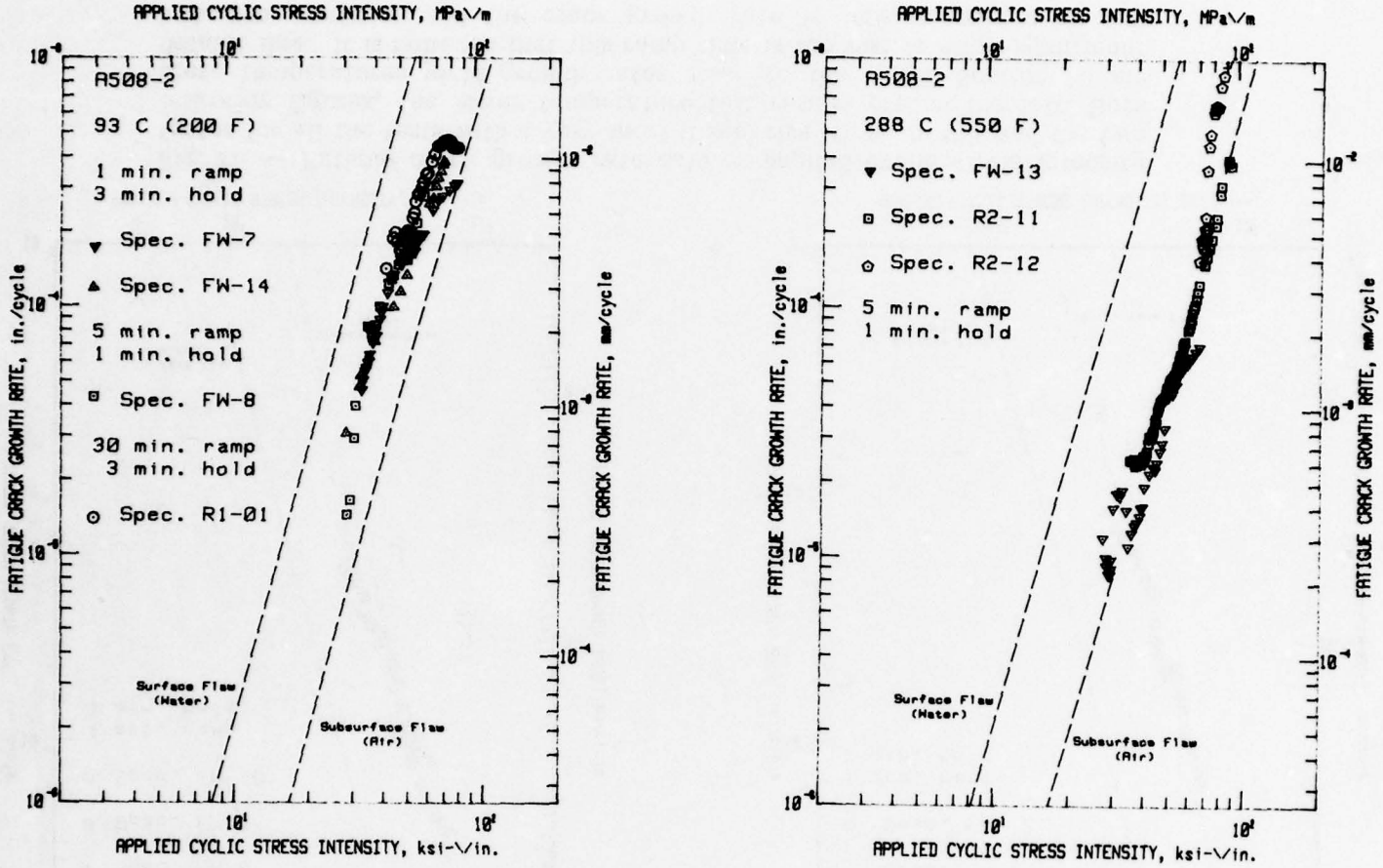

Fig. 28 — Fatigue crack growth rate data vs applied cyclic stress intensity factor for all the tests with both significant ramp times and hold times (1 min or greater for each). In the left hand data sets, the effect of the increase in crack growth rates due to the lower temperature is clearly seen. In this case, the test at low temperature shows the effects of hydrogen assistance, and the resultant fracture surfaces bear the characteristics of this mechanism. The higher temperature tests do not exhibit high growth rates, possibly because the formation of an oxide layer prevented significant hydrogen entry.

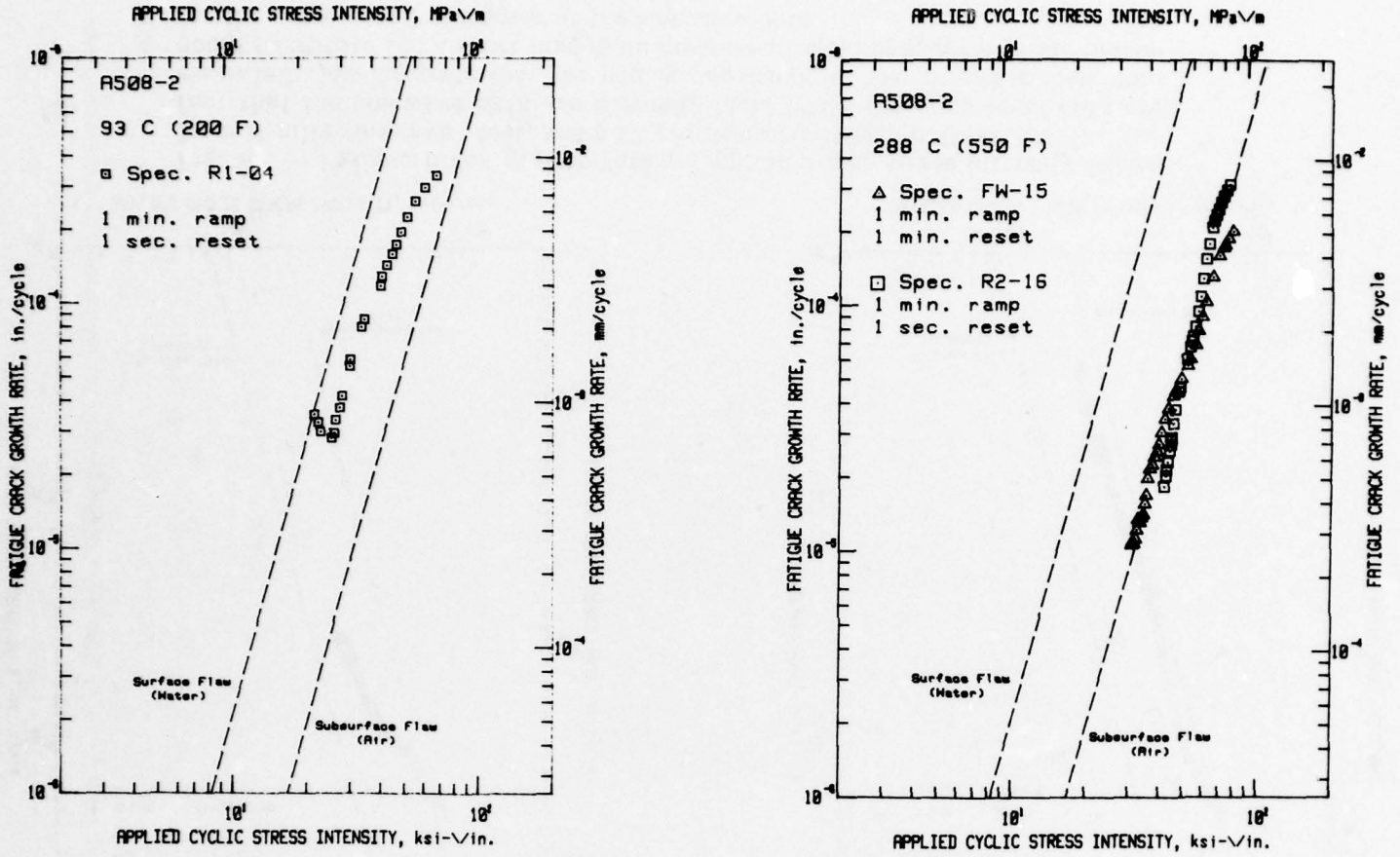

Fig. 29 — Fatigue crack growth rate data vs applied cyclic stress intensity factor for tests with a one min ramp, but no hold time. The fact that the low temperature test exhibits a high growth rate, and the high temperature test does not, is an indication of either the difference in the permeability of the oxide layer, or of the temperature dependence of the mobility of interstitial hydrogen.

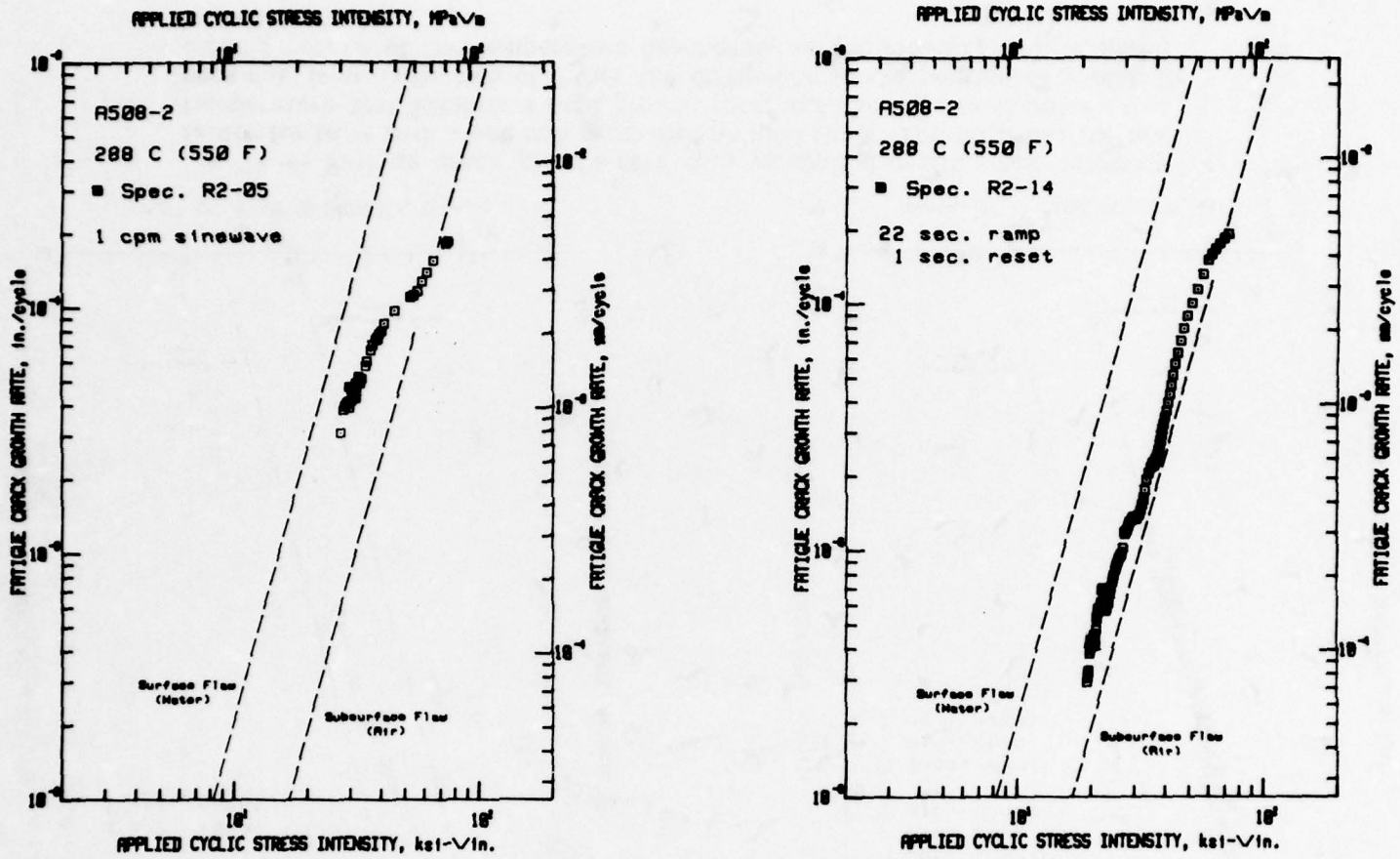

Fig. 30 — Fatigue crack growth rate vs applied cyclic stress intensity factor for a 17 mHz sinewave test, and a 22 sec ramp/reset test both at 288°C. The fact that the sinewave data are basically high, while the ramp reset data are essentially low suggests that the nearly zero slope at the sinewave maximum could substitute for a short hold-time component and might provide the reason for the accelerated character of the sinewave data.

the hold time are solely responsible for the low crack growth rate results. Figure 29 shows the results of tests involving 1 min ramp times, and no hold times, and the results for high temperature are again in the low category. Thus, it is clear that a hold time is not required to produce low growth rate data at the high temperature. This represents a modification of the conclusions given in Reference 14 and is the result of additional tests completed since release of that publication. On the other hand, at the lower temperature, a ramp time component is sufficient to produce a high growth rate, and comparison with Fig. 28 shows that a hold time component does not additionally aggravate the growth rates.

Lastly, Fig. 30 shows the results of a 17 mHz (1 cpm) sinewave test at 288°C and a 22 sec ramp/reset test at the same test temperature. This latter test was intended to confirm that ramp times of about 20 to 30 sec were sufficient to produce data in the high category for this temperature. However, the ramp test produced data that is basically in the low category and suggests that the 17 mHz sinewave results ("high") cannot be replicated by a waveform containing a ramp component alone, and that at least a short hold time component is necessary for accelerated crack growth. To seek confirmation of this, a test of a 22 sec ramp/4 sec hold/reset waveform, i.e., the trapezoidal approximation to the positive slope of a sinusoidal waveform, will be scheduled for FY-80.

As shown in Tables 3 and 4, several tests of main matrix items are underway, although none of these tests has run to completion and the FCGR data is not available for presentation in this report. During 1980, more than half of the NRL autoclave capacity, and three single specimen autoclaves at Westinghouse Laboratories, will be disposed to the testing of main matrix items. The balance of the NRL autoclaves will be used for tests of elements of the piping steels matrix and for tests of research topics of special interest, such as complex waveforms, water chemistry studies, and temperature or extra high load ratio effects studies.

Results of Fractographic Examinations

During the past year, there have been several fractographic studies and fractographically-related research efforts which have been carried out in support of the overall NRC-sponsored fatigue crack growth program at the NRL. The results of these studies are individually described in the following sections.

Fatigue of A302-B Steel Specimens. As a baseline study, the fatigue fracture surface of four A302-B steel fatigue crack growth specimens were examined. The results of this study are detailed in Ref. 16. These specimens were fatigued in an ambient temperature air environment at 10 Hz and the resultant data fell close to the ASME air default line. Two specimens were cut from each of the T-L and L-T orientations of the parent plate, and the fractographic observations were dependent on the orientation difference. Of the two specimens within each orientation group, one test was started at a ΔK value of $\sim$16.5 MPa$\sqrt{m}$, the other at $\sim$22 MPa$\sqrt{m}$. The crack growth rates of the two specimens were roughly the same for ΔK values below 33 MPa$\sqrt{m}$. Above this

ΔK value, the crack growth rate of the T-L specimen was higher, by a factor of about two.

SEM examination showed that the fracture surfaces of specimens cut in the T-L orientation were characterized by a microstructural texture running parallel to the macroscopic crack propagation direction (Fig. 31). This texture was not present on the fracture surfaces of the specimens cut in the L-T orientation. The fracture surfaces of these latter two specimens were characterized by the presence of small lamina-shaped holes (Fig. 32). For the T-L specimen tested with the lower starting ΔK, the parallel texture appeared only at crack lengths corresponding to ΔK values of 25 to 30 MPa$\sqrt{m}$, while for the other T-L specimen, the parallel texture was present along the entire crack length. Subsequent x-ray analysis showed that the parallel texture was due to elongated manganese-sulfide inclusions (Fig. 33). The lamina-shaped holes found in the fracture surfaces of the L-T specimens are believed to be inclusion bands in these specimens that are oriented perpendicular to the direction of the macroscopic crack propagation direction. The higher crack growth rates observed in both T-L specimens resulted from the inclusion bands that give rise to the texture that ran parallel to the main crack path. It appears that a preferential decohesion process occurs at the inclusion/matrix interface. This decohesion process became activated above some threshold stress level and resulted in higher crack growth rates in the T-L orientation.

Fractography of Preliminary Matrix Specimens. The fracture surfaces and the transverse sections of selected specimens from the preliminary matrix studies have been examined by optical metallography, scanning electron microscopy, and by energy dispersive x-ray analysis. Optical metallography was employed to examine the interaction between the material microstructure and the crack path. Scanning electron microscopy was employed to characterize the significant fractographic features, and energy dispersive x-ray analysis was used to identify the various microstructural components, such as inclusion particles, which played a role in the fatigue fracture process. The basic aims of the above microscopic examinations were to search for correlations and relationships between the microstructural features and the mechanical properties, and to gain additional insight into the mechanisms of failure of these materials as functions of the variables of these test matrices. Because of the wide range of variables of the preliminary test matrix, leading to the "low" and "high" trends of the fatigue results, the fractography on these specimens proved especially interesting and supportive of a proposed model for hydrogen-assisted fatigue crack growth to be presented later in this section.

The significant trends found in the fractographic examinations were as follows:

1. Specimens tested in air failed by a crack blunting process involving fatigue striation formation. Essentially, these same features characterized the fracture surfaces of specimens that had been tested in reactor grade water and which produced data in the "low" crack growth category. This includes specimens tested with a fast ramp time (= 1 sec) at either 93 or 288°C, and specimens tested with a long ramp time (>= 1 min) at 288°C. Examples of this type of behavior are shown in Fig. 34.

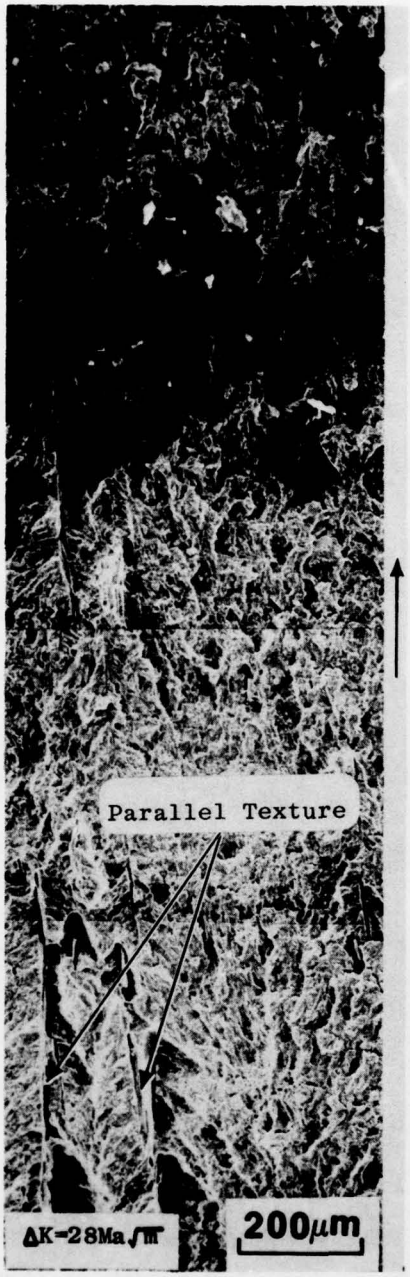

Fig. 31 — Fracture surface of A302-B ferritic steel specimen cut along T-L direction (VAB1), tested in air at room temperature with the lower starting ΔK value. Arrows show direction of macroscopic crack propagation. Series of SEM micrographs show transition region corresponding to 25 to 30 MPa $\sqrt{m}$ ΔK value, where inclusion bands begin to appear in fracture surface.

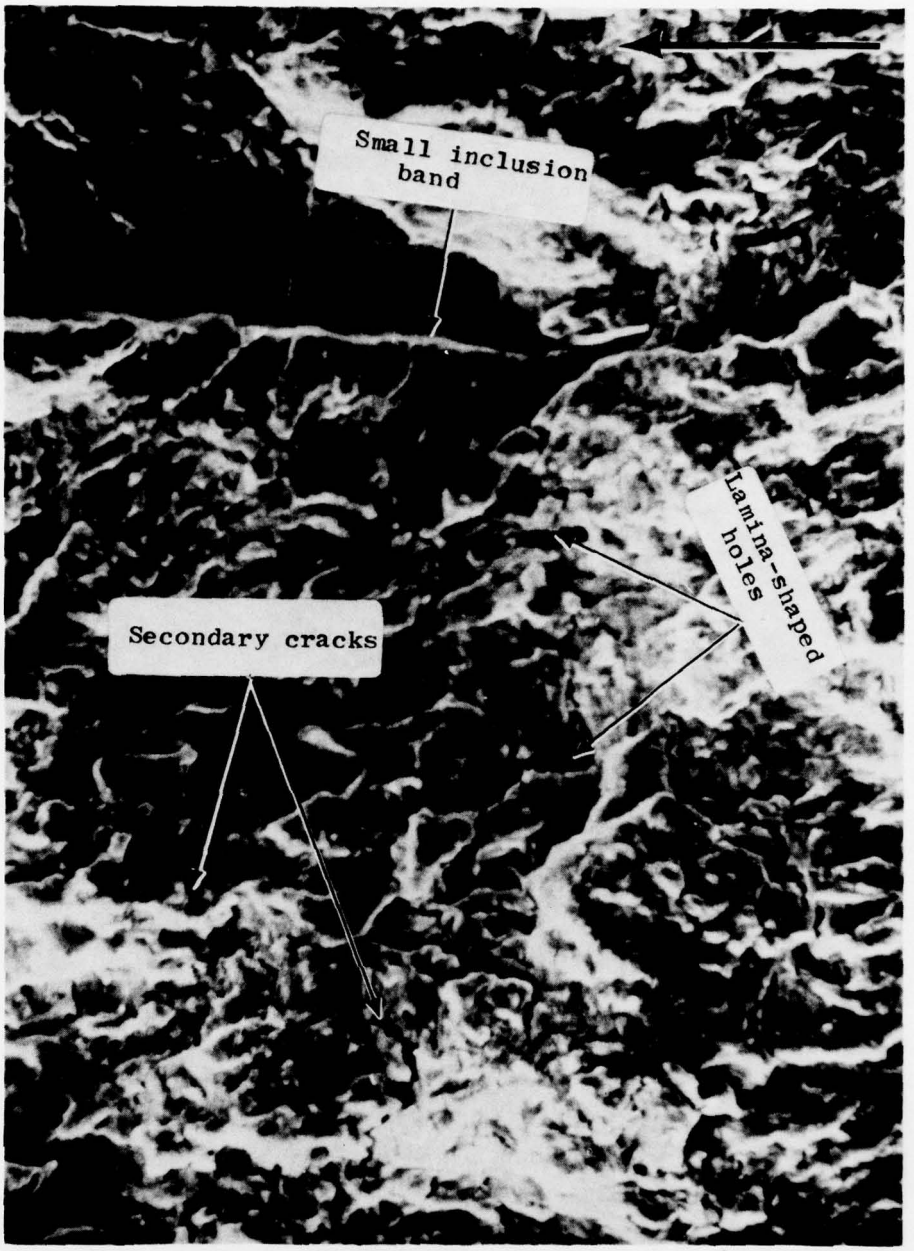

Fig. 32 — Fracture surface of A302-B ferritic steel specimen cut along L-T direction (VADA2) tested in air at room temperature. Arrow shows direction of macroscopic crack propagation. SEM micrograph shows small inclusions and lamina-shaped holes present in the fracture surface. The lamina-shaped holes are believed to represent the inclusion bands that are oriented perpendicular to main crack plane.

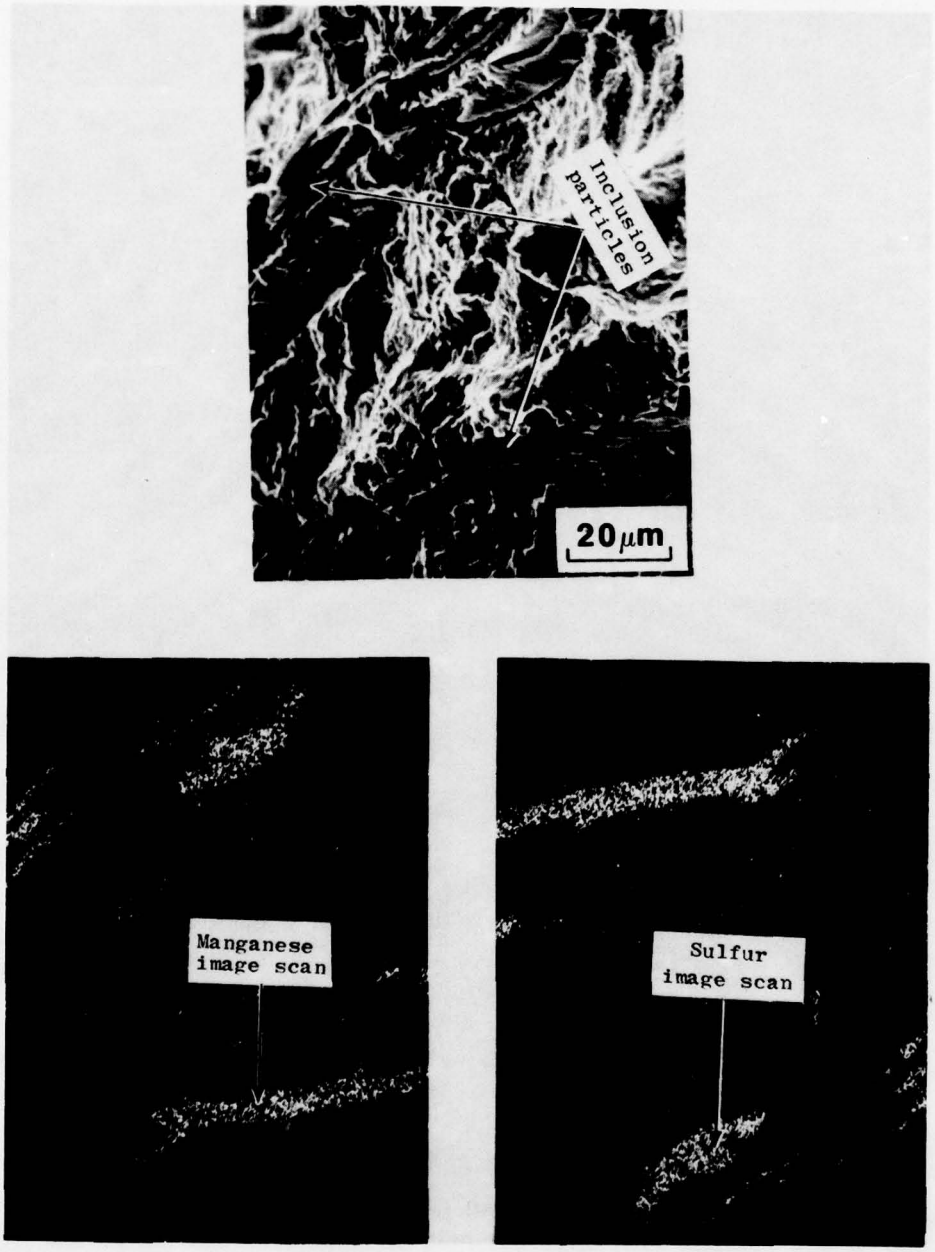

Fig. 33 — Fracture surface and corresponding energy dispersive x-ray point maps of A302-B ferritic steel specimen cut along T-L dirction (VABl) Arrow shows macroscopic crack propagation direction. SEM micrograph on top of the figure (micrograph a) clearly shows inclusion bands in the fracture surface that run parallel to the macroscopic crack propagation direction. Lower two micrographs are image scans obtained through energy dispersive x-ray micro-analysis showing that inclusion bands are manganese (left) and sulfur (right) second-phase particles.

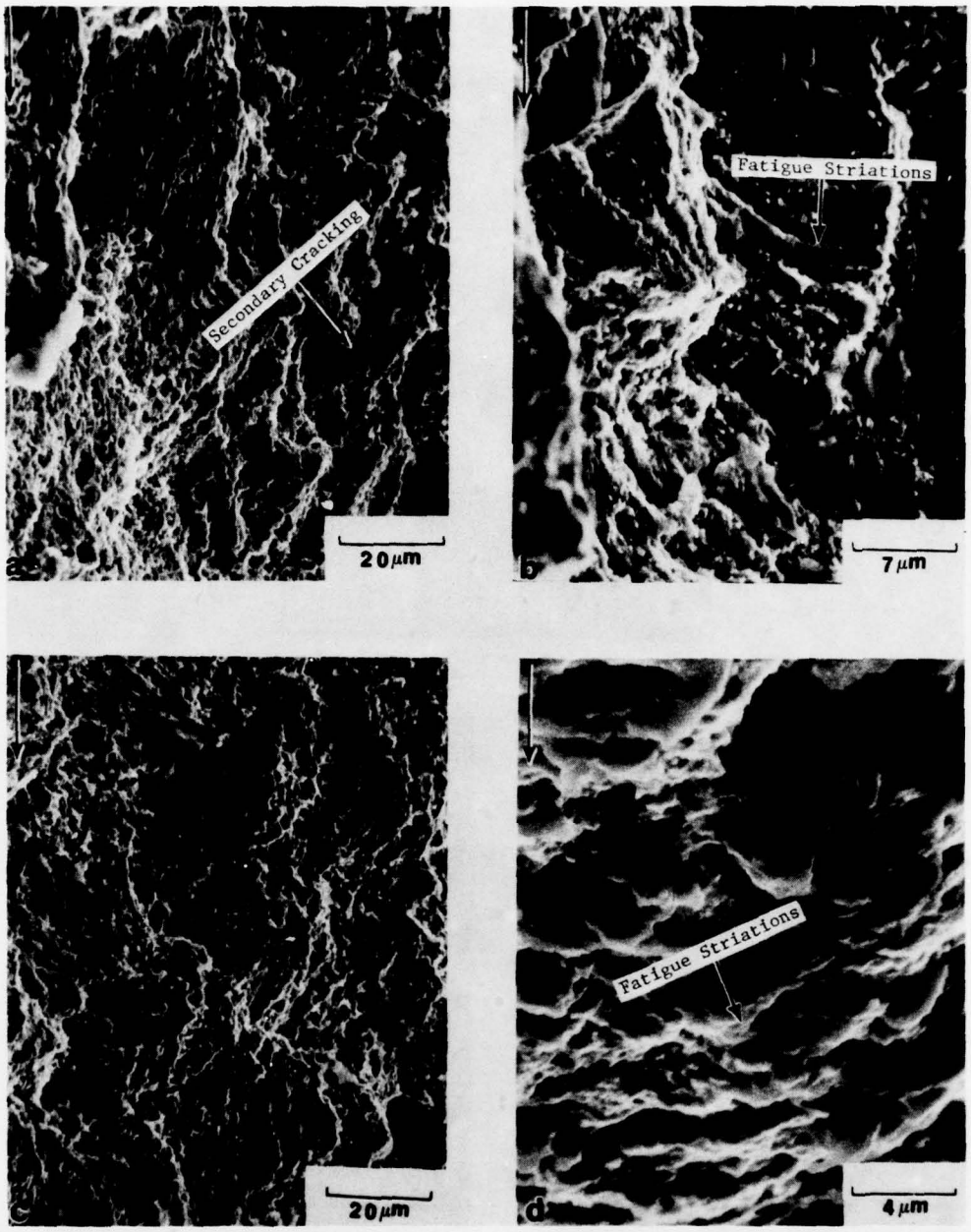

Fig. 34 — Fracture surfaces of A508-2 fatigue specimens tested in the water pot (93°C and 200°F), with different hold time periods but all with a ramp time of 1 sec. The SEM micrographs were taken at crack lengths that correspond to the following ΔK values: (a) 33 MPa$\sqrt{m}$ (30 ksi$\sqrt{in.}$), (b) 72.6 MPa$\sqrt{m}$ (66 ksi$\sqrt{in.}$), (c) 44 MPa$\sqrt{m}$ (40 ksi$\sqrt{in.}$)., and (d) 88 MPa$\sqrt{m}$ (80 ksi$\sqrt{in.}$). Arrows show direction of macroscopic crack propagation. The failure mode for these specimens is transgranular with fatigue striations and secondary cracking, as in the air tests shown in the previous figure.

2. The failure mode of specimens tested at 93°C with ramp times greater than one second, either with or without a hold time, was characterized by either intergranular or cleavage-like facets for the entire ΔK range. No fatigue striations were seen in these specimens. These features are illustrated by the SEM micrographs shown in Fig. 35. Taken together, these fractographic features suggest the possibility of a corrosion fatigue component being active under the above test conditions. This contention is reenforced by the fact that the crack growth rates for this group of tests fall in the "high" category.

3. The fractographic features observed in the sinewave tests in the autoclave were a function of the ΔK level. In the low ΔK regime, the failure mode was transgranular with fatigue striations. At intermediate ΔK levels the features were mostly cleavage-like, while in the high ΔK region the failure mode reverted to transgranular with fatigue striations. The failure modes found in the three regions of the fatigue test are illustrated by the SEM micrographs in Fig. 36. These three regions roughly correspond to three different regions present in the crack growth data of Fig. 30a.

Stress Corrosion Cracking Studies of A508 and A533-B. Subsequent to the identification of an environmentally assisted component of fatigue crack growth in the reactor grade water environment, static load tests were conducted on two pressure vessel steels to determine if stress corrosion cracking could be included at 93°C. The complete results of these tests will be presented at an ASTM Symposium on Fractography in Materials Science and published in the associated STP [17]. One uniform gage tensile specimen was machined from A533-B from the HSST Program (Plate No. 2), and a second specimen was machined from a rejected heat of foreign produced A508 Class 2 equivalent steel. After 2000 hours in the environment, at 75% of yield loading, the A508 forging specimen had developed several cracks along the gage section - the longest was about 10 x 3 mm (length x depth). No cracks were found in the A533-B specimen. Figure 37 shows three views of some of the largest cracks in the A508 specimen. Other smaller cracks in the same specimen are illustrated by the SEM micrograph in Fig. 38. Further research suggested that large amounts of segregation particles and manganese-sulfide inclusions in the A508 provided the most likely sites of stress corrosion initiation. Figure 39 shows a metallographic cross-section containing such a cleaved inclusion, with associated microcracks emanating from the inclusion stringer. Such phases were not present to the same degree in the A533-B.

Metallography of Fatigue Crack Morphology. Metallographic cross sections of fatigue crack traces were examined for specimens from a 93°C test showing "high" category growth rates (R1-01), and from an aborted 288°C test showing a net crack growth rate in the low category (R1-02). As shown in Fig. 40, the basic difference in the two crack profiles is the extent and type of crack branching (secondary cracking), emanating from the main crack path. The secondary cracks in the R1-01 are rather large and deep; in R1-02 they are smaller but more numrous. In fact, the average number of secondary cracks per unit length in R1-02 is 5 to 6 times larger than in R1-01. Moreover, an oxide

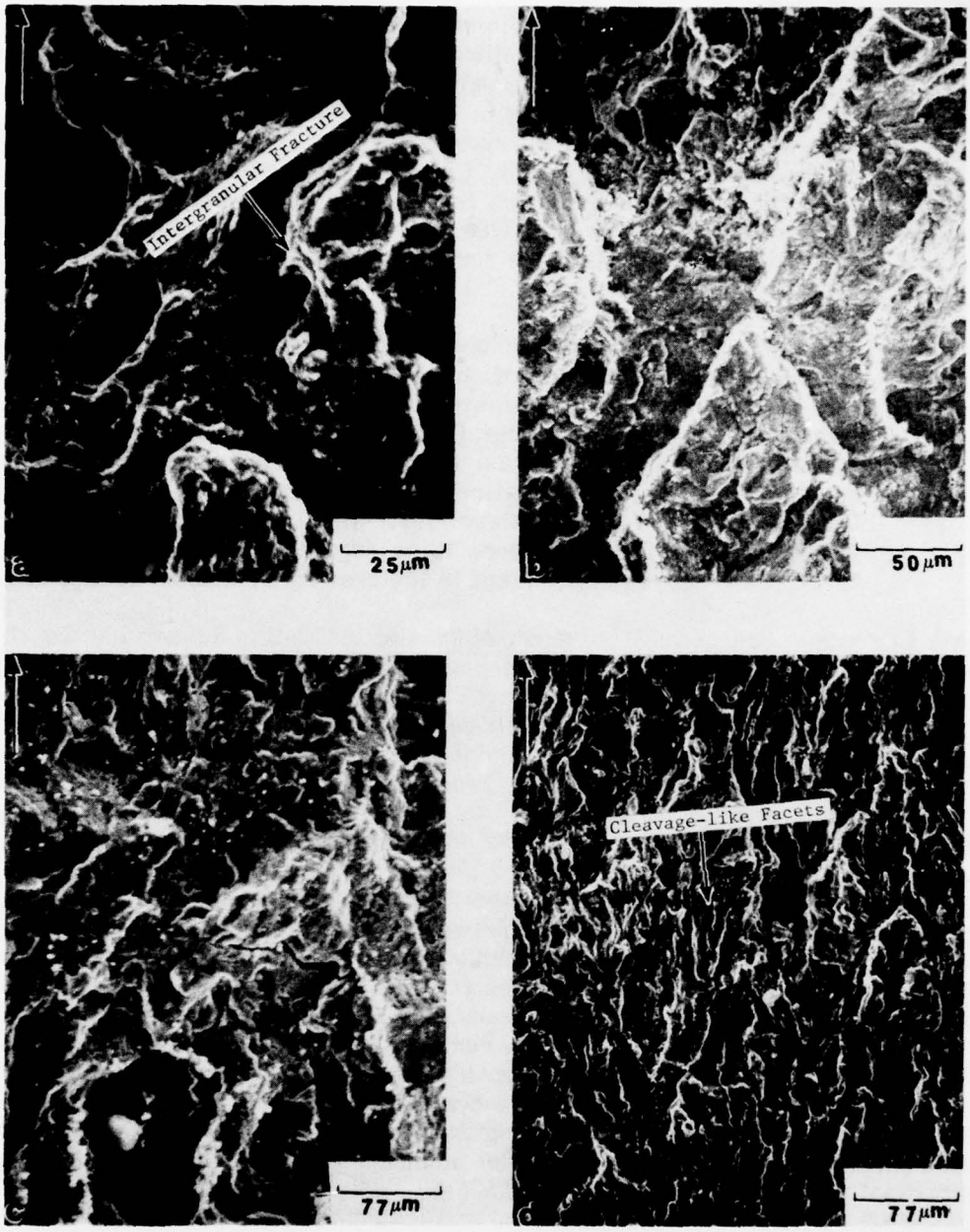

Fig. 35 — Fracture surfaces of A508-8 fatigue specimens tested in the water pot (93°C, 200°F) with significant ramp and hold times (1 min or greater for each). (a) and (b) specimen FW-8, (c) and (d) specimen FW-7. The SEM micrographs were taken at crack lengths that correspond to the following values of ΔK: (a) 38.5 MPa$\sqrt{m}$ (35 ksi$\sqrt{in.}$), (b) 57.2 MPa$\sqrt{m}$ (52 ksi$\sqrt{in.}$), (c) 33 MPa$\sqrt{m}$ (30 ksi$\sqrt{in.}$), and (d) 60.5 MPa$\sqrt{m}$ (55 ksi$\sqrt{in.}$) Arrows show direction of macroscopic crack propagation. As shown by the micrographs, the predominant failure mode is transgranular, but some regions of the fracture surfaces are characterized by transgranular failure and by cleavage-like facets.

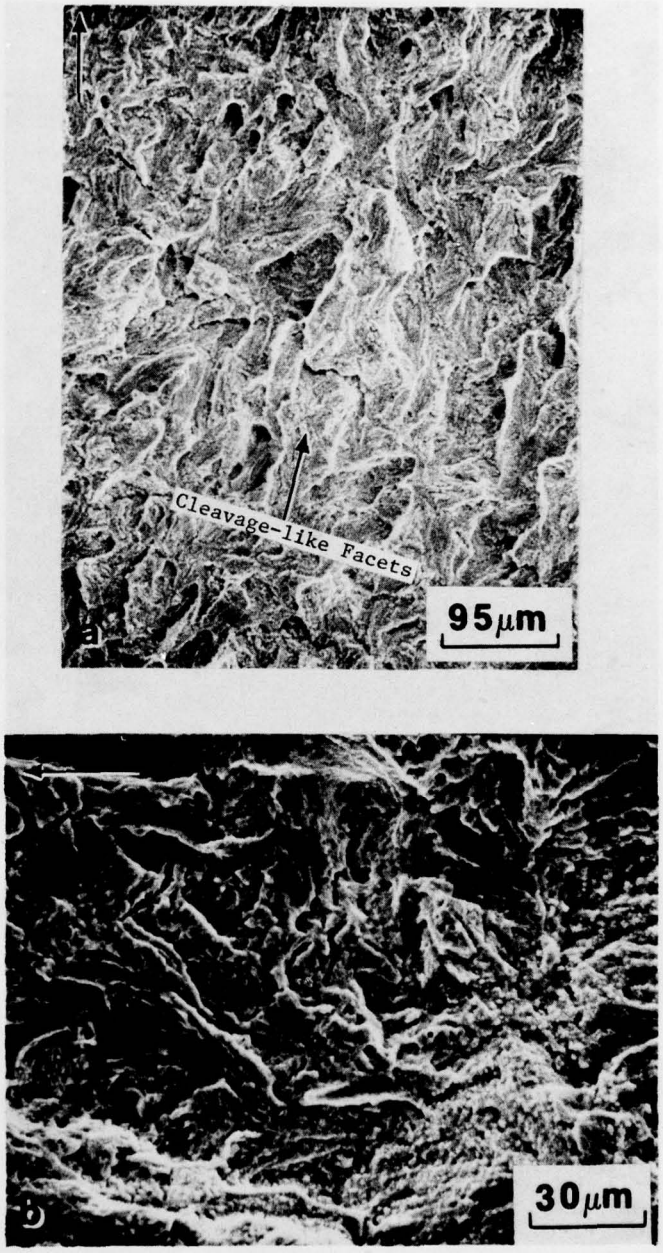

Fig. 36 — Fatigue fracture surfaces of A508-2 specimens tested in reactor grade water at 288°C. The SEM micrographs were taken at crack lengths that correspond to the following values of ΔK: (a) 32 MPa$\sqrt{m}$ (29 ksi$\sqrt{in.}$), and (b) 57.2 MPa$\sqrt{m}$ (52 ksi$\sqrt{in.}$). Arrows show direction of macroscopic crack propagation. In (a), the surface shows the cleavage-like facets produced by the environmentally-assisted crack growth; in (b), the growth rates have decreased and the morphology is transgranular cracking with fatigue striations.

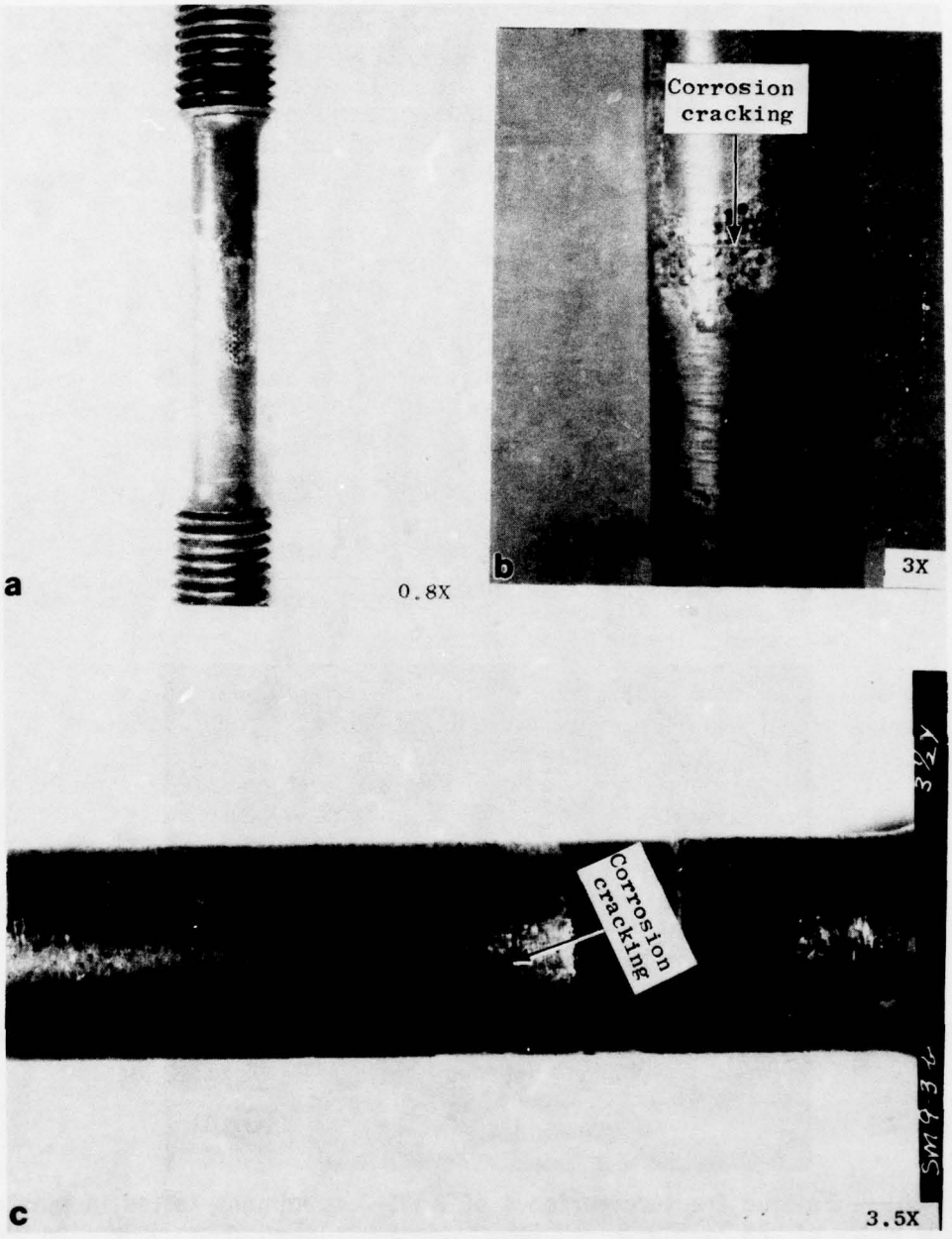

Fig. 37 — Optical photographs of the A508-2 tensile specimen subjected to 75% of yield load in 93°C reactor grade water. The entire specimen is shown in (a), while (b) and (c) show some of the larger cracks that developed during the test.

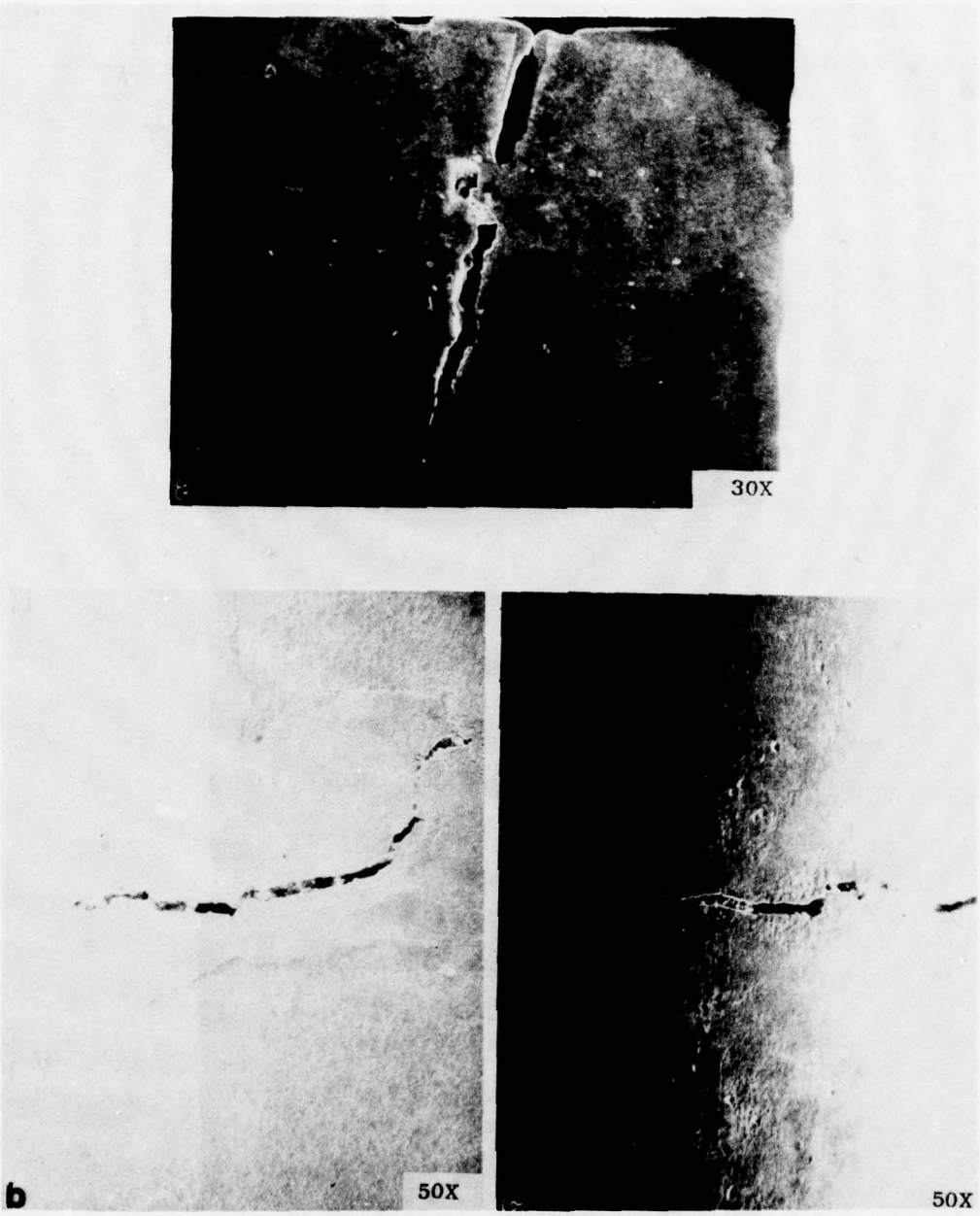

Fig. 38 — SEM micrographs of the specimen of Fig. 37. Fig. 38a is a transverse section showing the depth of the largest of the SCC cracks. Panels (b) and (c) show surface traces of two other cracks in the specimen.

Fig. 39 — Montage of SEM micrographs of the transverse section of A508-2 specimen. The montage shows one of the many microcracks found on this specimen after the SCC test. The microcrack that originated from the outside surface, propagates along the inclusion-matrix interface. A large number of segregation particles is present in the microstructure.

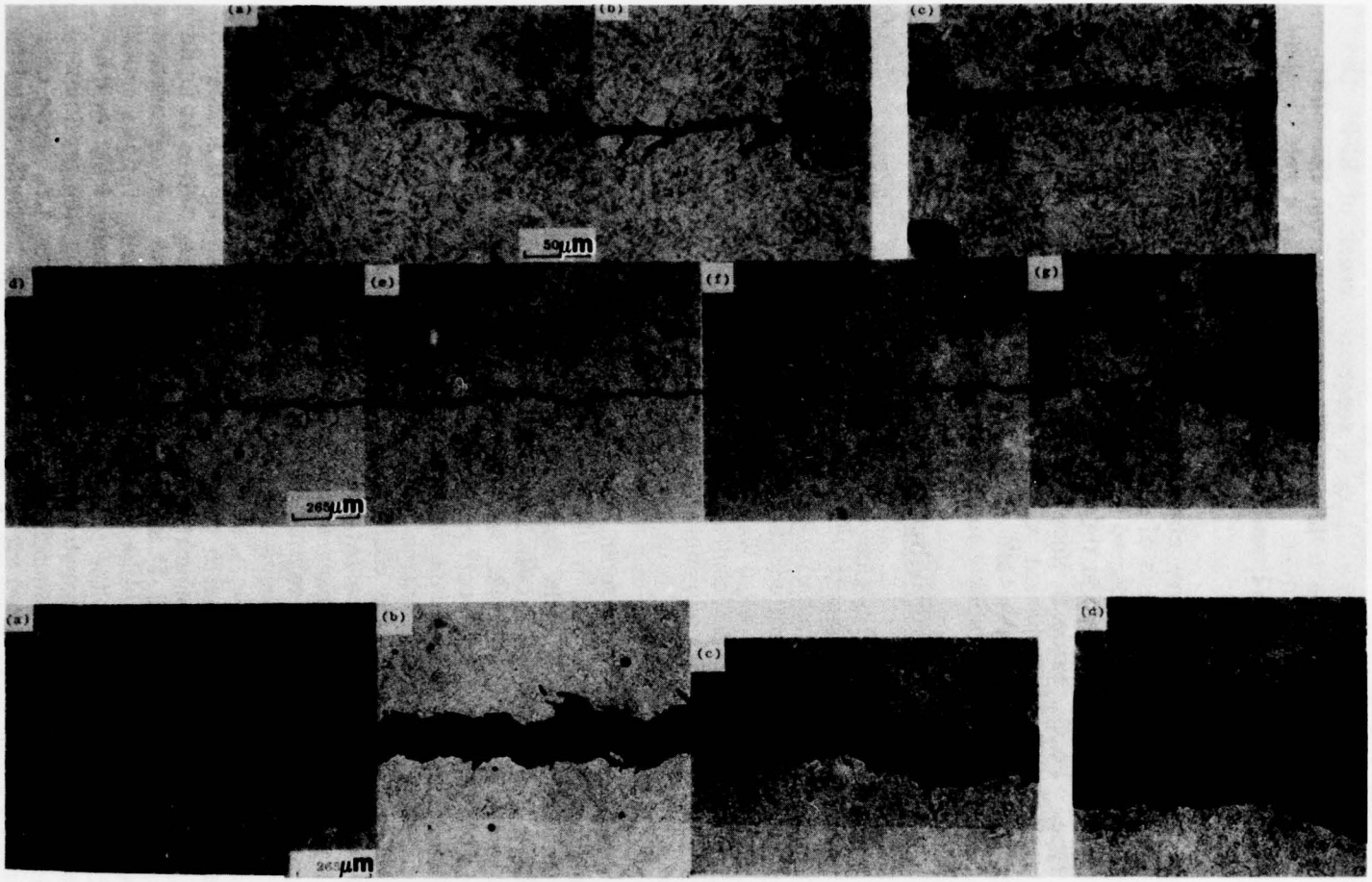

Fig. 40 — Optical micrographs of transverse sections of A508-2 fatigue specimens tested in the autoclave [top micrographs, (a)-(g), R1-2] and in the waterpot [bottom micrographs (a)-(d), R1-2]. The specimen tested in the autoclave shows extensive branching with small microcracks. In the specimen tested in the water pot, the microcracks were larger but they were fewer in number than in the autoclave test. The average density of microcracks per unit length is roughly 5 to 6 times greater in R1-2 than in R1-1.

layer covers the secondary cracks of R1-02; no oxide layer appears to be present in the microcracks of R1-01. The presence or the absence of this oxide layer is better shown by the SEM micrographs of Fig. 41, taken from the cross sections of the above two specimens. At the tip of a secondary crack of R1-01, this figure also shows a non-metallic particle partially separated from the matrix. As above, it is hypothesized that these inclusion particles play a role in the transportation of hydrogen, resulting in embrittlement, cracking, and accelerated growth.

Surface Oxide Studies. Preliminary chemical analysis on the type of oxide which forms on the fracture surfaces of specimens that are tested at both 93 and 288°C showed that the oxide formed in the waterpot specimens is mostly of the Fe_2O_3 type; the oxide formed in the autoclave specimens is of the Fe_3O_4 (magnetite) type. Fe_2O_3 oxide is known to be non-adherent and thus non-protective, while Fe_3O_4 is adherent and somewhat more protective. This suggests that for those autoclave tests in which the adherent oxide could be produced, the specimens might receive some protective advantage.

Results of ICCGR Round Robin Activities at NRL

As part of the NRL contribution to the activities of the ICCGR round robin tasks, we completed and submitted results of the calculational round robin and the first experimental test round robin. For the calculational round robin, the participating laboratories edited, differentiated, and plotted three a vs N data sets as graphs of da/dN vs ΔK. The objective was to determine if variations in individual methods resulted in significant variations in the final product. The results of this round robin will be published, in the future, by the coordinators of this task.

For the experimental round robin, each participating laboratory tested a compact specimen of A533-B steel in 288°C, 7 MPa, distilled, de-ionized, and deoxygenated water with a 17 mHz sinusoidal waveform. The initial starting ΔK was to be 27.5 MPa$\sqrt{m}$ (25 ksi$\sqrt{in.}$) and the load ratio was 0.2. The result of the NRL test is shown in Fig. 42. As expected for a 17 mHz sinewave, the data points fall in the high growth rate category, with the initial and final crack growth rates trending to the low category. As indicated above, examination of the fatigue fracture surfaces indicates morphologies which are commensurate with the high or low growth rate observations at various stages of the test. Figure 43 shows three views of the fatigue surface, (a) and (c) corrsponding to "low" growth rate regimes at the near-initial and near-final ΔK values for the test, while (b) corresponds to the regime of high growth rates for intermediate ΔK values. The arrows on the preceding Fig. 42 correspond to da/dN values for crack lengths corresponding very nearly to the areas at which the three micrographs were taken. The fourth panel (d) of Fig. 43 shows the cleaved surface resulting from post-test separation of the two specimen halves at liquid nitrogen temperature. Panel (d) is shown to establish the correspondence between the size of the cleavage-like features produced during fatigue crack growth, and the pure cleavage of the post-test fracture. These fractographic observations corroborate the observations described above for the preliminary matrix tests, that is, non-environmentally assisted growth rates, i.e., those near the ASME air default line, proceed via ductile mechanisms, involving striation formation and transgranular failure, while the growth with environmental

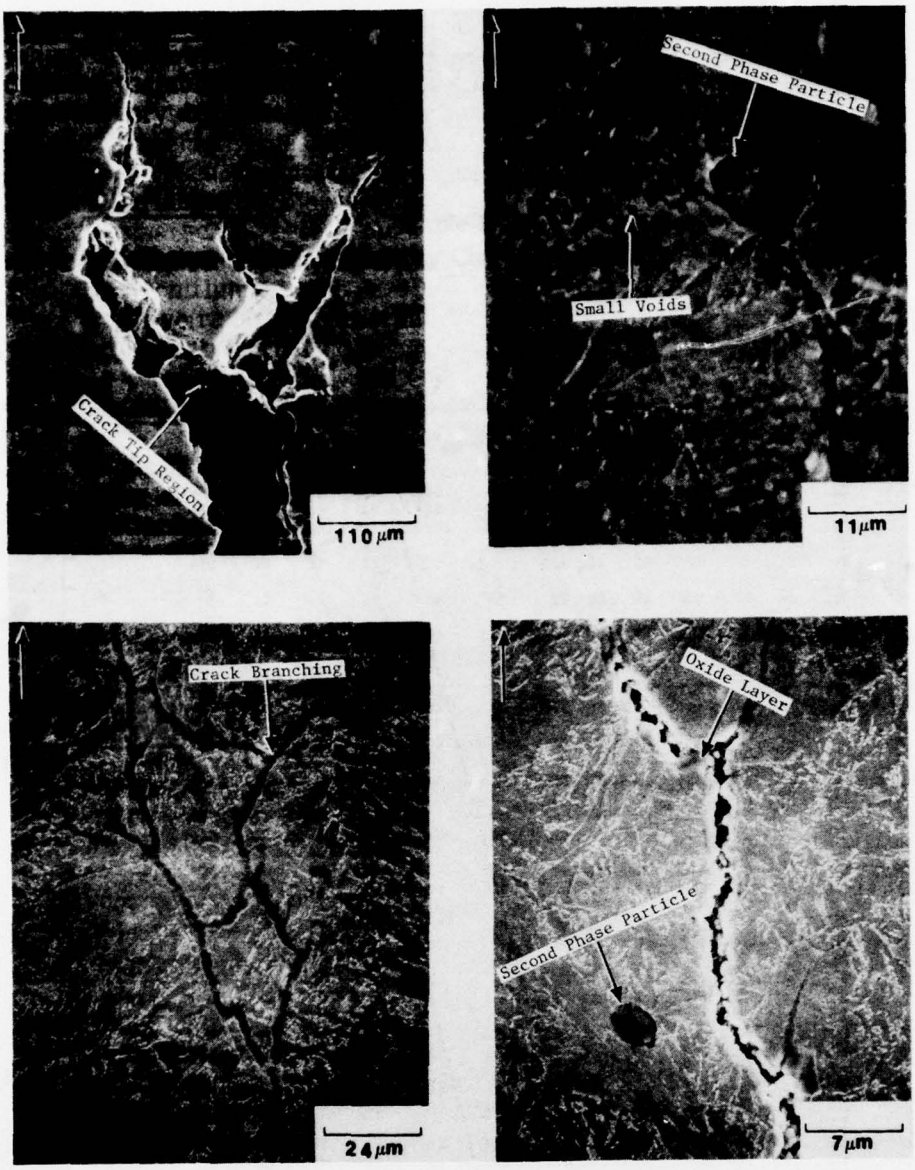

Fig. 41 – SEM micrographs of transverse sections of A508-2 fatigue specimens; one tested in the water pot (top micrographs, R1-1) and the other tested in the autoclave (bottom micrographs, R1-2). The arrow on top left corner of each micrograph indicates direction of macroscopic crack propagation. Previous to SEM examination, the sections were polished and then etched in 1% nitol solution. Micrograph (a) shows extensive crack branching; it is believed that the specimen has already yielded. The adjacent micrograph (b) is a higher magnification micrograph of a microcrack at the crack tip region. The tip of this microcrack shows a partially separated second phase particle surrounded by small voids. The bottom micrographs show crack branching and a second phase particle. The particle is not surrounded by small voids as in R1-1, while the crack path is covered by a protective oxide layer. No oxide layer was visible in specimen R1-1.

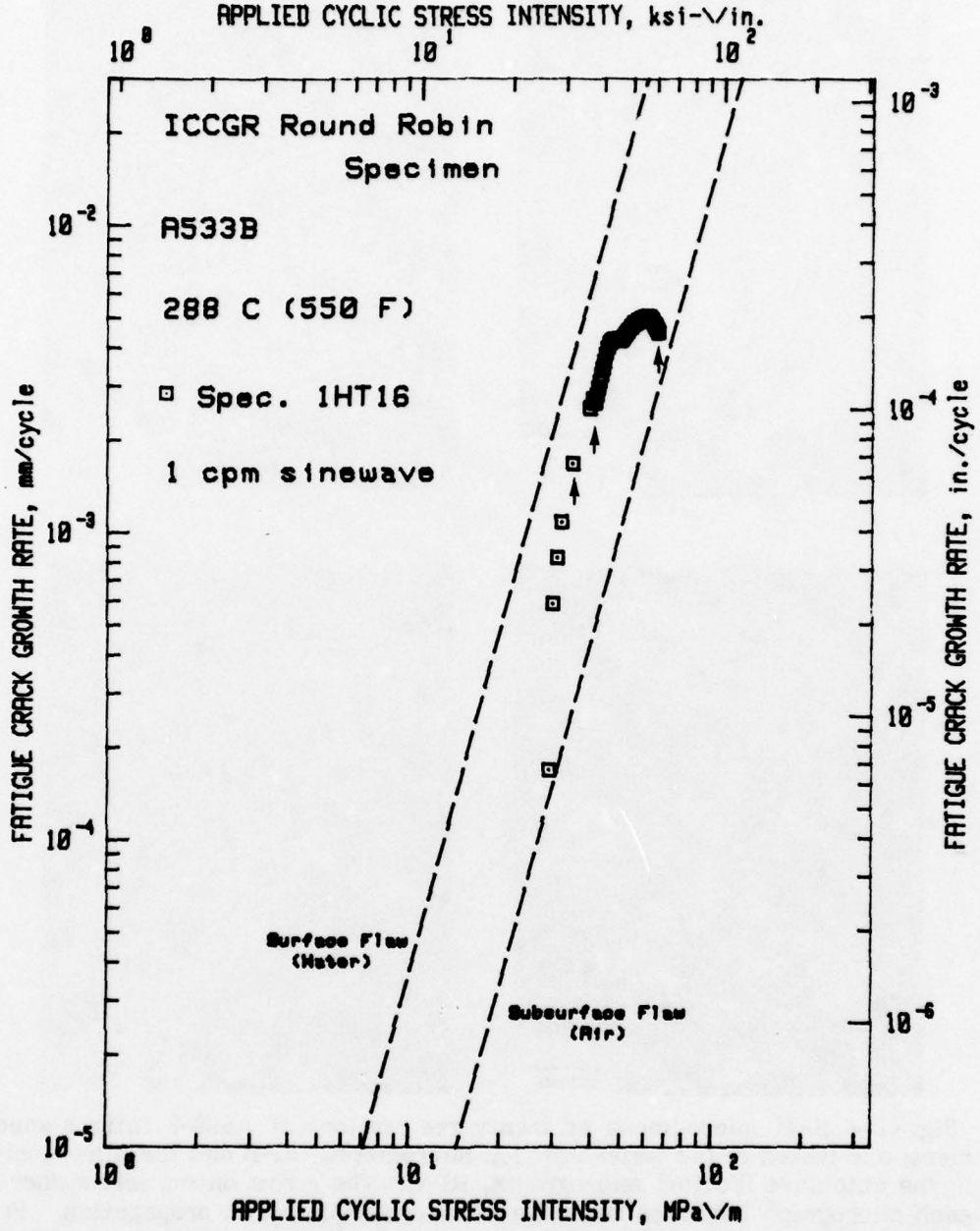

Fig. 42 — Fatigue crack growth rate vs applied cyclic stress intensity factor for the 17 mHz sinusoidal waveform round robin test of A533-B steel. The data exhibits a startup rate in the "low" category, but quickly moves to the "high" category for the mid-range ΔK values. Toward the end of the test, the FCGR's trended to the low category. The arrows indicate growth rates in the regions corresponding to the fractographs of the next figure.

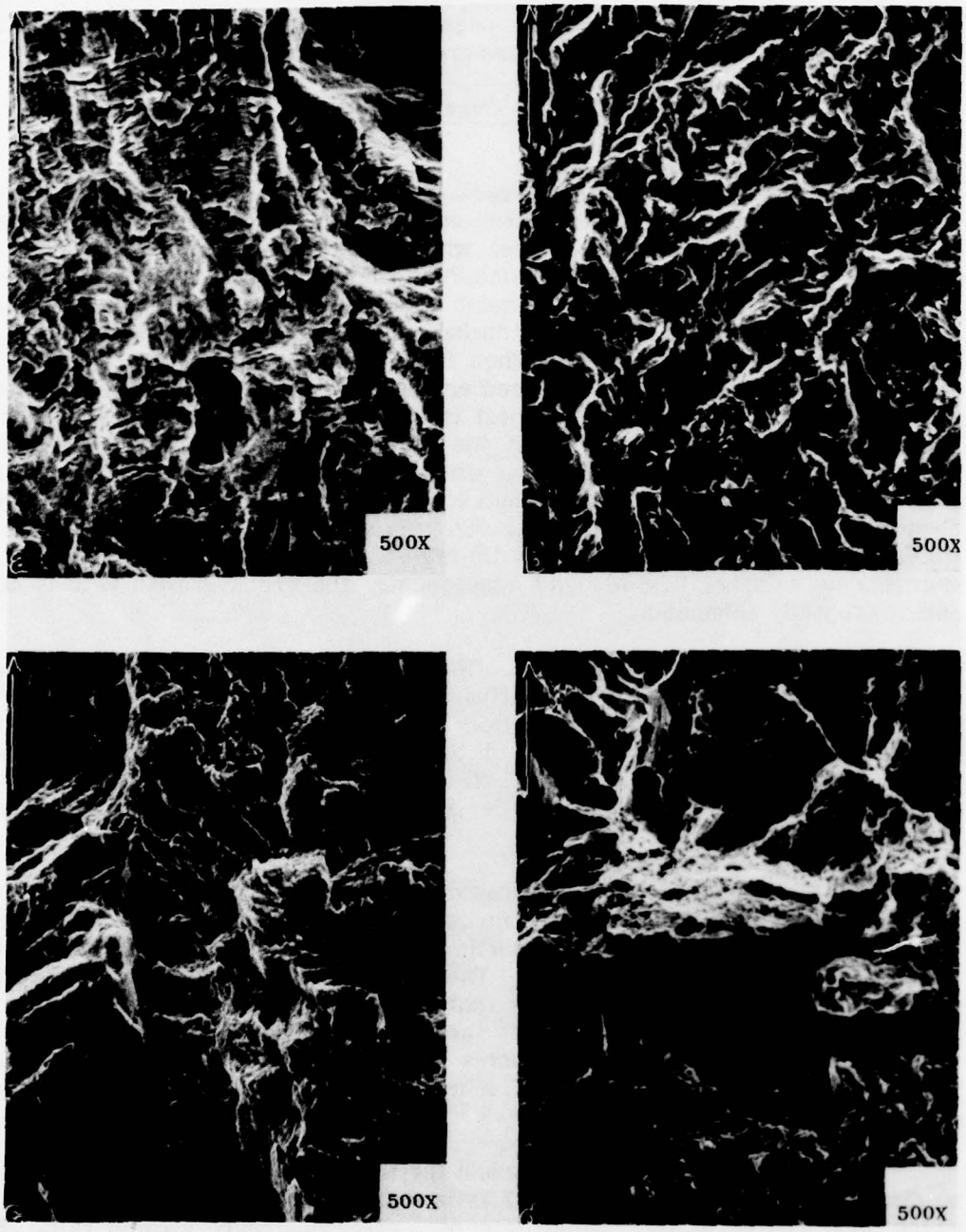

Fig. 43 — Fatigue fracture surfaces of the A533-B round robin specimen. The SEM micrographs were taken at crack lengths corresponding to the following ΔK values: (a) 31.9 MPa$\sqrt{m}$ (29 ksi$\sqrt{in.}$), (b) 37.5 MPa$\sqrt{m}$ (34.2 ksi$\sqrt{in.}$), (c) and (d) both at $\approx$66 MPa$\sqrt{m}$ (60 ksi$\sqrt{in.}$). Arrows indicating these ΔK values and the crack growth rates are shown in Fig. 42. Panel (d) includes some of the cleavage of the post-test fracture; this can be compared with the cleavage-like features, of about the same size, in panel (b).

assistance proceeds with a large cleavage-like component and little, if any, striation formation. Once again, the presence of the cleavage-like features is strongly indicative of hydrogen-assisted growth mechanisms.

Model for Hydrogen-Assisted Fatigue Crack Growth in Nuclear Coolant Environment

Consideration of the fatigue crack growth results, the fractography and the large volume of published research on corrosion-fatigue crack growth has led to the formulation of a model which describes the influence of the preliminary matrix variables: ramp time, hold time and temperature. The model assumes that in the water environment hydrogen is produced by a cathodic reaction at the crack tip. The event during which this reaction is most likely to occur is the period of rising load when fresh metal surface is exposed at the crack tip. The hydrogen thus produced enters the metal and diffuses along the stress gradient to the region of highest triaxial stress. It may also be trapped at the second phase particles or at the grain boundaries. The presence of hydrogen in this region causes local embrittlement that enhances the crack growth rate. On the other hand, hydrogen adsorption at the surface of the plastic enclave may be prevented, or seriously slowed by the development of a stable, protective oxide at the crack tip region. In such a case, local hydrogen embrittlement is not possible and consequently the crack growth rate is not environmentally enhanced.

Ramp times of one second, at either 93 or 288^{o}C, are too short for the hydrogen to be produced in quantities sufficient for embrittlement of the plastic enclave at the fatigue crack tip. Thus the crack growth rates for these tests fall in the "low" category, and the failure mode is characterized by fatigue striation formation as in Fig. 34. No obvious features were observed on the fracture surfaces that could be associated with a corrosion fatigue mechanism.

On the other hand, the accelerated crack growth rates observed for the specimens tested with longer than one second ramp times, at 93^{o}C, indicates that these ramp times are quite sufficient for the hydrogen embrittlement mechanism to become established. The corresponding fractography on this group of specimens showed features that are usually associated with environmentally-assisted fatigue failures. In fact, the fracture surfaces showed both intergranular and cleavage-like facets (Fig. 35), while fatigue striations, which would be more indicative of a non-assisted, or normal fatigue crack growth mechanism, were absent.

The observations on the mechanism for the higher temperature tests must be discussed in two sections. The 17 mHz sinewave tests, which yielded data which was mostly in the "high" category, correspondingly showed (Fig. 36) cleavage-like features. All the other tests at autoclave temperatures produced data in the "low" growth rate category and exhibited the fractographic features of normal fatigue crack growth. Mechanistically, the 17 mHz test received hydrogen assistance, but the other tests, at both shorter or longer equivalent ramp times, did not. Based on these behaviors, it seems likely that a trade-off is occurring between the tendency for hydrogen adsorption/diffusion and oxide

layer formation/passivation. On one hand, increasing the ramp time provides the necessary interval for the hydrogen to be produced, while at the same time, affording an opportunity for oxide passivation. For ramp rates in the neighborhood of 20 to 25 sec (equivalent to a sinewave frequency of 17 mHz), the hydrogen mechanism out-paces the oxide formation, but at longer ramp times, the formation of very stable Fe_3O_4 prevents this.

Other research results provide evidence which increase the credibility of the proposed model. The identification of the difference in oxide type, mentioned earlier, (Fe_2O_3 at 93°C vs Fe_3O_4 at 288°C) helps to substantiate the mechanistic differences between these tests. Also, the differences in degree of crack branching indicates that there may be mechanistic differences. Lastly, the production of stress corrosion cracks in an (albeit, inferior quality) A508 forging specimen, indicates that overt segregation and inclusion content could lead to hydrogen embrittlement mechanisms much like the one described above.

If one chooses a fixed, mid-range value of ΔK, and constructs a three-dimensional plot of da/dN (at a given ΔK) vs rise time on one axis and temperature on the other, the result will be close to that shown in Fig. 44. The rates at the low temperature (back edge of the plot) are low for the short ramp times, and go high for ramps of 60 sec duration and longer. On the other hand, at high temperature, the rates are low, then go high at about 25 sec, returning to low for ramps of 60 sec duration or longer.

Because of the lack of exact correspondence between the 17 mHz sinewave test ("high"), and the 22 sec ramp test (between "low" and "high"), it is evident that there is still some mechanistic fine-tuning to be worked out. However, the gross aspects of the model seem to be in good order.

ONGOING TESTS

The overall plan of the main matrix for both unirradiated and irradiated materials was presented in the Program Overview and several items from that matrix are currently under test as indicated in Table 3. It is expected that work on this matrix will continue through 1980. Most of the specimens for this matrix are now available, with the exception of the weld made up with Linde 80 flux. This weld metal is due to be received in early 1980.

In addition to the ongoing main matrix tests, we have in progress one test of A508-2 steel in reactor grade water at 93°C (200°F). The waveform for this test is a 22 sec ramp/reset, and the initial ΔK was 11 MPa$\sqrt{m}$ (~10 ksi $\sqrt{in.}$). This test will provide some information on the near-threshold FCGR behavior of this material.

At the close of 1979, two specimens of A106-Gr. C piping were under test, with a one min ramp/reset waveform and load ratios of 0.2 and 0.7. Additionally, the variable amplitude test is on A516 steel, also a typical piping material. As indicated in Table 5, other specimens of A351 stainless, A515, A106, some stainless-to-stainless welds, and mixed metal (stainless-to-low alloy) welds are being fabricated. Much of this same material being tested in the fatigue program is also being tested in fracture programs at Naval Ship

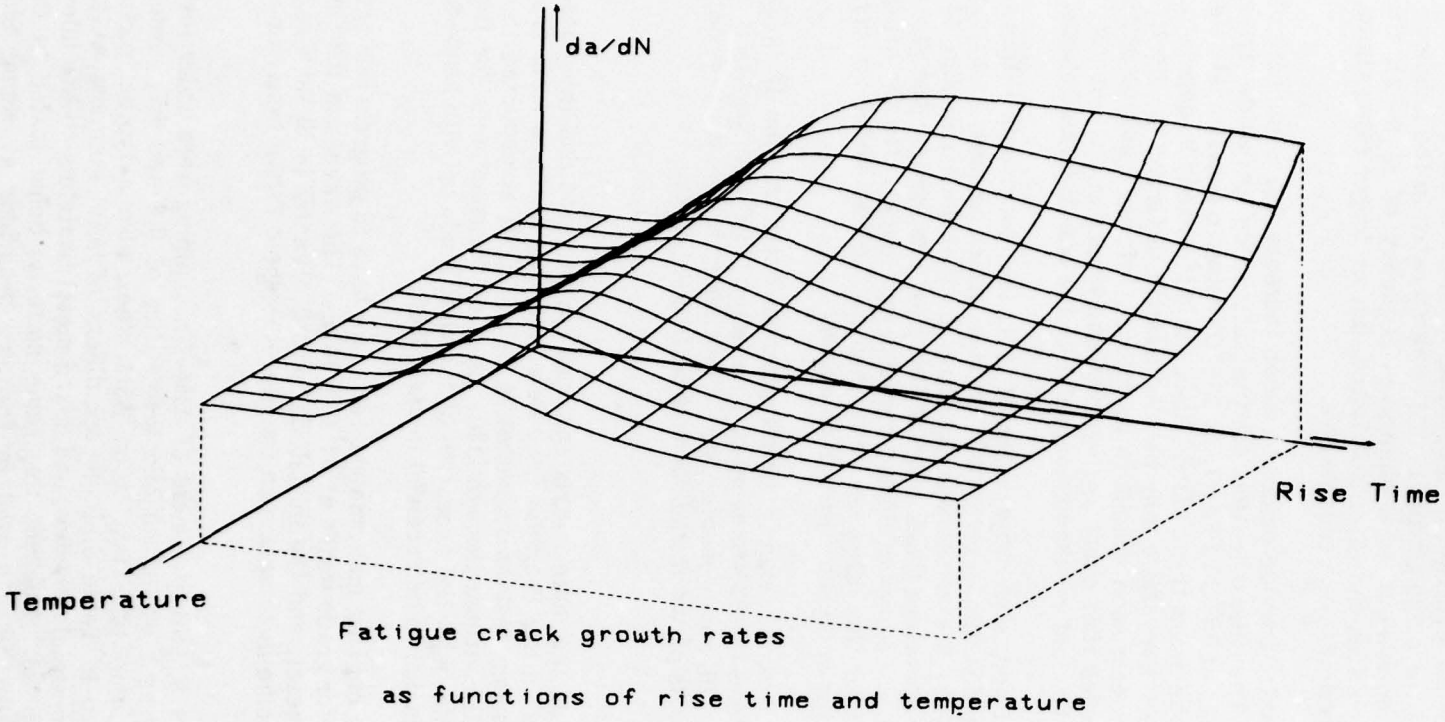

Fig. 44 — A conceptualized three-dimensional surface of crack growth rates, for some fixed value of ΔK, as functions of ramp time and temperature. The edge closest to the viewer depicts the growth rate behavior at higher test temperature ($\approx 288^{o}C$), beginning with low growth rates for fast ramps, then high growth rates for 17 mHz sinewave equivalent ramps, and reverting to low growth rates for long ramp times.

Research and Development Center (NSRDC), Annapolis, Maryland, and at Battelle Northwest Laboratory, Richland, Washington.

In September 1979, a variable amplitude loading test of A516-Gr. B piping steel was initiated in a single specimen autoclave. The specimen is subject to the usual PWR coolant environment (14 MPa, 288°C, ~1 ppb dissolved oxygen content). The load waveform characteristics are based on cold leg axial stresses and transients of an operating nuclear reactor. The same data are being used in a mathematical modeling study at Battelle-Columbus. A list of the largest and most frequently observed transients and associated load ratios and cyclic counts is shown in Table 6.

An MTS model 433 Processor Interface, and the associated PDP 11/05 computer were adapted for use with the servohydraulic control unit for this autoclave system. Subsequently, a computer program was written to generate a waveform which adequately duplicated the stress transients as given in Table 6. The individual cycles are mixed and are applied with the same maximum load for each cycle. Thus the appropriate load ratio for each type of cycle is achieved by varying only the minimum load. The frequencies for each cycle were not specified for the actual measured transients and have been conservatively chosen on the basis of the preliminary matrix results. A segment of the actual waveform is shown in Fig. 45. A 2T-WOL specimen is being used for this test and the initial applied K_{max} was 44 MPa$\sqrt{m}$ (40 ksi$\sqrt{in.}$). The test results could be plotted in several ways, but one method of computing an independent variable related to the applied cyclic stress intensity factor (ΔK_i) of the individual cycles is to compute a centroid of ΔK according to a root mean cube expression:

$$\Delta K_{cent} = \sqrt[3]{\frac{N_i \, \Delta K_i^3}{N_{total}}} \qquad (1)$$

in which N_i is the number of cycles applied for each ΔK_i [18,19] At the close of this quarter, the results from this test to date were not sufficient for accurate differentiation.

Since termination of the round robin test, the 1T autoclave has been undergoing renovation to prepare it for irradiated specimen testing. In addition to the modifications to enable remote loading of the specimen, the autoclave was altered to provide generally improved performance, and the water chemistry analysis system was upgraded. This first test of an irradiated specimen will be at PWR conditions, using a 17 mHz sinusoidal waveform. The material will be A533-B irradiated to a flux (>1 MeV) of 3.3×10^{19}.

OVERALL PROGRESS

While the progress to date, at NRL, together with the other laboratories, has been significant and encouraging, there remain certain aspects of this research which are somewhat less than conclusive in their findings. In many

Table 6 - Transients, Load Ratios and Cyclic Counts for Variable Amplitude Test

Transient No.	Transient Description	Load Ratio	Number of Cycles
1	Start-up/Shutdown	0.151	240
5,6	Step Increase/Decrease	0.804	8000
8	Reactor Trip	0.667	470
7	Turbine Trip	0.704	390
9	Rapid Depressurization	0.682	80
12	Hydro Test	0.139	20
16	Steam Line Failure	0.565	1

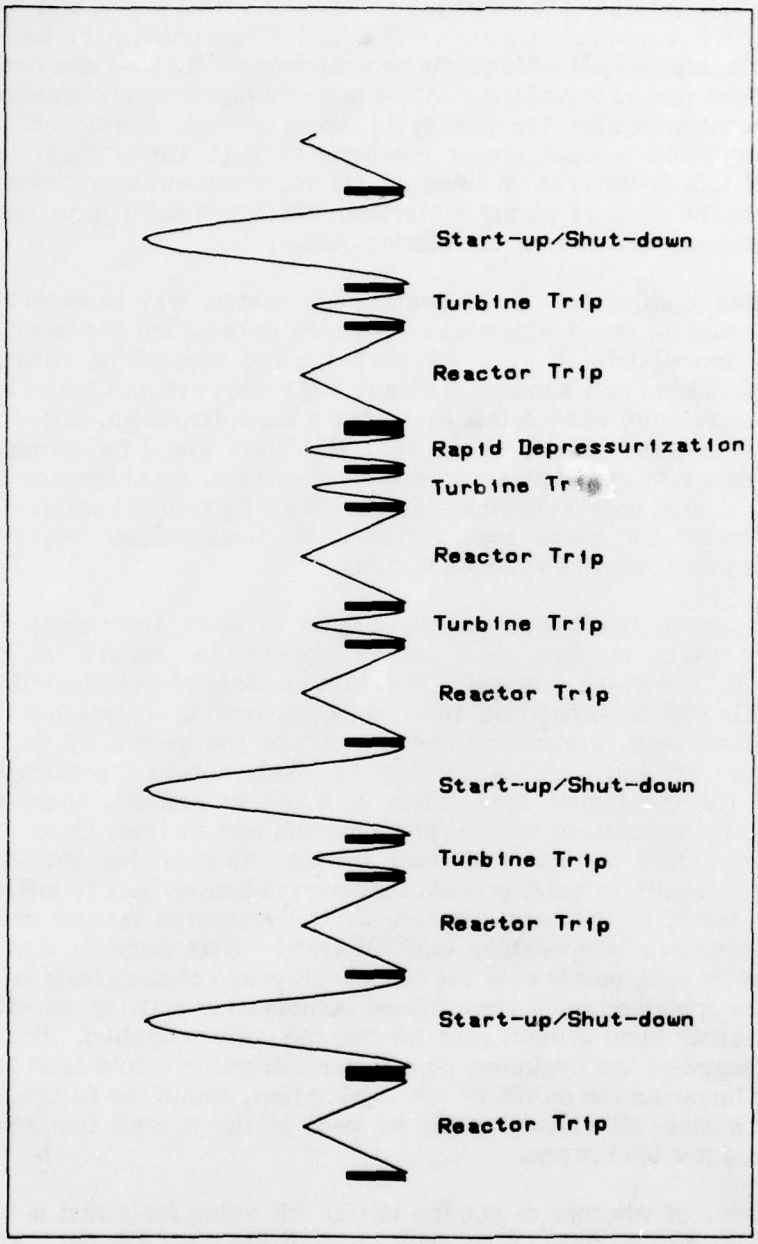

Fig. 45 — A section of the command signal waveform for the variable amplitude test in progress at the end of this fiscal year. All components of the waveform have the same load maximum, but various load minimums. The frequencies run from 0.017 to 1Hz, depending on the type of cycle.

cases, the research necessary to address and correct these deficiencies, which are outlined in this section, is currently underway, and some additional results are expected in the near future. To date (the close of FY-79), the bulk of the published fatigue data is for a load ratio of 0.2 or lower, and most of that is for the PWR coolant chemistry. The test frequencies have been centered about 17 mHz, but ranged sufficiently to each side so that we can conclude that extremely long period waveforms do not produce higher crack growth rates but, in fact, probably reduce the per cycle crack growth increment. However, operating reactors sustain stress components with rather high load ratios, (≥ 0.7), and this is an area in need of far more research and understanding, especially in the case of piping materials, which are subject to the high load ratio mechanical vibrations of circulation pumps.

A primary objective of the preliminary matrix was to determine if any conditions could be found which would produce data which exceeded the ASME Section XI water default line. A very limited amount of data have been previously published [20] showing that a 17 mHz sinewave and a load ratio of 0.2 would just marginally exceed this limit, but a much larger amount of data for R = 0.6 [21-24] and 0.7 [25-31] shows that the limit would be exceeded over a significant range of cyclic stress intensity. However, consideration of the NRL preliminary matrix data indicates that the ASME Section XI water default line is not exceeded for these load ratios (0.2), temperature (93, 288°C), and waveform (ramp/hold, sinewave) conditions.

As shown in the review of the results to date, the ramp/hold type of waveforms result in data sets which appear to satisfy a power law ($da/dN = C \Delta K^n$) over the range of ΔK values which have been tested. However, in both NRL and Westinghouse tests using sinusoidal waveforms, there is a definite, often very pronounced "bend-over" in the graphs of da/dN vs ΔK (Figs. 30 and 42) and Refs. 25 through 31. This behavior seems particularly aggravated for the higher load ratios of 0.7. At present, there is no solid mechanistic interpretation for this phenomenon, and in fact, there needs to be better experimental definition of these trends. As indicated in the section on experimental results to date, present evidence indicates that 17 mHz sinusoidal waveforms result in the maximization of the measured fatigue crack growth rates for autoclave temperature (288°C) tests. It is possible that the near-vertical rise of data points over the initial ΔK range of such tests is merely the result of the specimen/environment/load combination settling into the equilibrium (and rather high) growth rate for the ΔK values applied. Extending this conclusion suggests the beginning at a lower ΔK value would tend to "straighten out" or linearize the da/dN vs ΔK log-log plot, and in the future, such tests, with lower initial ΔK values, should be part of the overall test schedule, for both high and low load ratios.

The issue of whether or not the initial ΔK value for a test is itself a test variable might also be resolved by such tests. It has been alleged that the lower of the starting ΔK, the higher the overall crack growth rates throughout the entire ΔK range for the test [26, 27]. For three series of tests at NRL [14, 32] (see Fig. 27 and 28 of this report), we have not been able to substantiate this effect, however, the controversy will continue, until several independent investigations support one position or the other.

Resolution of these high and low load ratio sinewave trends, and more data generation for high load ratios is necessary before a truly comprehensive micromechanistic model can be finalized. In addition to the somewhat tenuous explanation of the 288°C, 17 mHz sinewave behavior for R = 0.2, the model cannot, because of lack of data, be extended to the lower ΔK regime. Similarly, no attempt has been made to extend the model to the high load ratio case. There is virtually no available data for the ramp and hold configuration at R>= 0.7.

Thus, the additional experimental work suggested above will simultaneously close several gaps in our current understanding of FCGR's in nuclear pressure vessel coolant environments and stress profiles. It is clear that the high load ratio data now available exceeds the ASME Code requirements. Hence, these suggestions will provide both a better empirical basis for establishment of more viable ASME Code limits, and a better basis for development or refinement of our understanding of the micro-mechanisms of fatigue crack growth.

In a previous section detailing the development of a hydrogen assisted crack growth model, a three-dimensional surface, describing the crack growth rate levels as functions of ramp time and temperature was shown in Fig. 44. This figure is conceptual; it is not the result of a curve-fitting procedure or experimentally measured data points. The issue here is that we do not have any data at intermediate temperatures (between ~100 and 300°C) and this indicates an area for additional research. While crack growth rates for such intermediate temperatures are not expected to deviate too significantly from those suggested by the conceptualized surface, these tests should be undertaken for completeness and scientific integrity.

The effect of water chemistry is also difficult to delineate at the present time, and this indicates an area for additional effort. Most of the results in BWR chemistries emanate from the General Electric Laboratories in San Jose, California [21-24], or from Japan Atomic Energy Research Institute, Ibaraki, Japan [33-34]. Study of these results indicate that, unlike the PWR results, decreasing the test frequency monotonically increases the crack growth rates. If this is true, then the higher oxygen content of the BWR environment could be the cause, indicating that a mechanism other than, or in addition to, hydrogen-assisted crack growth is operative. Studies on the above topics are being continued and expanded at these two laboratories, and additional studies, comparing effects of PWR and BWR, are scheduled for initiation at Babcock and Wilcox in 1980.

As these basic tasks, involving waveform, load ratio, temperature and water chemistry are carried out and the results are interpreted and understood, we will be in a better position to initiate tests which combine and vary these variables, to better imitate the actual operating reactor conditions. The variable amplitude test now in progress at NRL is indicative of the beginnings of this advance, and additional research tasks will be developed and carried out in the future. In this test, for which K_{max} is constant for all cyclic components, the interactions between individual cyclic excursions will be minimized. Tests with more randomized load schemes, and better, more typical

frequency spectra should be carried out, even though it will be more difficult to reconcile the crack growth rate data with the existing body of constant amplitude FCGR data.

The current main test matrix includes a series of tests (Table 4) on irradiated steels, and some results will become available during FY-80. At NRL, we have one autoclave currently located in a hot cell and we have demonstrated that an irradiated specimen can be instrumented and loaded into the autoclave using remote handling techniques. The autoclave is in the final stages of outfitting for this first irradiated specimen test in the simulated coolant environment. A second autoclave, capable of testing 2T or 4T specimens, is scheduled for installation in a hot cell during 1980.

SUMMARY AND CONCLUSIONS

While the specification of the various conclusions of these fatigue studies has been included in the appropriate sections, and the conclusions from the preliminary matrix studies have been previously published, these most important points are condensed and again presented here.

a. Characteristics of high-temperature, pressurized water fatigue crack growth rates for pressure vessel steels fall in one of two categories, "low," i.e., near the ASME air line, because of a lack of hydrogen assistance component, or "high," i.e., located midway between the ASME air and water default lines, because of the presence of a hydrogen-assisted crack growth mechanism.

b. Ramp/hold type waveforms for load ratios $\sim$0.2 do not exceed the ASME water default line, and for other waveforms, only a few data points have been published which do. Based on the test results available to date, for this load ratio, the overall positioning of the ASME water defaul line is safely conservative.

c. The situation is different for high R ($\sim$0.7 and larger) data. Much of these data exceed the ASME water default line [25-31], and ongoing ramp/reset tests, together with the variable amplitude test at NRL, should help show the degree to which crack growth rate data exceeds the present ASME Code.

d. Fractographic observations indicate that the fatigue fracture morphology for tests involving "high" category growth rates contain a large cleavage-like component and essentially no striation formation component. Low growth rate morphologies are composed of striations and other ductile rupture components.

FUTURE PLANS

During FY-80, the predominant NRL effort will be the testing of items in the main matrix for pressure vessel steels and weld metals, and the piping matrix of piping materials. As part of the main matrix effort, the 1T autoclave will be heavily disposed toward the testing of irradiated specimens. The

remaining few tests to complete the basis for hydrogen-assisted crack growth model development for load ratios of 0.2 are planned, and if possible, tests to obtain results for extension of the model for intermediate temperature and /or high load ratios will be initiated.

Since the computerized facility for the generation of complex waveforms is now in place, variable amplitude load and frequency tests could be initiated to study load interactions or synergistic effects.

Finally, our program involving NRL appointments of foreign scientists, the active participation in the ICCGR coop program, and visits to our facility by representatives of nuclear power plant research and design representatives, both national and foreign, will be actively continued.

III. RADIATION SENSITIVITY AND POSTIRRADIATION PROPERTIES RECOVERY

A. Notch Ductility Degradation by Low-to-Intermediate Neutron Fluence Exposures

J. R. Hawthorne

INTRODUCTION

The embrittlement of reactor structural steels by neutron fluence typically is assessed from changes in Charpy-V (C_v) notch ductility. The progressive increase in embrittlement with neutron exposure is known to be non-linear with fluence ($n/cm^2 > 1$ MeV) and, in addition, has been shown to be dependent on the content of copper and phosphorus impurities in the steel. Through C_v data compilations and analyses, radiation embrittlement trends have been evolved for application in reactor vessel design and for guidance of fracture safe vessel operation. One example of the development of embrittlement versus fluence curves is the U. S. Nuclear Regulatory Commission Guide 1.99 [35] While significant progress has been made, trend development efforts have been greatly impeded by a lack of radiation data for the extremes of the fluence range of interest. Projected end-of-life (EOL) fluences for many currently operating reactor vessels are on the order of 3 to 5 x 10^{19} n/cm^2. A large volume of data exists for 2 to 4 x 10^{19} n/cm^2 fluences; however, data for exposures below this fluence interval are scarce. This study was undertaken with the objective of improving knowledge of both the extent and trend of C_v notch ductility changes in reactor vessel steels (plate and weld metals) at low-to-intermediate fluences, that is, between 0.1 and 1 x 10^{19} n/cm^2. A second objective was to obtain an experimental assessment of the level of conservatism in current embrittlement projection methods. A full report on the study has been prepared [36] and was presented to the Third ASTM-EURATOM Symposium on Reactor Dosimetry.

MATERIALS AND MATERIALS IRRADIATION

The plates and weld deposits selected for the investigation are identified by NRL code number and composition in Table 7 and were fully representative of reactor vessel materials now in service. The A302-B plate is also the ASTM reference correlation-monitor steel used extensively in reactor surveillance programs. The C_v test specimens (ASTM Specification E-23, Type A) were taken from the quarter thickness location in plates and from through-thickness locations in weld deposits.

Material irradiations were conducted at a nominal 288°C (550°F) at the State University of New York at Buffalo using its 2 MW pool reactor (UBR). Irradiation temperatures were monitored by multiple thermocouples in each specimen array. The ambient neutron flux was on the order of 7 x 10^{12} n/cm^2-sec. Fluence determinations were based on measurements with iron neutron dosimeter wires placed among the specimens.

TABLE 7

TEST MATERIALS[a]

Material	NRL Code	Chemical Composition, wt.%										
		Cu	P	C	Mn	S	Si	Ni	Cr	Mo	V	Other
A302-B Plate[b]	F26	.20	.011	.24	1.34	.023	.23	.18	.11	.51	.01	Al .038
A533-B Plate	N27[c]	.13	.008	.17	1.21	.007	.20	.56	-[d]	.50	.02	Al .015
	EBB	.10	.009	.19	1.28	.013	.25	.61	.04	.55	.004	
	EDB	.14	.009	.20	1.31	.012	.22	.62	.08	.59	.004	
	3MU[e]	.12	.011	.20	1.26	.018	.25	.56	.10	.45	-	Al .034
A533-B S/A Weld	MY	.36	.015	.14	1.38	.012	.22	.78	.07	.55	-	
	W1	.35	.020	.09	1.45	.013	.68	.57	-	.39	-	
	NRL 1	.19	-	-	1.43	-	-	.56	.08	.36	-	
	NRL 2	.29	-	-	1.56	-	-	.65	.08	.39	-	
	NRL 3	.30	-	-	1.53	-	-	.68	.08	.40	-	
	NRL 4	.16	-	-	1.51	-	-	.58	.08	.37	-	
	NRL 5	.39	-	-	1.60	-	-	.58	.10	.39	-	
	NRL 6	.16	-	-	1.49	-	-	.58	.09	.39	-	
	NRL 7	.27	-	-	1.42	-	-	.56	.06	.36	-	
	NRL 8	.32	-	-	1.51	-	-	.68	.07	.39	-	
	W[f]	.29	.020	09	1.50	.014	.56	.62	.16	.37	<.01	
	62N(1)[f,g]	.18	.019	.08	1.55	.008	.60	.55	.17	.38	.01	
	62N(2)[f]	.24	.013	.08	1.42	.008	.57	.50	.07	.37	.01	
	63N[f]	.31	.017	.10	1.62	.010	.65	.69	.09	.42	.01	

[a] Material thickness range: 15.2 to 26.6 cm

[b] ASTM A302-B Reference Plate

[c] NRL A533-B Demonstration Melt

[d] Not determined

[e] IAEA Reference Plate (HSST Plate 03)

[f] Approximate composition

[g] Two weld filler wires used

RESULTS

Experimental C_v results for the individual materials are summarized in Table 8 and are entered on the NRC Regulatory Guide 1.99 graphs for projecting transition temperature and upper shelf changes in Figs. 46 and 47. In the discussion below, ductile-to-brittle transition behavior is indexed to the 41 J (30 ft-lb) temperature unless noted otherwise.

Observations for 1 to 2 x 10^{18} n/cm^2

Data for the low fluence condition indicate that radiation effects on notch ductility are first becoming significant at this fluence level. Transition temperature increases are on the order of 14 to 31°C (25 to 55°F). In contrast, upper shelf reductions are notably absent. It thus appears that the transition temperature elevation begins with fluence in advance of the upper shelf reduction and that the mechanisms responsible for each are not the same.

Observations for 3 to 4.5 x 10^{18} n/cm^2

In this fluence interval, both a transition temperature elevation and an indication of upper shelf reduction were observed for all but one (weld NRL 5) of the materials tested. Tests of the plates were not conducted in this range. Overall, transition elevations ranged from about 39 to 100°C (70 to 180°F). Percentage upper shelf reductions ranged from 0 to 15%. The irradiation effect generally was found proportional to material copper content. The nonconformance of weld, NRL 5, to this pattern at this fluence level is being investigated; no explanation can be offered at this time.

Observations for 6. 5 to 9.5 x 10^{18} n/cm^2

Here, large transition temperature elevations ranging from 69 to 133°C (125 to 240°F) were observed for the welds along with large reductions in upper shelf energy (15 to 44%). Of special interest, Figs. 48 and 49 demonstrate that upper shelf levels can be reduced to 68 J (50 ft-lb) or lower at this intermediate fluence level. In the case of weld 63N (Fig. 49), the upper shelf was reduced to 49 J (36 ft-lb) by 7.8 x 10^{18} n/cm^2. Isolation of the metallurgical reason(s) for such poor upper shelf retention should be an urgent task.

Observations for >10 x 10^{18} n/cm^2

A few of the materials were irradiated to fluences greater than 10 x 10^{18} n/cm^2. The data indicate a trend of increasing radiation embrittlement with increasing fluence but at a much reduced rate. On this point, a large volume of data from test reactor irradiations exist for >2 x 10^{19} n/cm^2 fluences which clearly show increasing radiation effects with fluence. For surveillance irradiations, on the other hand, recent data by Westinghouse suggest a saturation of radiation effects at ~ 1 x 10^{19} n/cm^2 when the flux is low, ~5 x 10^{10} n/cm^2-sec [37]. Confirmatory research, however, is clearly needed. For one, a closely controlled set of test reactor experiments should be performed to verify the suggested saturation, using flux and fluence levels comparable to those of the power reactor results. Secondly, higher fluence irradiations will

Table 8
Summary of Charpy-V Notch Ductility Changes with 288°C (550°F) Irradiation

Material/Code	Fluence 10^{18} n/cm^2 (>1 MeV) (Φ^{cs})	Transition Temperature: Unirradiated C_v 41J °C	°F	C_v 68J °C	°F	Irradiated C_v 41J °C	°F	Δ°C	Δ°F	C_v 68J °C	°F	Δ°C	Δ°F	Upper Shelf: Unirradiated J	ft-lb	Irradiated J	ft-lb	ΔJ
A302-B Plate																		
F26	1.2	-18	0	10	50	4	40	22	40	32	90	22	40	117	86	117	86	0
A533-B Plate																		
N27	1.2	-62	-80	-43	-45	-62	-80	0	0	-40	-40	0	0	187	138	187	138	0
	6.6	-62	-80	-43	-45	-34	-30	28	50	-9	15	33	60	187	138	171	126	16
	21.0[a]	-62	-80	-43	-45	16	60	78	140	46	115	89	160	187	138	~134	~99	53
EBB	1.3	-12	10	13	55	≤2	≤35	≤14	≤25	29	85	17	30	137	101	137	101	0
EDB	1.3	1	30	21	70	18	65	19	35	41	105	19	35	160	118	160	118	0
3MU	17.0	-1	30	29	85	43	110	44	80	77	170	47	85	138	102	136	100	0
S/A Weld																		
MY	1.2	-34	-30	-15	5	-4	25	31	55	21	70	36	65	145	107	142	105	0
	6.6	-34	-30	-15	5	99	210	133	240	124	255	139	250	145	107	103	76	42
	26.0[a]	-34	-30	-15	5	141	285	175	315	174	345	189	340	145	107	76	56	69
W1	1.4	-29	-20	2	35	2	35	31	55	-	-	-	-	94	69	94	69	0
NRL 6	16.0	-23	-10	7	45	88	190	111	200	107	225	100	180	107	79	77	57	30
NRL 1[b]	4.2	-15	5	4	40	27	80	42	75	82	180	78	140	107	79	103	76	4
	9.5	-15	5	4	40	66	150	81	145	104	220	89	160	107	79	90	66	17
NRL 2	4.2	-34	30	41	105	57	135	58	105	96	205	56	100	104	77	91	67	13
	9.5	-34	30	41	105	93	200	94	170	129	265	89	160	104	77	81	60	23
NRL 3	3.9	-9	15	27	80	57	135	67	120	93	200	67	120	100	74	96	71	4
	8.5	-9	15	27	80	85	185	94	170	121	250	94	170	100	74	81	60	19
NRL 4[b]	3.6	-18	0	18	65	27	80	44	80	46	115	28	50	98	72	90	66	8
	7.6	-18	0	18	65	52	125	69	125	77	170	58	105	98	72	76	56	22
NRL 5	3.9	16	60	52	125	-1	30	53	95	113	235	61	110	83	61	83	61	0
	9.0	16	60	52	125	88	190	72	130	127	260	75	135	83	61	79	58	4
NRL 7	3.2	-26	-15	7	45	13	55	39	70	49	120	42	75	111	82	106	78	5
	6.7	-26	-15	7	45	43	110	69	125	79	175	72	130	111	82	90	66	21
NRL 8[b]	3.9	-9	15	24	75	63	145	72	130	93	200	69	125	106	78	90	66	16
	9.0	-9	15	24	75	91	195	100	180	116	240	92	165	106	78	79	58	27
W	8.9	-29	-20	-1	30	60	140	89	160	-	-	-	-	104	77	65	48	39
62N(1)	8.9	-29	-20	4	40	60	140	89	160	102	215	97	175	103	76	79	58	24
	12.1	-29	-20	4	40	71	160	100	180	-	-	-	-	103	76	68	50	35
63N	7.8	4	40	~38	~100	135	275	131	235	-	-	-	-	87	64	49	36	38

[a] Prior data.

[b] Upper shelf values taken at 160°C (320°F).

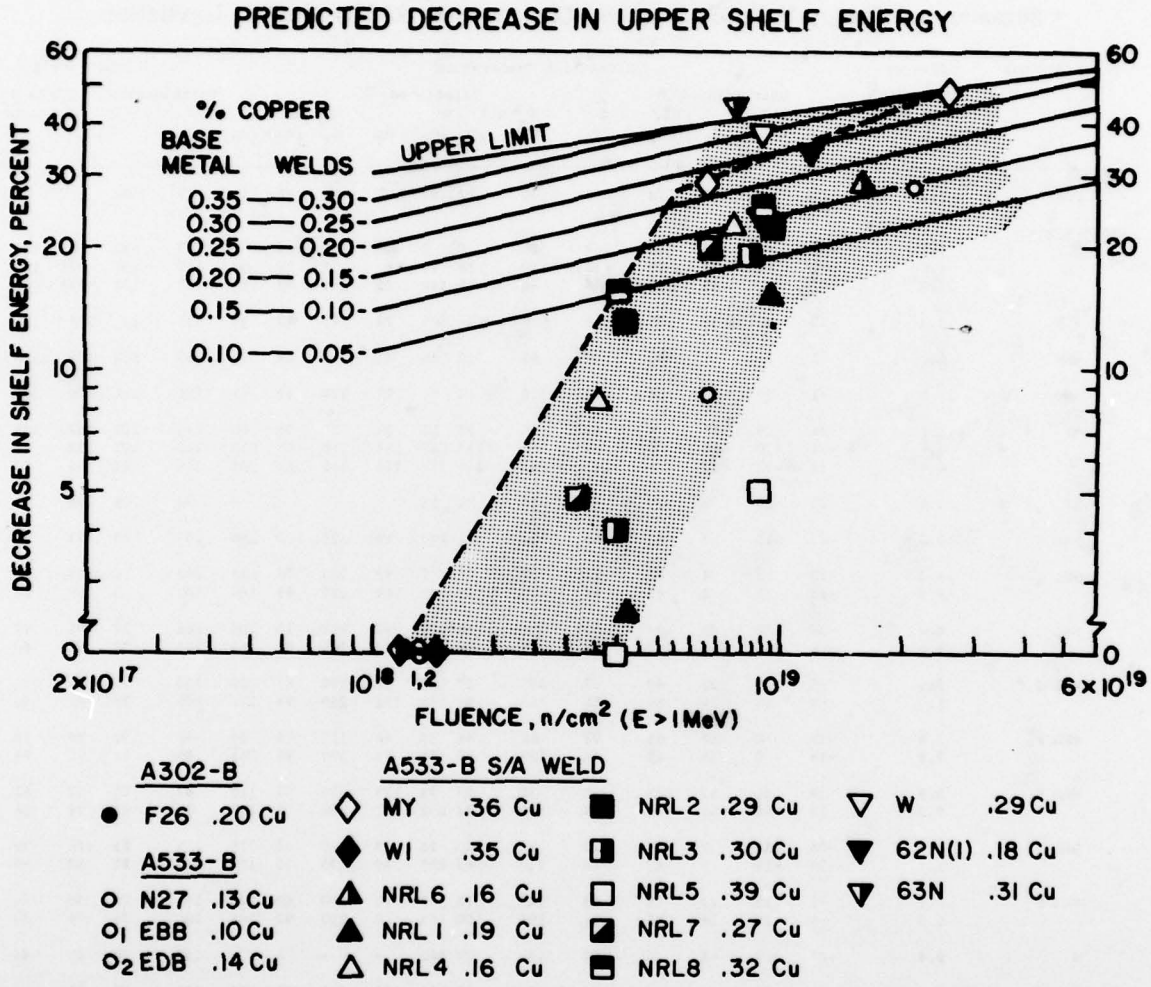

Fig. 46 — NRC Regulatory Guide 1.99 graph for projecting the upper shelf reduction with fluence. Results of the present study are superimposed. The data suggest that a set of bi-linear curves might better describe the upper shelf trend. The dashed line represents the behavior of submerged arc weld, Code MY.

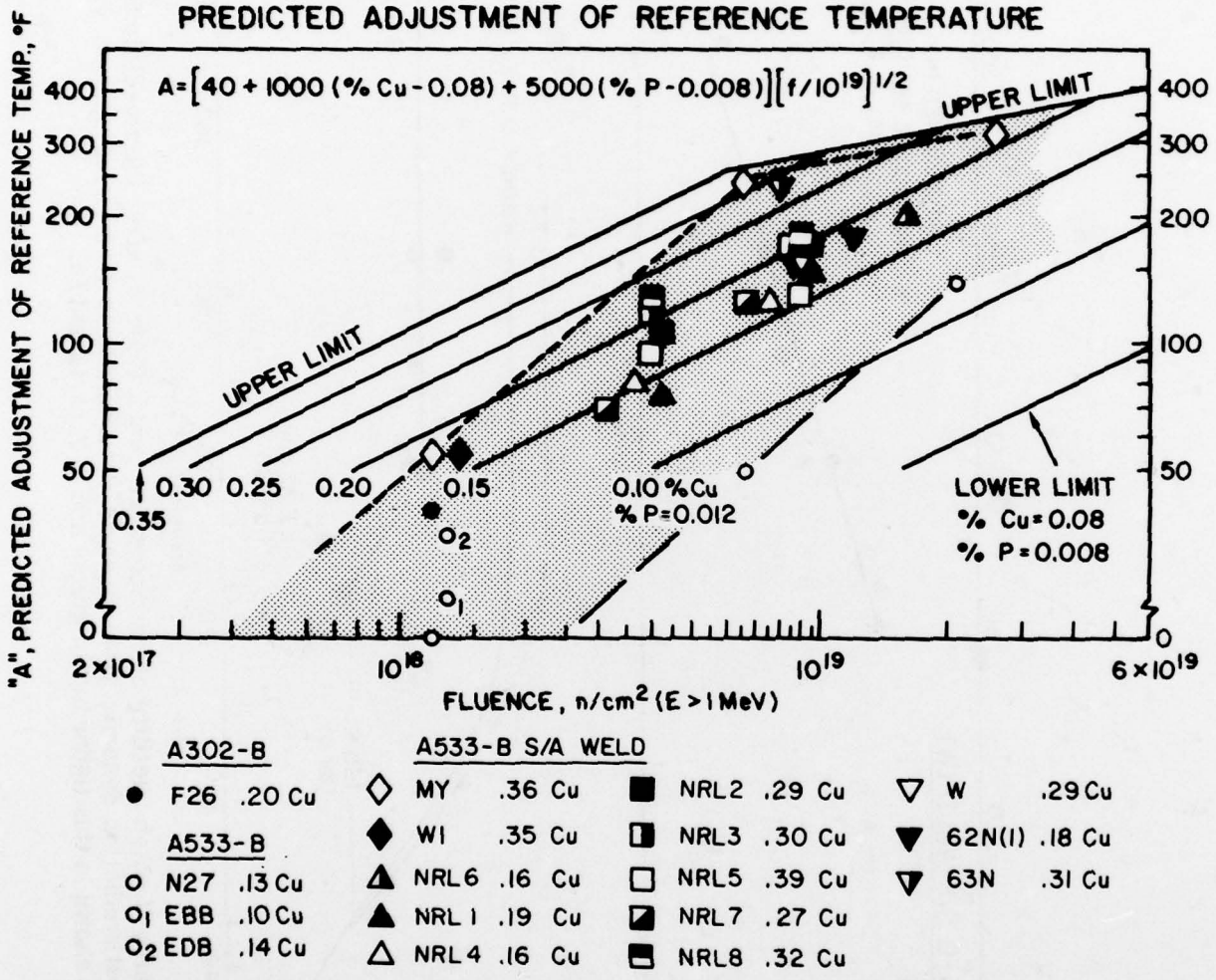

Fig. 47 — NRC Regulatory Guide 1.99 graph for projecting the reference temperature elevation with fluence. Results of the present study are superimposed. Note the degree of conservatism in Guide projections at low fluence.

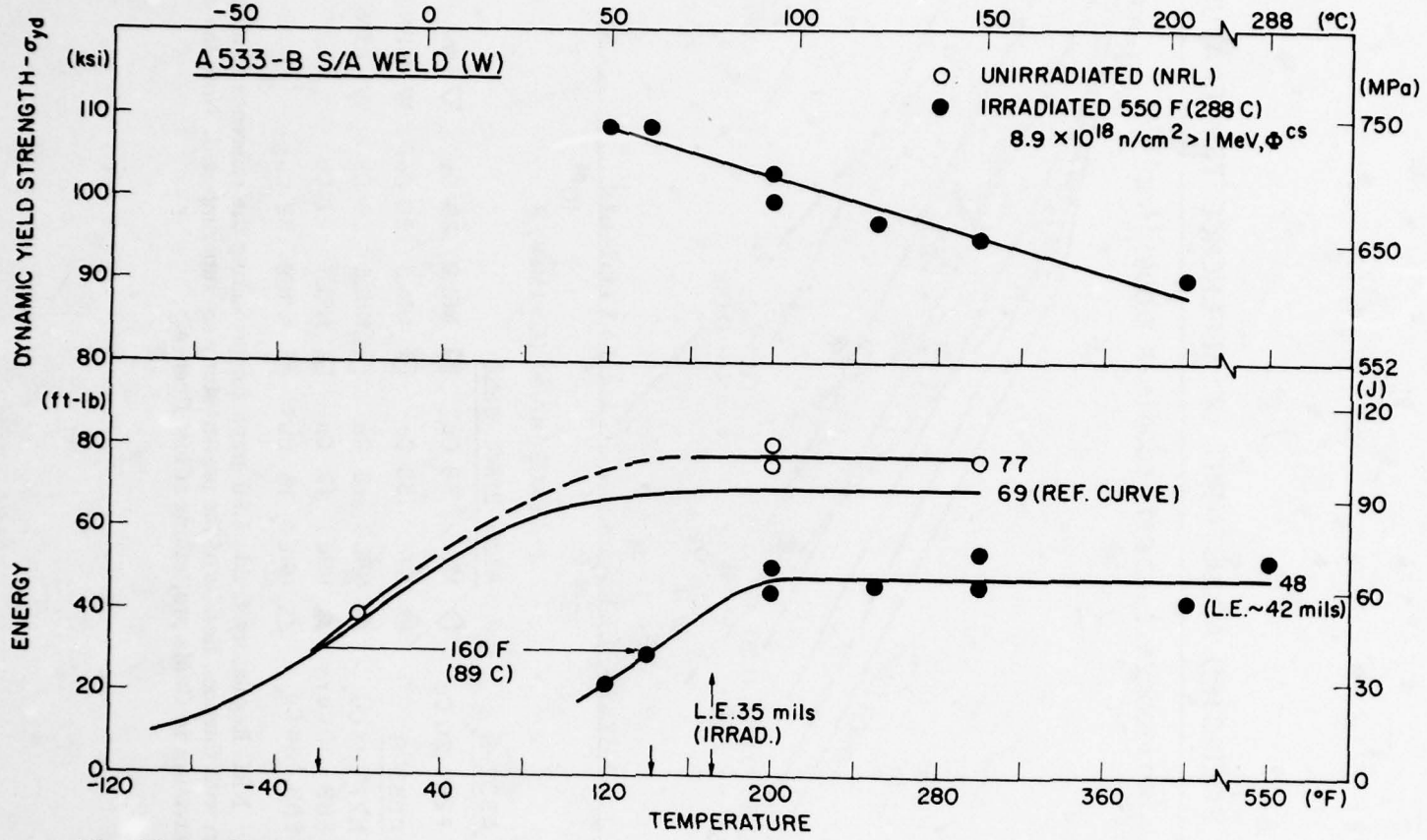

Fig. 48 — Charpy-V notch ductility of submerged arc weld, Code W, after intermediate fluence irradiation. Postirradiation dynamic yield strength determinations from Dynatup load vs time traces are also shown in this figure (upper graph) and in Figs. 49 and 50.

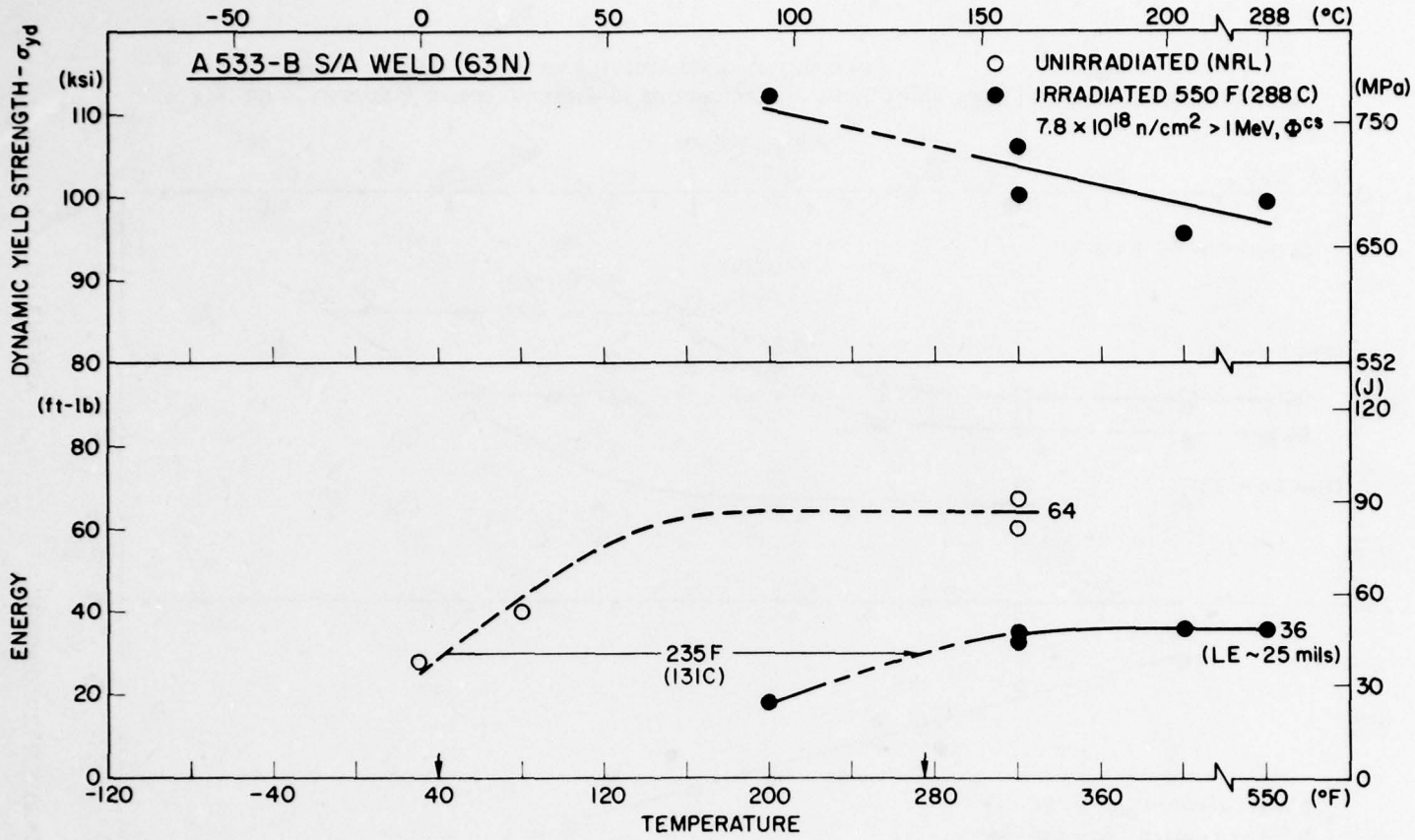

Fig. 49 — Charpy-V notch ductility of submerged arc weld, Code 63N, after intermediate fluence irradiation

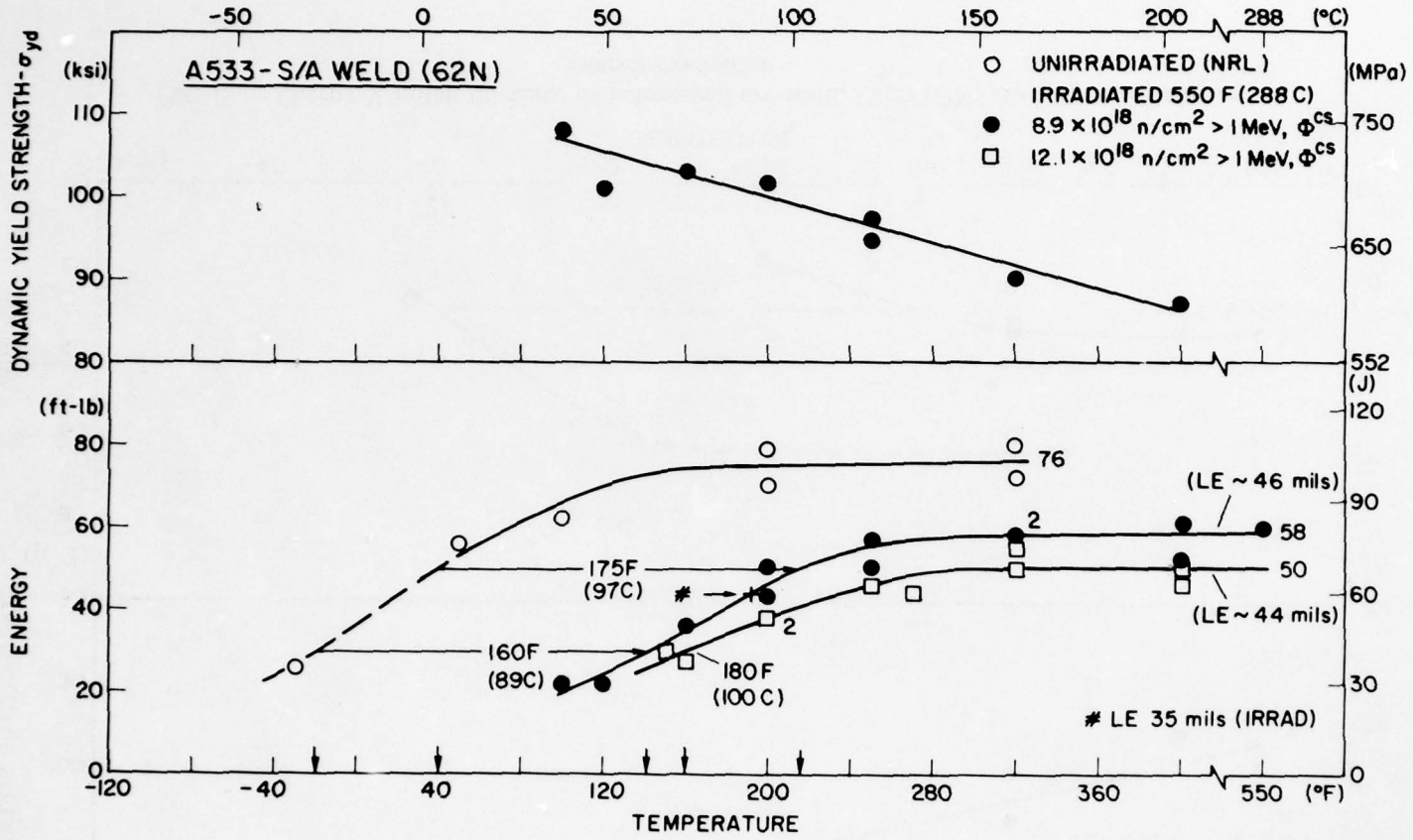

Fig. 50 — Charpy-V notch ductility of submerged arc weld, Code 62N(1), after irradiation to two intermediate fluences

AD-A081 004 NAVAL RESEARCH LAB WASHINGTON DC F/G 18/10
STRUCTURAL INTEGRITY OF WATER REACTOR PRESSURE BOUNDARY COMPONE--ETC(U)
DEC 79 F J LOSS
UNCLASSIFIED NRL-MR-4122 NUREG-CR-1128 NRC-RES-79-103 NL

2 OF 2
AD
A081004

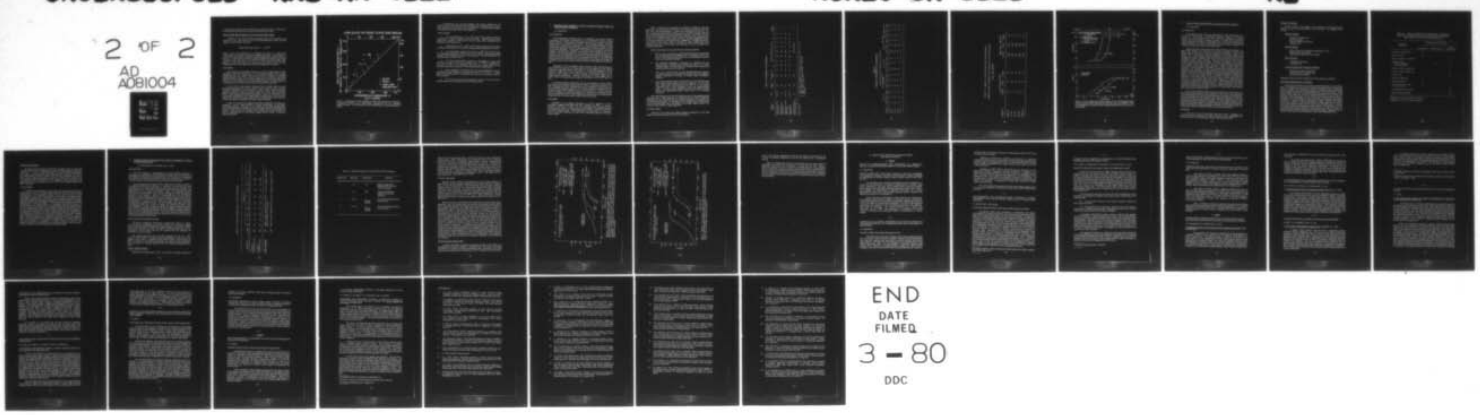

END
DATE
FILMED
3-80
DDC

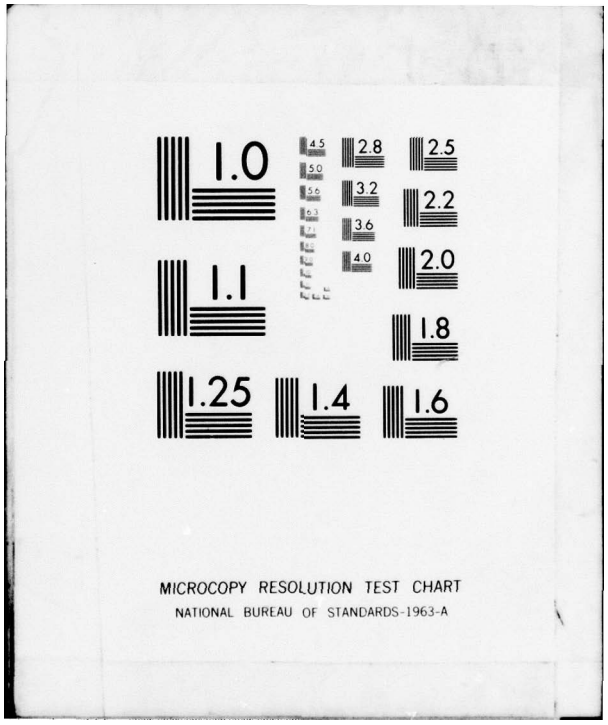
1.0
1.1
1.25
1.4
1.6
1.8
2.0
2.2
2.5
2.8
3.2
3.6
4.0
4.5
5.0
5.6
6.3
MICROCOPY RESOLUTION TEST CHART
NATIONAL BUREAU OF STANDARDS-1963-A

be important to confirm that the effect is not temporary, that is, restricted to a certain fluence interval only, since EOL fluences can be high.

Trend of Upper Shelf Reduction at Low-to-Intermediate Fluence

Analysis of the data relating percentage upper shelf reduction and fluence for the weld metals in the low-to-intermediate fluence interval suggests a relationship of the form:

$$\text{Upper Shelf Reduction (\%)} = A\,(\Phi^{cs})^{n}$$

where A and n are constants for a material. The value of A varies with material and is an indicator of material radiation sensitivity. The exponent, n, on the other hand, appears relatively material independent and has a value of about 2.3. Welds NRL 2 and NRL 8 which exhibited the largest upper shelf reduction of the materials at 4×10^{18} n/cm^2 depart from the primary data pattern. In these two cases, lower values of n are required to fit the data. Investigations to further explore the trend relationship are in progress.

DISCUSSION

One objective of the present study was to test the conservatism of NRC Regulatory Guide 1.99 projections in the low-to-intermediate fluence range, recognizing that only sparse data were previously available for defining property-change limits in this interval. Entry of the new data on the graphs indicates that the Guide may be overly conservative in projecting upper shelf reductions at low fluences and at intermediate fluences. A lesser degree of overconservatism is noted for its transition temperature projections.

In Fig. 46, the data suggest that upper shelf change might be more accurately described by a set of bilinear curves such as used to project transition temperature behavior (Fig. 47). Similar evidence from surveillance programs, however, would be required before new curves could be promulgated. Unfortunately, surveillance data appear to be more scattered in this format and are illustrative of a broad range of performance at low fluences. Appreciable reductions in upper shelf have been observed for some long term reactor surveillance irradiations to further cloud the analysis.

In Fig. 51, measured and projected transition temperature increases are compared. Here, a broad scatter is evident, particularly at the higher embrittlement levels. The source of the scatter has not been established but may be due partially to the lack of a term for nickel content in the projection formula. That is, data are available which indicate that nickel content can cause a reenforcement of the primary copper content effect on radiation sensitivity [38,39].

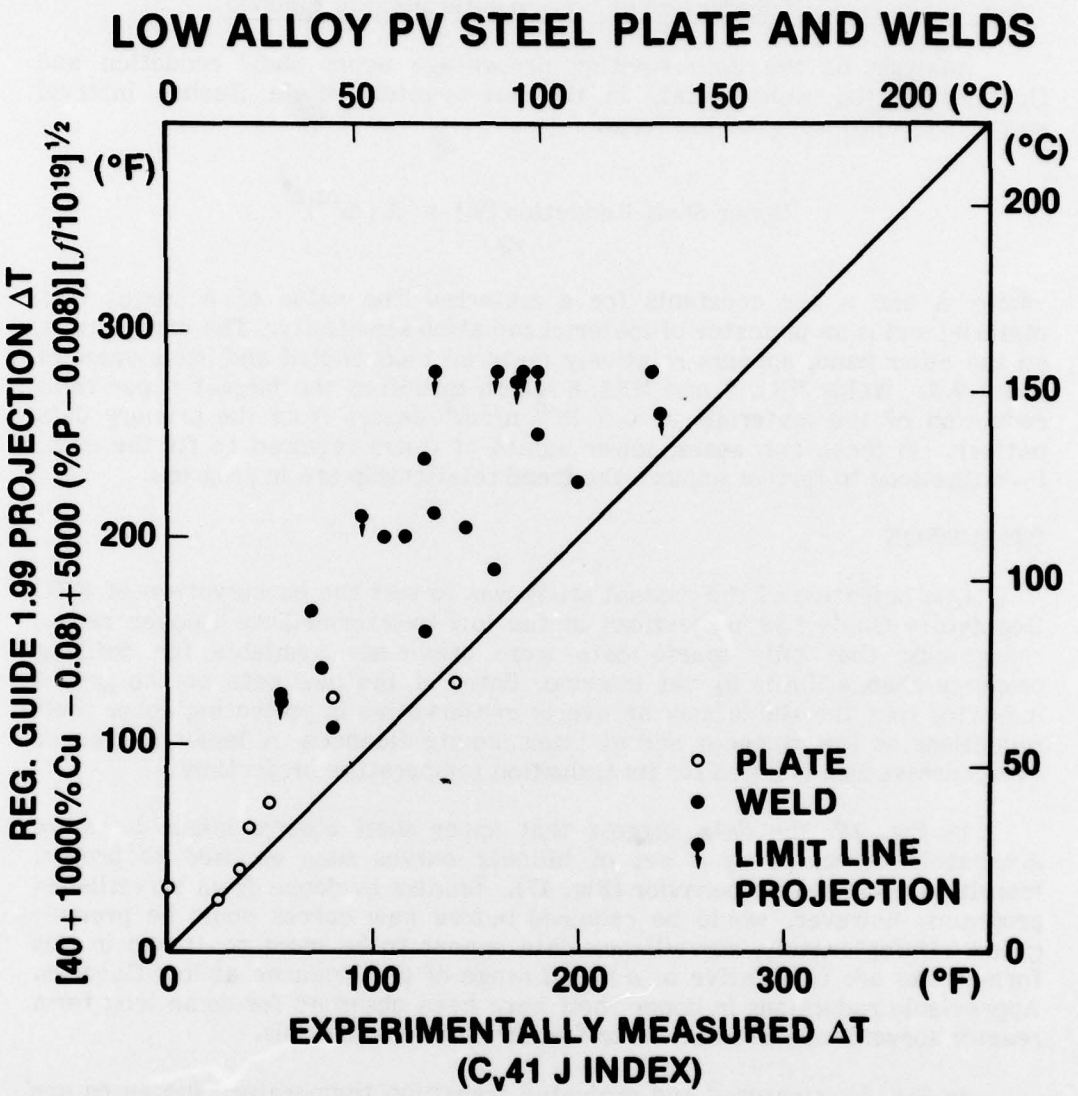

Fig. 51 — Comparison of NRC Regulatory Guide 1.99 projection of transition temperature elevation with experimental measurement for the individual plates and welds. A wide variation in the conservatism of Guide projections is noted.

To summarize, the new data suggest that current penalties at low fluence could be reduced provided that reasons for inconsistencies in surveillance data become understood. The possibility for a reduced penalty appears to be greatest for upper shelf energy properties.

CONCLUSIONS

1. At low fluences of 1 to 2 x 10^{18} n/cm^2, high radiation sensitive steels begin to exhibit changes in notch ductilitiy. Transition temperature elevations in excess of 11^{o}C (20^{o}F) but not upper shelf reductions were observed at this fluence level.

2. Fluences of 3 to 4.5 x 10^{18} n/cm^2 produced transition temperature elevations of 39 to 100^{o}C (70 to 180^{o}F) and upper shelf reductions of 0 to 15%.

3. At intermediate fluences of 6.5 to 9.5 x 10^{18} n/cm^2, large transition temperature elevations of 69 to 133^{o}C (125 to 240^{o}F) and large reductions in upper shelf energies of 15 to 44% were observed. One weld exhibited 49 J maximum after 7.8 x 10^{18} n/cm^2.

4. For low-to-intermediate fluences, a relationship of upper shelf reduction to fluence of the form, Reduction (%) = A $(\Phi^{cs})^n$, is suggested by the data for most of the materials. The value of A varies with material radiation sensitivity; the value of n is relatively material independent.

5. NRC Regulatory Guide 1.99 may be overly conservative in projecting upper shelf reduction at fluences less than 5 x 10^{18} n/cm^2. A lesser degree of overconservatism was indicated by the data for transition temperature projection.

6. The trend of log percent upper shelf reduction with log neutron fluence appears best described by a set of bilinear curves.

B. Evaluation and Comparison of IAEA Coordinated Program Steels and Welds with 288°C Irradiation

J. R. Hawthorne

BACKGROUND

The International Working Group on Reliability of Reactor Pressure Components (IWG-RRPC), sponsored by the International Atomic Energy Agency (IAEA), is conducting a coordinated study of the radiation embrittlement behavior of pressure vessel steels. The research program, formally identified as "Analysis of the Behavior of Advanced Reactor Pressure Vessel Steels Under Neutron Irradiation," was approved by the IAEA Director General in December 1976 [40]. A main goal is to undertake a cooperative study of the radiation embrittlement behavior of improved steels produced in various countries. The stated purpose is to "demonstrate that careful specification of reactor steels can eliminate the problem of potential failure including that caused by neutron irradiation and to demonstrate whether or not knowledge has advanced to the point where steel manufacture and welding technology can routinely produce steel reactor pressure vessels of high radiation resistance" [40].

Materials for the investigation (plate, forging, weld), representing current production practices, are being supplied to the program by the Federal Republic of Germany, France and Japan. A United States-produced A533-B steel plate (HSST Plate 03) is being used as a reference material in a role similar to that played by the ASTM A302-B steel reference plate [41] in reactor vessel surveillance. Material irradiations are being carried out at $290^{\circ}C \pm 10^{\circ}C$. The target fluence range for the study is 1 to 3×10^{19} n/cm^2 >1 MeV.

The Naval Research Laboratory (NRL) is a participant in the IWG-RRPC study under IAEA Research Agreement No. 1661/CF. Particular interest of the NRL investigations include determinations of the irradiation characteristics of the coordinated program materials, the relative radiation resistance of USA versus non-USA steel production, and the correlation of C_v notch ductility, fracture toughness and strength changes with irradiation. Projected results will be of significant value to NRC Regulatory Guide 1.99 [35] for foreign steel evaluations and to current reactor vessel construction codes.

PROGRESS

Standard C_v and fatigue precracked C_v (PCC_v) specimens of five coordinated program materials have been irradiated at 288°C to approximately 1.5×10^{19} n/cm^2 >1 MeV. Four of the materials were supplied by Japan and include two plates, one forging and one weld deposit. The fifth material is the IAEA reference plate. The irradiations were conducted in two experiments in the State University of New York at Buffalo, using its 2 MW pool reactor (UBR).

Table 9 identifies the materials by producer, chemistry, and heat treatment. It will be noted that Plate LG was the parent plate for Weld JW 502. Pre- and postirradiation C_v results are summarized in Table 10. The PCC_v results are summarized in Table 11 and are tentative pending additional tests of the unirradiated condition. Figure 52 compares C_v and PCC_v test data for the A533-B reference plate. Here it will be noted that K_{Jd} determinations by the PCC_v method are not necessarily the K_{Jd} initiation toughness because of the use of maximum load values for the computation. J-integral determinations made on this basis imply the absence of stable (rising load) crack extension and will, in some cases, over estimate the K_J at initiation (see discussion, Section I).

Several observations were made from the results as follows:

1. The C_v 41 J, C_v 68 J and K_{Jd} 100 MPa$\sqrt{m}$ transition temperatures for the Japan-produced materials were considerably lower than those of the IAEA reference plate for the unirradiated condition and for the irradiated condition.

2. The transition temperature elevations by irradiation for the Japan-produced materials were smaller than that for the IAEA reference plate. Of the former, the forging showed the greatest transition elevation with irradiation.

3. The C_v 41 J and the PCC_v K_{Jd} 100 MPa$\sqrt{m}$ transition temperature elevations by irradiation are in good agreement and suggest a possible correlation of benefit to reactor vessel surveillance programs.

4. All of the materials exhibited high ($\geq$135 J, $\geq$ 275 MPa$\sqrt{m}$) upper shelf energy levels before and after irradiation. For the most part, upper shelf reductions were less than 14 J. The largest reductions ($\geq$41 J) were exhibited by the two Japan-produced plates. However, the preirradiation upper shelf levels of these plates were significantly greater than those of the remaining materials.

The observations permit the conclusion that each of the Japan-produced materials have a high resistance to embrittlement by 288°C irradiation. Additionally, these materials showed a greater resistance to radiation than the IAEA reference plate. In this regard, the somewhat poorer performance of the reference plate can be attributed to its higher copper content (i.e., 0.12%Cu versus 0.04%Cu, Japan production.

FUTURE PLANS

Plans for the coming year include parallel evaluations of the IAEA program materials produced in France and Germany.

Table 9 — Identification of Test Materials

Material/ Producer	Codes	Thickness (mm)	Yield Strength (MPa)	Chemical Composition (wt.%) C	Mn	Si	P	S	Ni	Cr	Mo	Cu	Heat Treatment
HSST A533-B Plate 03 (Lukens Steel)	3MU, 3NE	305	464	.20	1.26	.25	.011	.018	.56	.10	.45	.12	1
Japan A533-B Plate (Nippon Steel)	107	251	442	.18	1.48	.22	.007	.007	.66	.20	.57	.01	2
Japan A508-3 Forging (Japan Steel)	212, 213	302	462	.18	1.35	.27	.007	.005	.76	.12	.49	.04	3
Japan S/A Weld (Mitsubishi)	502, 503	248	530	.07	1.20	.32	.008	.003	.89	.06	.50	.04	4
Japan A533-B Plate (Parent Plate Weld 502)	LG	245	444	(Not Available)									5

Heat Treatments:

1. 843 to 899°C - 4 hr, WQ; 649 to 677°C - 4 hr, AC; 607 to 635°C - 20 hr, FC.
2. 880°C - 8 hr, WQ; 660°C - 6 hr, AC; 620°C - 26 hr, FC.
3. 870 to 900°C - 6.4 hr, WQ; 635 to 645°C - 7.8 hr, AC.
4. (PWHT) - 615°C - 26 hr, FC.
5. Not known.

Table 10
Summary of Preirradiation and Postirradiation

Charpy-V Notch Ductility Properties of Test Materials

Material	Transition Temperature C_v 41J (°C)			Transition Temperature C_v 68J (°C)			Transition Temperature C_v 0.9 mm (°C)			Upper Shelf Energy (J)			Upper Shelf Lateral Expansion (mm)		
	Initial	Irrad.	Change	Initial	Irrad.	Change	Initial	Irrad.	Change	Initial	Irrad.	Change	Initial	Irrad.	Change
HSST 03	- 1	43	44	29	76	47	24	80	56	138	136	∿0	2.0	1.6	0.4
JP 107	-46	-29	17	-35	-21	14	-38	-21	17	> 270	212	≥58	2.3	2.1	0.2
JF 212	-63	-32	31	-54	-21	33	-54	-21	33	∿ 233	∿218	∿15	∿2.1	∿ 2.0	∿ 0.1
JW 502	-42	-23	19	-29	-12	17	-34	- 7	28	184	184	∿ 0	2.2	2.0	0.2
JW(BP) LG	-37	-23	14	-32	-15	17	-34	-15	19	> 270	-228	≥ 37	2.2	1.9	0.3

Table 11 - Summary of Preirradiation and Postirradiation Dynamic Fracture Toughness (K_J) Properties of Test Materials (PCC_V Test Method)

Material	K_{Jd} 100 MPa $\sqrt{m}$ (°C) Initial	Irrad.	Change	Upper Shelf (MPa $\sqrt{m}$) Initial	Irrad.	Change
HSST 03	33	77	44	>240	>235	~0
JP 107	- 1	16	17	>305	>305	~0
JF 212	2	35	33	>325	>295	~0
JW 502	-17	16	33	>290	>290	~0
JW(BP) LG	- 1	16	17	>305	>295	~0

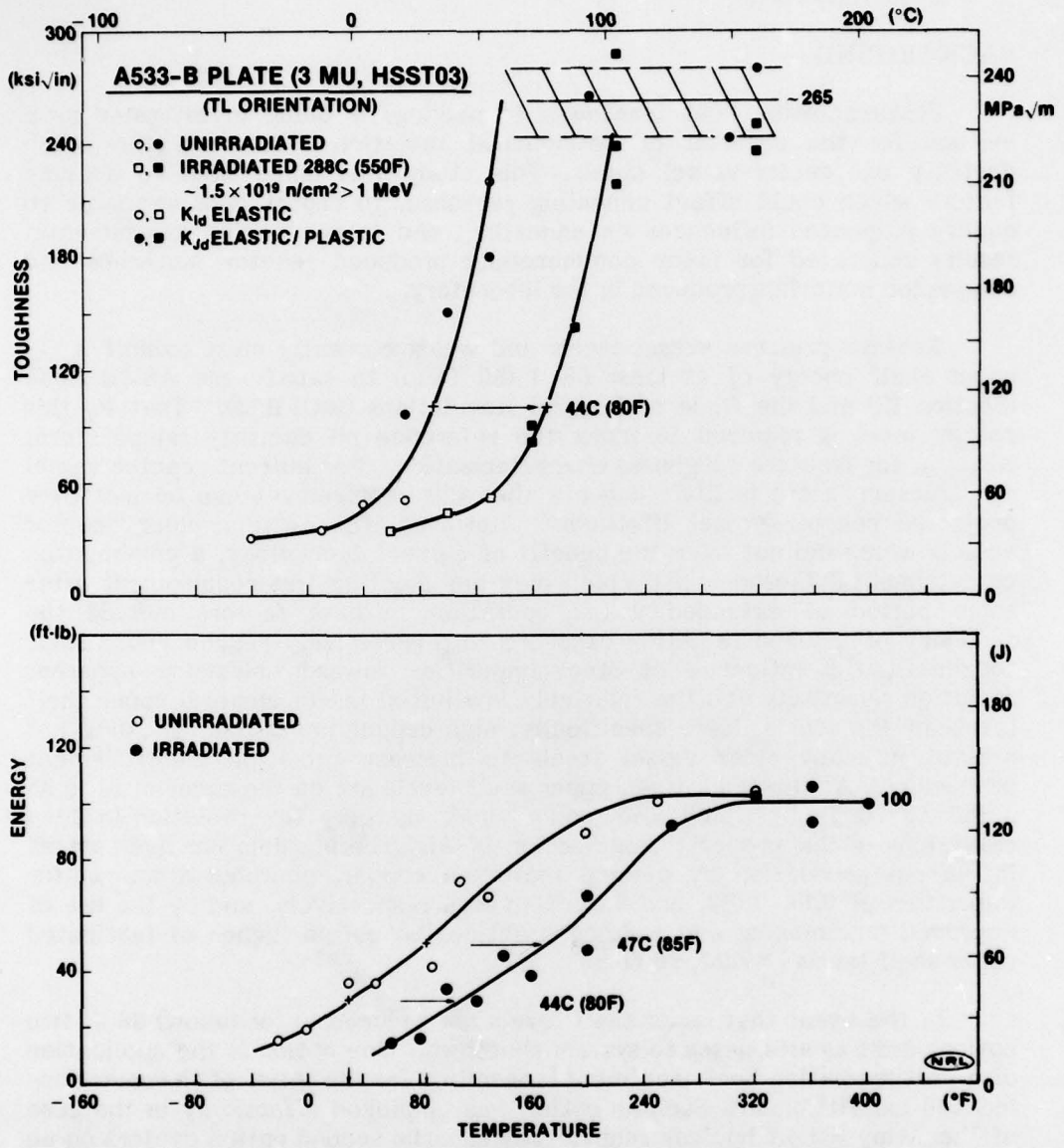

Fig. 52 — Notch ductility and fracture toughness of the United States-produced A533-B steel plate (HSST Program Plate 03) before and after irradiation. Note the good agreement of radiation effects changes determined by the C_v and PCC_v test methods.

C. Survey of Embittlement Relief by Postirradiation Heat Treatment

J. R. Hawthorne

BACKGROUND

Postirradiation heat treatment (annealing) is being investigated as a method for the reversal of detrimental radiation effects to the notch ductility of reactor-vessel steels. This study was undertaken to analyze factors which could affect annealing response, to report data available to qualify suspected influences on annealing, and to summarize experimental results generated for many commercially produced reactor materials and companion materials produced in the laboratory.

Reactor pressure vessel steels and welds currently must exhibit a C_v upper shelf energy of at least 68 J (50 ft-lb) to satisfy the ASME Code (Section III) and the Code of Federal Regulations (10CFR50). That is, this energy level is required to index the reference nil ductility temperature, RT_{NDT}, for fracture toughness characterization. For current reactor vessel construction, there is little concern that this requirement can be met over projected reactor vessel lifetimes. However, for certain older reactor vessels which did not have the benefit of current technology, a combination of detrimental factors exist which may bar meeting this requirement after some period of extended vessel operation. These factors include the tendency of neutron radiation exposure to progressively reduce upper shelf toughness, the influence of steel impurities toward enhancing apparent radiation sensitivity and the relatively low initial (as-fabricated) upper shelf levels of the steels. More specifically, high copper impurities ($\geq$0.20%) are present in many older vessel steels to increase radiation embrittlement tendencies. At the same time, upper shelf levels are on the order of 81 to 95 J (60 to 70 ft-lb) which allow only small margins for radiation-induced reductions in this property (see Section III-A). The problem has been solved in current production by placing limits on copper, phosphorus and sulfur impurities of 0.10, 0.012, and 0.015% (max.), respectively, and by the use of improved steelmaking and welding practices to obtain higher as-fabricated upper shelf levels [>122J, 90 ft-lb].

In the event that upper shelf levels are reduced to (or below) 68 J, two options exist as alternates to system shutdown. One option is the application of a postirradiation heat treatment (annealing) for the relief of the radiation-induced embrittlement. Such an option was employed effectively in the case of the Army SM-1A nuclear reactor vessel. The second option centers on an essentially complete volumetric examination of the beltline region of the vessel and the performance of a fracture mechanics analysis which conservatively demonstrates, making appropriate allowances for all uncertainties, the existence of adequate margins of safety for continued operations.

PROGRESS

A full report on the study [42] has been issued. Highlights are presented here to illustrate the state-of-the-art and to demonstrate the current promise of the annealing method for embrittlement relief.

Analysis of Variables

Several variables were judged to have potential for influencing notch ductility recovery by postirradiation heat treatment. By category these include:

Service Variables

Irradiation temperature,
Neutron fluence,
Relative radiation resistance,
Applied stress,

Steel Metallurgy

Impurity element composition (including Cu, P, S),
Alloy element composition,
Product form (plate, weld, or forging),

Heat Treatment

Annealing temperature,
Annealing time,

Cyclic Irradiation and Annealing Conditions

Annealing time and temperature,
Fluence before first anneal, and
Fluence between anneals.

Synergistic effects between variables were also judged to be possible.

Experimental Qualification of Variables

Within the limitations of the existing experimental data, the contributions or importance of certain of the factors were assessed by the study using direct or indirect test comparisons. Table 12 identifies where assessments were permitted by the data and the qualification made in each case. Among those variables identified as contributing factors, annealing temperature and duration were ranked as having the greatest influence on the recovery of properties. This relationship in turn is reflected in the importance of heat-treatment time and conditions selected for cyclic annealing and reirradiation treatments. Impurity-element composition (copper content) was ranked second in importance. A detrimental effect of a high copper content (0.30% Cu) on upper shelf recovery was demonstrated for A302-B steel. A similar effect for companion weld deposits is quite possible. Of those factors yet to be qualified, four were identified for first priority (see Table 12). Here, the roles of relative radiation resistance and alloying-element composition are of interest to preclude technical surprises in future annealing operations.

Table 12. Status of Experimental Assessments of Variables Suspected of Contributing to the Alleviation of Radiation Embrittlement by Postirradiation Annealing

Variable Description	Experimental Qualification		
	Contributing	Noncontributing	Not Established
Irradiation temperature	X		
Neutron fluence	X[a]		
Relative radiation resistance			X[b]
Applied Stress:			
During irradiation		X	
During annealing			X
Impurity element composition	X		
Alloying element composition			X[b]
Product form			X
Annealing temperature	X		
Annealing duration	X		
Cyclic anneal conditions (temp., time)	X		
Fluence before first anneal			X[b]
Fluence between anneals			X[b]

[a]Dependent on the heat treatment condition.

[b]Suggested priority for future research.

Survey of Existing Data

The data survey indicated that 343°C annealing does not have high promise for reactor vessel applications having first cycle fluences exceeding 1 x 10^{19} n/cm^2 > 1 MeV. On the other hand, it is clear that 399°C annealing or annealing at a somewhat higher temperature does hold significant promise for the embrittlement relief of vessels. With this heat treatment, the survey showed that transition-temperature recoveries of about 55% minimum and 75% maximum can be expected for most materials. More importantly, full upper-shelf recovery for fluences up to 3 x 10^{19} n/cm^2 appears typical with 399°C annealing.

CONCLUSIONS

Although major progress has been made, the study concludes that the present state of the art is insufficiently advanced to permit an immediate consideration of the annealing method for the relief of reactor vessel embrittlement. One basis for this opinion is that experimental data describing property changes with reirradiation are too sparse to confidently base engineering judgments and property projections for this condition. An equally important basis is that knowledge of factors governing reirradiation behavior (senisitivity) is extremely limited. To compound both issues the rate of reembrittlement of annealed material is significantly different (greater) from that of nonannealed material at an equivalent fluence level (see Section III-D). The trend in upper-shelf reduction with reirradiation likewise appears to be significantly different from that of nonannealed material. Beyond first-cycle behavior, information on notch ductility trends with multiple annealing and reirradiation cycles is, in comparison, practially nonexistent. Accordingly, while high-temperature annealing shows promise for embrittlement relief, further research must precede its application. On-going studies at NRL and elsewhere are designed to provide answers to many of the paramount questions on variables and to develop an adequate data bank upon which to judge the merits of annealing for individual cases.

D. Irradiation-Anneal-Reirradiation (IAR) Program Investigation of Charpy-V Notch Ductility Trends

J. R. Hawthorne, H. E. Watson and F. J. Loss

BACKGROUND

The IAR Program is investigating the notch ductility behavior of submerged arc weld deposits with irradiation (I) followed by two full cycles of postirradiation annealing (A) and reirradiation (R). The intent of the program is to identify the merits and potential of in-situ heat treatments for control of radiation induced embrittlement buildup in reactor pressure vessels.

In a preceding section (Section IIIC), reasons for the current interest in the annealing method were reviewed. It is sufficient to say here that vessel annealing is one of three options open in the event that the Charpy-V (C_v) upper shelf level of the vessel steel is reduced to (or below) 68J such that code requirements can no longer be satisfied. Where the annealing option is exercised for embrittlement relief, detailed knowlege of vessel reirradiation behavior will be required. Also, it is conceivable that, for some plants, application of the annealing treatment may be necessary more than once over the system lifetime to maintain the minimum required toughness in the vessel. Unfortunately, a paucity of data exists for single cycle and multicycle annealing and reirradiation behavior. The IAR Program was conceived by NRL in conjunction with NRC to gain an insight into properties behavior under these conditions. Two heat treatment options are being investigated including 343°C (650°F) annealing, representing the use of nuclear or pump heating to attain the vessel annealing temperature and 399°C (750°F) annealing representing the use of auxiliary heat sources. Two welds (Table 13), made commercially with different welding fluxes, were obtained for the study of high versus low (initial) upper shelf level trends.

IRRADIATION EXPERIMENT MATRIX

The plan of irradiation experiments is illustrated in Table 14. Objectives were (1) the development of material test data at the end of each phase of the irradiation-annealing sequence, (2) an irradiation temperature of 288°C (550°F), (3) evaluation of 343°C and 399°C annealing treatments, and (4) development of both notch ductility and fracture data for assessing the potentials of the IAR method.

The target fluence for the first phase exposure was set at 1×10^{19} n/cm^2 >1 MeV because of its approximate correspondence to the knee of the radiation trend curve of transition temperature increase versus fluence at 288°C. Fluences for reirradiation exposures were lower and were dependent upon the degree of recovery observed with the individual annealing treatments.

INITIAL OBSERVATIONS

Findings from Experiments 1 and 2 on IA, IAR, and IARA trends (see

Table 13 - Chemical Compositions of IAR Program Welds

Material	Code	Weight (%) Cu	C	Mn	Si	P	S	Ni	Mo	V	Cr
S/A Weld 1 (Linde 1092 flux)	V84	.35	.14	1.56	.14	.013	.011	.62	.53	.002	.03
S/A Weld 2 (Linde 80 flux)	V86	.35	.08	1.60	.55	.016	.013	.69	.40	.006	-

Heat Treatment	V84	Stress relief annealed 593 to 621°C - 50 hr, furnace cooled to 316°C at 6°C/hr, air cooled.
	V86	Stress relief annealed 621°C -40 hr, furnace cooled to 316°C.

Table 14 - Radiation Experiment Plan (288°C (550°F) Irradiation)

Experiment	Specimen	Designation	Objective
1	C_v	IA	Explore recovery by 343 and 399°C (650 and 750°F) annealing
2	C_v	IAR	Explore reirradiation response of all three materials
3	CT, C_v	I through IARAR	Determine IARAR performance of Weld 1
4	CT, C_v	I through IARAR	Determine IARAR performance of Weld 2

Table 14) have been reported [43]. In brief, the results of these experiments revealed that a 343°C intermediate heat treatment may not be a practical method for the control of radiation embrittlement in reactor vessels because of the high frequency of annealing which would be required. A 399°C heat treatment, on the other hand, showed definite promise for the control of radiation effects buildup in vessels. That is, both welds showed better notch ductility after 399°C annealing and reirradiation than after the first cycle of radiation exposure. Based on this finding, 399°C-168 hr annealing conditions were selected for investigation in Experiments 3 and 4. The target reirradiation fluence was $\sim 0.6 \times 10^{19}$ n/cm^2 > 1 MeV.

RECENT PROGRESS

Charpy-V notch ductility determinations for the IARAR condition of welds V86 and V84 were completed recently; experimental results are shown in Figs. 53 and 54 respectively. Weld properties after the initial radiation exposure (curve I) and after the second intermediate 399°C-168 hr annealing treatment (curve IARA) are also shown for reference. Neutron dosimetry results are not yet available; however, the fluences received during the first radiation cycle (I) and by the second and third (repeat) irradiation cycles (R) are estimated at 1.2, 0.7, and 0.7 x 10^{19} n/cm^2 > 1 MeV respectively. Accordingly, the total fluence received by the IARAR condition is estimated at 2.6 x 10^{19} n/cm^2.

Several important observations are permited by the third-cycle irradiation data. First, the results clearly demonstrate the benefits of intermediate 399°C annealing and that the benefits can be retained through two cycles of reirradiation. Specifically, the upper shelf level of the IARAR condition is significantly higher, in each case, than that of the I condition of the weld. At the same time, the C_v 41J transition temperature for the IARAR condition is significantly lower than that of the I condition. Second, the results confirm the earlier observation [43] for the IAR condition that the rate of reembrittlement of annealed material is higher than that of non-annealed material for the same increment of additional fluence. Third, the upper shelf reduction and transition temperature elevation experienced by the welds during the third cycle of irradiation are about the same as those changes observed for the second cycle of irradiation. If additional data confirm this trend, it would appear that notch ductility changes can be maintained below prefixed limits by carefully selected annealing schedules for individual materials. Moreover, the results indicate a good possibility for optimizing annealing schedules once the effectiveness of 399°C annealing, in terms of residual embrittlement after an anneal and the material reembrittlement rate, is established. The acquisition of further insight into such factors is an important objective of the continuing IAR Program.

STATUS AND FUTURE PLANS

A report providing a complete review and summary of the Phase 1 C_v investigations by the IAR Program is in preparation. The report will include information on hardness and lateral expansion trends observed for the welds during cyclic annealing and reirradiation as well as energy trend information.

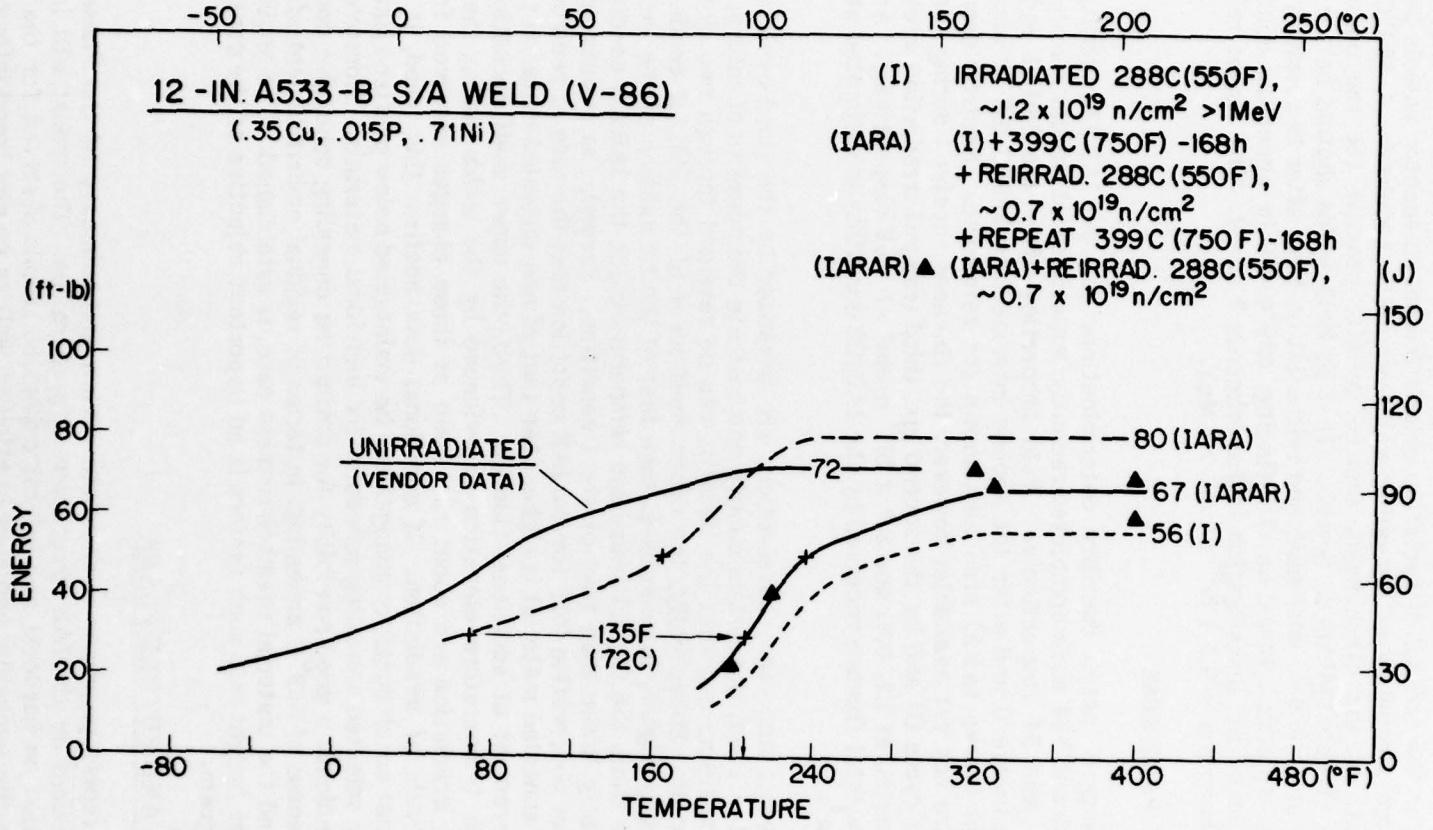

Fig. 53 — Charpy-V notch ductility of Weld V86 after two cycles of intermediate 399°C (750°F)-168 hr annealing and 288°C (550°F) reirradiation. The dashed curves labeled (I) and (IARA) represent the first cycle irradiation and second cycle annealed conditions respectively. A significant benefit of cyclic irradiation and annealing to notch ductility retention is indicated.

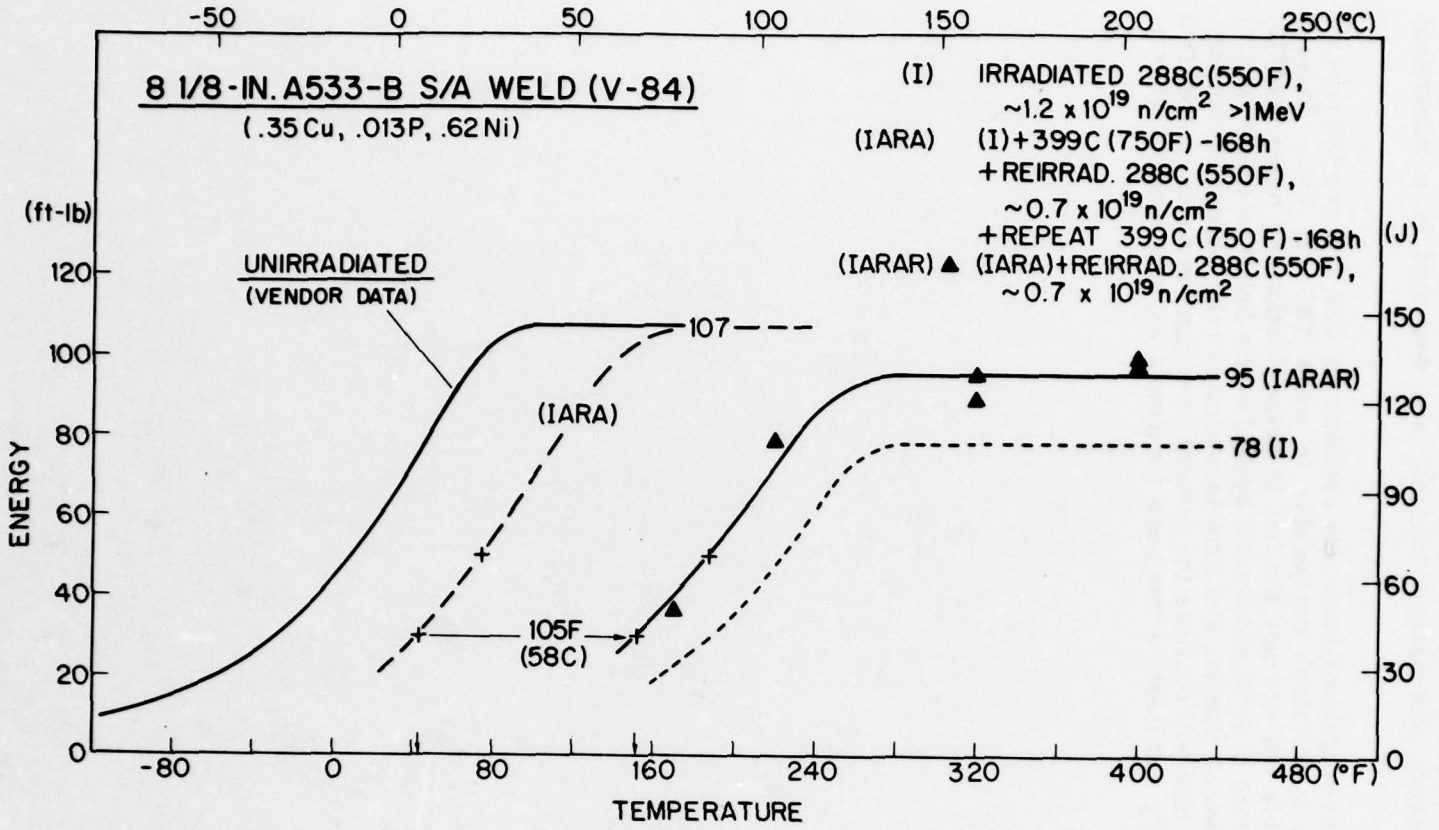

Fig. 54 — Charpy-V notch ductility of Weld V84 after two cycles of intermediate 399°C (750°F) -168 hr annealing and 288°F (550°F) reirradiation. Curves (dashed) indicate properties of the (I) and (IARA) conditions for reference.

Tests of the compact toughness (CT) specimens included in Experiments 3 and 4 have commenced; observations thus far are described in a subsequent section.

Phase 2 investigations have also commenced with the procurement of additional weld metal stock comparable to welds V86 and V84. Phase 2 objectives include but are not limited to determinations of notch ductility trends as functions of first and second cycle fluence levels, reembrittlement rate as a function of fluence, and time-temperature relationships in recovery. Phase 2 studies also will continue the present investigation on the correlation of notch ductility and fracture toughness for irradiated, annealed and reirradiated conditions.

IV. ABSTRACTS OF REPORTS AND PUBLICATIONS FOR FISCAL YEAR 1979

A. Reports

SURVEY OF POSTIRRADIATION HEAT TREATMENT AS A MEANS TO MITIGATE RADIATION EMBRITTLEMENT OF REACTOR VESSEL STEELS

J. R. Hawthorne

NUREG/CR 0486; NRL Report 8287; February 14, 1979; also Proceedings, IAEA Specialists' Meeting on Irradiation Embrittlement, Thermal Annealing and Surveillance of Reactor Pressure Vessels, Vienna, Austria, 26-28 February 1979.

Postirradiation heat treatment (annealing) is being investigated as a method for the alleviation of radiation embrittlement to reactor vessel steels. Objectives of this study were to identify those service and metallurgical variables which can affect annealing response, to report data comparisons available for qualification of suspected influences, and to survey experimental results from commercially produced reactor materials and duplicate materials from the laboratory.

Twelve factors are identified as having potential for affecting the postirradiation heat treatment response of low-alloy pressure vessel steels. A tentative qualification of six factors as significant contributing variables is made on the basis of experimental comparisons. Of these, heat-treatment temperature was observed to exert the largest influence on the embrittlement relief by annealing. The evidence indicates that a 399°C heat treatment, but not a 343°C heat treatment, is a practical and effective method for reducing and controlling radiation embrittlement in reactor vessels.

* * *

SIGNIFICANCE OF COPPER, PHOSPHORUS, AND SULFUR CONTENT TO RADIATION SENSITIVITY AND POSTIRRADIATION HEAT TREATMENT OF A302-B STEEL

J. R. Hawthorne

NUREG/CR 0327; NRL Report 8264; April 12, 1979

The effects of three levels of copper content and phosphorus content and two levels of sulfur content on radiation sensitivity and postirradiation heat treatment response were explored for a reactor pressure vessel steel, Type A302-B. Test plates for the investigation were produced from 182-kg (400-lb) laboratory melts. The contributions of individual elements were assessed from Charpy-V (C_v) notch ductility changes with 288°C (550°F) irradiation and with a 343°C (650°F)-168 hour postirradiation heat treatment.

Limited studies of properties recovery by postirradiation 399°C (750°F) heat treatment were also made.

Radiation embrittlement sensitivity, as shown by C_v transition-temperature elevation and C_v upper shelf reduction, generally increased with increased copper and phosphorus content and with decreased sulfur content. Certain ranges of phosphorus and copper content were found to be more critical than others.

Response to 343°C (650°F) postirradiation heat treatment, as evidenced by transition temperature recovery in degrees C, appeared to be independent of copper, phosphorus, and sulfur content for the ranges investigated. Response to heat treatment also appeared to be independent of the magnitude of the prior transition temperature elevation by irradiation. On the other hand, a dependence of percentage recovery on impurity-element content was observed. A dependence of upper shelf recovery on copper content was also found.

Six of the eight plate compositions exhibited full upper shelf recovery but only small transition temperature recovery after 343°C (650°F) heat treatment.

* * *

FRACTOGRAPHIC AND MICROSTRUCTURAL ANALYSIS OF FATIGUE SPECIMENS OF A302 GRADE B STEEL TESTED IN AIR AT ROOM TEMPERATURE

G. Gabetta[a] and V. Provenzano

NUREG/CR 0968; NRL Memorandum Report 4062; September 28, 1979

Microscopic studies were undertaken to characterize the failure processes and to establish correlations with fatigue crack propagation data of Type A302-B ferritic steel tested in air at room temperature. A cooperative program was established between the Naval Research Laboratory (NRL) and the Centro Informazioni Studi Esperienze (CISE) to investigate the fatigue properties of this ferritic steel for nuclear pressure vessel applications. Failed specimens have been examined by scanning electron microscopy (SEM), by metallographic techniques, and by energy dispersive X-ray microanalysis. SEM examinations of the fracture surfaces of specimens cut in the T-L direction revealed the presence of inclusion bands above an observed ΔK threshold value. Subsequent X-ray image scans and corresponding energy spectra showed that the bands were manganese-sulfide inclusions. The inclusion bands resulted in increased crack growth rate in these specimens compared to those cut in the L-T orientation specimens. The ΔK threshold value necessary to activate the inclusion bands is thought to be a measure of the cohesive strength between the inclusions and the material matrix. The failure mode of all the specimens tested was transgranular; extensive microcracking was also present in the fracture surfaces. The microcracking did not appear to have affected the crack propagation behavior.

[a]Permanent address, Centro Informazioni Studi Esperienze (CISE), Research Labortories, Milan, Italy

* * *

FATIGUE CRACK GROWTH OF A508 STEEL IN HIGH-TEMPERATURE, PRESSURIZED REACTOR-GRADE WATER

W. H. Cullen, V. Provenzano, K. Torronen,[a] H. E. Watson, and F. J. Loss

NUREG/CR 0969; NRL Memorandum Report 4063; September 28, 1979

Fatigue crack growth tests of A508-2 pressure vessel steel have been conducted at two test temperatures (93° and 288°C) using a variety of constant amplitude waveforms. The load ratios were either 0.1 or 0.125, and the water chemistry was carefully monitored and controlled so as to simulate the nominal pressurized water reactor chemistry. The test procedures are described, and an examination of all the data indicates that the results fall into one of two rather clearly defined categories. One band of data, termed "low", lies close to or essentially on, the ASME Section XI Code air environment default line. The other band of data, termed "high", resides approximately midway between the ASME Section XI air and water environment default lines.

The two bands of data are the result of certain combinations of the waveform and temperature variables listed above and are determined by the following rules:

(1) A ramp time in excess of one second is needed to obtain the high crack growth rate.

(2) The application of a hold time, together with a high temperature, serves to depress a normally high crack growth rate test (i.e., one with a long ramp time) and force it into the low category.

A hydrogen embrittlement model is used as a basis for the explanation of this behavior. During the longer ramp times (∿ one second) hydrogen, formed by aqueous hydrolysis, diffuses into the plastic zone, resulting in local embrittlement. However, if the test involves a waveform with a hold time component and a high temperature, the hydrogen diffuses out of the plastic enclave and the crack growth rates are not accelerated from the "low" to the "high" category. Short ramp times (∿one second) at either temperature, do not allow a significant production of hydrogen ions, and the growth rates remain in the "low" category.

The suggested mechanism is supported by fractographic observations of increased intergranular and quasi-cleavage components for the hydrogen assisted fatigue crack growth modes, while the fatigue fracture surfaces of specimens from the low growth rate category showed a higher percentage of striation formation and transgranular growth modes.

---

[a]Technical Research Center of Finland

---

* * *

NOTCH DUCTILITY DEGRADATION OF LOW ALLOY STEELS WITH LOW-TO-INTERMEDIATE NEUTRON FLUENCE EXPOSURES

J. R. Hawthorne

NUREG/CR 1053; NRL Report 8357, November 1979; also proceedings, Third ASTM-EURATOM Symposium on Reactor Dosimetry, Ispra, Italy, 1-5 October 1979

The extent and trend of Charpy-V (C_v) notch ductility changes in reactor vessel materials with fluences of 1×10^{18} to 10×10^{18} n/cm^2 >1 MeV were investigated with several thick section steel plates and submerged arc weld deposits irradiated at 288°C (550°F). The materials were fully represen tative of reactor vessels now in service and had copper contents ranging from 0.10 to 0.40% and phosphorus contents ranging from 0.008 to 0.020%. Material irradiations were performed in a 2 MW pool reactor.

The steels with high radiation sensitivity indicated an onset of notch ductility change at fluences of $\sim 1.5 \times 10^{18}$ n/cm^2 by an elevation in the ductile-to-brittle transition temperature. Reductions in upper shelf were not observed at this fluence level but were in the range of 0 to 15% at $\sim 4 \times 10^{18}$ n/cm^2 and beteween 15 to 44% at $\sim 8 \times 10^{18}$ n/cm^2. The data trend suggest a power law relationship of upper shelf reduction to fluence at low-to-intermediate fluences.

The C_v transition temperature elevation and upper shelf reduction with irradiation are compared to embrittlement projections by U. S. Nuclear Regulatory Commission Guide 1.99. A limited experimental comparison of radiation effects to dynamic fracture toughness and notch ductility is also presented.

B. Books

EXPLORATORY INVESTIGATIONS OF CYCLIC IRRADIATION AND ANNEALING EFFECTS ON NOTCH DUCTILITY OF A533-B WELD DEPOSITS

J. R. Hawthorne, H. E. Watson, and F. J. Loss

in Irradiation Effects on the Microstructure and Properties of Metals, ASTM STP 683, 1979.

Postirradiation heat treatment (annealing) is being investigated as a possible method for the periodic relief of radiation embrittlement to reactor vessel steels. This report describes a study of the Charpy-V (C_v) notch ductility of two representative A533-B weld deposits under two full annealing and reirradiation cycles. The welds were specially chosen for their high sensitivity to radiation effects and for their difference in as-fabricated C_v uppershelf energy levels. Notch ductility properties were developed at each point in the irradiation-annealing sequence. Heat treatment temperatures

were selected to represent the two heat treatment options open for vessel annealing.

The results demonstrate that a 399°C (750°F)-168 hour heat treatment is highly effective for reducing radiation embrittlement accrual in service; in contrast, a 343°C (650°F)-168 hour heat treatment is shown to be ineffective for the fluence conditions investigated. A greater rate of radiation embrittlement was observed for the heat treated material (both conditions) compared to non-heat treated material. The investigations also revealed a significant difference between upper shelf energy and transition temperature response to heat treatment.

* * *

A COMPUTERIZED DATA ACQUISITION SYSTEM FOR A HIGH TEMPERATURE, PRESSURIZED WATER FATIGUE TEST FACILITY

W. H. Cullen, B. H. Menke, H. E. Watson and F. J. Loss

in Computerized Automation of Materials Testing, ASTM STP 710 , 1979.

The hardware and software of a data acquisition system for a high-temperature, high-pressure water fatigue crack growth facility is described in this article. This system monitors crack lengths of fifteen specimens, together with water pressures, temperatures and water chemistry data such as dissolved oxygen content, pH and specific conductance. The measurement strategy is defined by the cyclic count: each of the specimens has its unique measurement targets and measurement interval. The computer constantly compares the instantaneous accumulated count with the count targets of the fifteen specimens and enters a data acquisition subprogram when any count target is reached. The methods of data acquisition, data reduction, file management, input/output and system status modification are described.

* * *

DYNAMIC FRACTURE ANALYSIS OF NOTCHED BEND SPECIMENS

S. Mall[a], A. S. Kobayashi[b], and F. J. Loss

in Crack Arrest Methodology and Applications, ASTM STP 711 , 1979.

A dynamic finite element code was used to determine dynamic initiation fracture toughness, K_{Id}, in 25.4 mm (1 in.) thick notched bend specimens of A533-B steel and a 15.9 mm (5/8 in.) thick dynamic tear (DT) specimen of 6061 aluminum alloy. These specimen types can reflect varying dynamic fracture response due to differences in test temperature, specimen geometry and material as well as notch tip sharpness. Measured load-time histories were applied to the tup as modeled by finite elements and the dynamic stress intensity factor was computed by a calibrated COD procedure. Dynamic stress intensity factors were also computed by the ASME E-399 procedure using a load based on local dynamic strain measurements and a static K-calibration.

Reasonable agreements between measured and computed dynamic strains in the vicinity of the crack tip verified the accuracy of the dynamic finite element model. The attendant agreement between measured versus computed time-varying dynamic stress intensity factors also verified, for the first time, the applicability of the ASTM E-399 procedure for the computing dynamic initiation fracture toughness, K_{Id} on the basis of local dynamic strain measurements.

---

[a]Assistant Professor, Mechanical Engineering, University of Maine, Orono, Maine 04473

[b]Professor, Department of Mechanical Engineering, University of Washington, Seattle, Washington 98195

---

* * *

DUCTILE FRACTURE ANALYSIS AND SAFETY OF NUCLEAR PRESSURE VESSELS

F. J. Loss

in Risk and Failure Analysis for Improved Performance and Reliability, Plenum Publishers, New York, 1979.

The current status of fracture characterization procedures has been reviewed for light water reactor structures. These methods are contained in the ASME Boiler and Pressure Vessel Code, Sections III and XI, as well as in Federal Regulations. The Code rules are based upon linear elastic fracture methods as a rational tool to provide a quantitative assessment of the margin of safety against fracture. In combination with associated ASTM Standards and Nuclear Regulatory Guides, the current procedures provide rules for materials testing, test and acceptance standards, standards for radiation damage assessment, and a means for relating material toughness to the requirements of the application.

While these procedures provide a relatively conservative-analytical approach for the avoidance of non-ductile failure, there are areas where improvement must be sought to provide more rigorous or less assumptive bases. An assessment of our current status has shown that more information is required in the areas of low upper shelf energy and interpretation of surveillance specimen results. The potential problems associated with low shelf energy can affect several USA plants and this results primarily from the use of beltline weld metals that are unusually sensitive to irradition. Currently available analyses are inadequate to deal with this problem. Also, the C_v upper shelf energy expected in these plants in the near future has not been rigorously related to the flaw size tolerance of the pressure vessel nor to the margin of safety available. If this problem is not successfully resolved by analysis, it still appears possible to extend plant lifetime by producing

embrittlement relief though periodic heat treatment for thermal correction (annealing) of radiation embrittlement.

Much of the future progress in fracture characterization rests in the advancement of elastic-plastic fracture. Of the various approaches to this area, a major research effort exists to investigate applications of the J integral. This method projects a significant advantage in the use of small specimens to characterize the toughness of large structures, such as reactor vessels, which are subject to a higher mechanical constraint. Current investigations with the J integral are promising for use with irradiated materials, including surveillance specimens. With respect to structural integrity, a new approach is described that deals with the topic of tearing instability. This method offers potential for the analysis of vessel integrity when the material exhibits a low upper shelf toughness as well as high toughness.

In conclusion, it is believed that the past decade has produced significant research information and related codes and rules which help assure the safety and reliability of nuclear structures. Future research in the areas outlined will enhance our abilities to quantify the margin of safety, to assure the continued reliability of nuclear power, and may even allow some relaxation of current conservatisms.

* * *

J-R CURVE CHARACTERIZATION OF IRRADIATED NUCLEAR PRESSURE VESSEL STEELS

F. J. Loss, B. H. Menke, R. A. Gray, Jr., and J. R. Hawthorne

in Proceedings, CSNI Specialist Meeting on Plastic Tearing Instability, St. Louis, Missouri, 25-27 September 1979

The J-R curve trends of an A533-B plate and a submerged arc weld deposit having a high copper impurity content have been charcterized by means of the single specimen compliance technique. The program involved 1T compact specimens with 20% side grooves which were irradiated to a nominal fluence of 1×10^{19} n/cm^2 >1 MeV. The R curve for these steels exhibits a power law behavior. This curvature precludes both an exact determination of J_{Ic} by the proposed ASTM multispecimen standard as well as the calculation of a single value of tearing modulus to represent the initial R-curve slope. An alternative measurement procedure for J_{Ic} is proposed whereby this quantity is taken as the J value corresponding to a fixed level of crack extension which exceeds that due to crack-tip blunting. This procedure provides a straightforward means for evaluating J_{Ic} for cases of cleavage failure for which the maximum ductile crack extension exceeds that due to blunting by a relatively small amount.

After irradiation the plate material exhibited only a slight decrease in J_{Ic} within the upper shelf temperature regime. On the other hand, the tearing modulus, taken as a least squares fit to the initial portion of the R

curve, decreased to 65 which represents one half of the value for the unirradiated material. The upper shelf J_{Ic} of the weld deposit exhibited a greater degradation with irradiation than did J_{Ic} for the plate. The J_{Ic} of the weld was reduced to one half of its preirradiation value, i.e., 65 kJ/m^2 (373 in.-lb/in.^{2}); this corresponds to a K_{Jc} value of 113 MPa $\sqrt{m}$ (103 ksi $\sqrt{in.}$). Similar to the plate material, the tearing modulus exhibited a greater decrease with irradiation than did J_{Ic}. The former was reduced to a level of 30 which reflects approximately one third of its preirradiation value.

* * *

REVIEW OF IAEA SPECIALISTS' MEETING ON IRRADIATION EMBRITTLEMENT, THERMAL ANNEALING AND SURVIELLANCE OF REACTOR PRESSURE VESSELS

L. E. Steele

Proceedings, IAEA Specialists' Meeting, Vienna, Austria, 26-28 February 1979

The basic theme of the meeting was the exposition of knowledge which will permit the evaluation or projection of the reactor pressure vessel condition after neutron irradiation so as to assure vessel integrity for the reactor's economic life. This applies both to current and future light water reactors (LWR) systems. With this basis, the participants, organizers, authors, and discussors freely provided the latest available information as well as ideas for added research and development to meet the theme goal.

Papers from Belgium, Czechoslovakia, France, the Federal Republic of Germany, India, Japan, The Netherlands, Sweden, the United Kingdom and the United States covered various topics within the framework of studies on irradiation embrittlement, surveillance, and thermal annealing to correct radiation damage. It was agreed that the collective result in the long run would be to provide the basic data on which to base criteria for assurance of LWR vessel integrity. Such information is considered of value to those companies (or nations) now owning operating reactors and to those companies (or nations) contemplating the acquisition of a nuclear power plant or plants.

The technical papers and technical discussion emphasized new developments in our understanding of irradiation embrittlement, the influence of individual component elements of vessel steels on sensitivity to neutron radiation, the fracture response of steels to conventional (usually Charpy V-notch) fracture tests, the potential value of new, less conventional fracture mechanics (quantitative) tests as applied both before and after irradiation, the current national or company approaches to surveillance of fracture response of vessel steels and the potential for radiation damage correction by postirradation heat treatment or annealing. The latter included discussions of the factors responsible for the engineering feasibility of this process which would be applied only as "last resort."

* * *

STEELS AND WELD METALS USED FOR WATER-COOLED NUCLEAR REACTOR VESSELS

J. R. Hawthorne

Proceedings, International Atomic Energy Agency Technical Committee Meeting on Accuracies in Correlation Between Property Change and Exposure of Vessel Steel Irradiations, Julich, Germany, 22-29 September 1979

The application of steels and weld metals in the construction of reactor vessels and material fabrication, heat treatment and qualification practices are reviewed in relation to vessels produced in the USA, Japan and Western Europe. A use of comparable materials is evident. Material state variations in as-fabricated properties and variations in response to the nuclear environment are also reviewed. Significant progress is reported in the development and use of advanced steels and weld metals in reactor vessel construction. Specific improvements are cited in preservice (unirradiated condition) properties and in steel resistance to detrimental radiation effects. The need for and general objectives of on-going research on steel radiation sensitivity are also discussed.

* * *

C. Journals

FIFTH INTERNATIONAL CONFERENCE ON STRUCTURAL MATERIALS IN REACTOR TECHNOLOGY

L. E. Steele

European Scientific Notes, Office of Naval Reseach-London, 1979.

Detailed information on the organization, purpose and content of the meeting are presented. Particular attention is given to the Post-Conference Seminar on Assuring Structural Integrity of Steel Reactor Pressure Vessels which was a part of the general conference. Topics covered in this seminar included design, materials selection, fabrication, problems of in-service degradation and provisions for dealing safely with these, as well as the national codes, standards, and regulations which impinge upon the design, construction, and operation of nuclear power plants and especially the primary vessel.

A panel discussion, drawing together experts from the various subject areas treated, concentrated upon design and fabrication technology, as well as experience in the operation of nuclear power plant and how these together permit one to project the potential for structural reliability. Much of the discussion centered on probabilistic versus deterministric approaches to integrity evaluation and on lessons learned from a post-accident review of Three Mile Island.

* * *

U. S. METAL PROPERTIES COUNCIL ACTIVITIES PERTINENT TO REACTOR VESSEL INTEGRITY

L. E. Steele, T. R. Mager[a], A. O. Schaefer[b], and J. J. Koziol[c]

Proceedings, First International Conference on Structural Mechanics in Reactor Technology, Berlin, Germany, 13 August 1979, Nuclear Engineering and Design, November 1979.

This invited paper was prepared so as to describe the goals and organization of The Metal Properties Council (MPC) and its particular activities in support of the subject conference. The organizational support by MPC of nuclear power which has been through the ASTM, ANSI, ASME, the Pressure Vessel Research Committee, the Electric Power Research Institute, and the Edison Electric Institute, were reviewed along with a more detailed review of the technical support. The latter covered mainly the activities of three task groups since 1973.

The first of the technical task group activities was a combined task group of the MPC and PVRC on fracture toughness of nuclear components which resulted in a massive program sponsored by the Electric Power Research Institute and an ongoing series of working groups on fracture toughness properties of reactor vessel steels including the dynamic fracture toughness of such steels, a working group on elastic-plastic analysis, a problem for the future now undergoing review, and a working group on crack arrest analysis. This represents the activities described for the task group on fracture toughness.

A second task dealt with prediction of the brittle-to-ductile transition of irradiated reactor pressure vessels. This involved a statistical analysis of all of the data, both from experimental and surveillance programs, for irradiation embrittlement of reactor pressure vessel steels. The results of this study, just completed, are to be made available to the public soon. The study indicated significant trends, the most striking being divergence between accelerated and low irradiation exposure rate studies.

A third major activity now ongoing was described. This involves a task group on reactor vessel surveillance, data collection and analysis. The major goal of this is a book to be published within the next year with chapters from all major reactor vendors in the United States, emphasizing their views, particularly on future reactor vessel surveillance, relative advancements affecting surveillance analysis, as well as a major analysis of results from approximately 30 reactors which have produced surveillance results. This book is being edited by the presenter and will be published by the American Society for Testing and Materials as a serial to an earlier volume published in 1970.

---

[a]Westinghouse Electric Corporation, Pittsburgh, PA.

[b]Executive Director, The Metal Properties Council, New York, NY.

[c]Combustion Engineering, Inc., Windsor, CT.

REFERENCES

1. F. J. Loss, Editor, "Structural Integrity of Water Reactor Pressure Boundary Components, Quarterly Progress Report, April-June 1979," NUREG/CR-0943, NRL Memorandum Report 4064, September 28, 1979.

2. S.J. Hudak, Jr., A. Saxena, R.J. Bucci, and R.C. Malcolm, "Development of Standards Methods of Testing and Analyzing Fatigue Crack Growth Rate Data - Final Report," AFML TR 78-40, Air Force Materials Laboratory, May 1978.

3. F.J. Loss, Editor, "Structural Integrity of Water Reactor Boundary Components - Progrss Report Ending 30 Nov 1977," NRL Memorandum Report 3782, May 1978.

4. G.A. Clarke and J.D. Landes, "Evaluation of J for the Compact Specimen," Scientific Paper 78-ID3-JINTF-P1, Westinghouse R&D Center, Pittsburgh, PA., June 12, 1978.

5. P. Paris, H. Tada, A. Zahoor, and H. Ernst, "A Treatment of the Subject of Tearing Instability," NUREG-0311, Nuclear Regulatory Commission, Aug. 1977.

6. J.A. Joyce, and J.P. Gudas, "Computer Interactive J_{Ic} Testing of Navy Alloys," ASTM STP 668, American Society for Testing and Materials, April 1977, Philadelphia, PA, pp. 451-568.

7. J.R. Hawthorne, Editor, "The NRL-EPRI Research Program (RP886-2), Evaluation and Prediction of Neutron Embrittlement in Reactor Pressure Vessel Materials, Annual Progress Report for CY 1978," NRL Report 8327, August 30, 1979.

8. "The Determination of the Elastic-Plastic Toughness Parameter, J_{Ic}," ASTM Committee E24.08.04, ASTM, Philadelphia, PA, Sep. 14, 1979.

9. H. Tada, personal communication.

10. F. J. Loss, editor, "Structural Integrity of Water Reactor Pressure Boundary Components, Progress Report Ending 29 February 1976," NRL Report 8006, NRL-NUREG-2, August 26, 1976.

11. F. J. Loss, J. R. Hawthorne, and C. A. Griffis, "Fracture Toughness of Light-Water Reactor Pressure Vessel Materials, Progress Report Ending 28 February 1979," NRL Memorandum Report 3036, April 1975.

12. "Standard Method of Test for Plane-Strain Fracture Toughness of Metallic Materials, E399-74," Book of ASTM Standards, Part 10, ASTM, Philadelphia, Pa., 1975.

13. S. Mall, A. S. Kobayashi, and F. J. Loss, "Dynamic Fracture Analysis of Notched Bend Specimens," in Crack Arrest Methodology and Applications, ASTM STP 711 (in press).

14. W.H. Cullen, et al., "Fatigue Crack Growth of A508 Steel in High-Temperature, Pressurized Reactor-Grade Water," NUREG/CR-0942, NRL Memorandum Report 4063, Sep. 28, 1979.

15. W.H. Cullen, et al., "A Computerized Data Acquisition System for a High-Temperature, Pressurized Water Fatigue Test Facility," in Computer Automation of Materials Testing, ASTM STP 710, American Society for Testing and Materials, Philadelphia, Pa. 19103 (pending publication).

16. G. Gabetta and V. Provenzano, "Fractographic and Microstructual Analysis of Fatigue Specimens of A302 Grade B Steel Tested in Air at Room Temperature," NUREG/CR-0968, NRL Memorandum Report 4062, Sep. 28, 1979.

17. V. Provenzano, et al., "Fractographic and Microstructural Analyses of Stress Corrosion Cracking of A533 Grade B Class 1 Plate and A508 Class 2 Forging in Pressurized Reactor Grade Water at 93°C," in Proceedings of Symposium on Fractography and Materials Science, Williamsburg, Va., 27-28 November 1979.

18. P. Albrecht and K. Yamada, "Simulation of Service Fatigue Loads for Short Highway Span Bridges," Symposium on Service Fatigue Loads Monitoring, Simulation and Analysis, ASTM STP 671 (1977).

19. P. Albrecht, et al., "Fatigue Strength of Overloaded Bridge Components," Report FHWA-MD-R-76, Dept. of Civil Engineering, University of Maryland, College Park, Maryland 20742.

20. W.H. Bamford and L.J. Ceschini, "Effects of High Temperature Primary Water on the Fatigue Crack Growth of Reactor Vessel Steels," in HSST Quarterly Progress Report for July-September 1977, ORNL/NUREG/TM-166, pp. 38-45 (April 1978).

21. T.L. Gerber, J.D. Heald, and E. Kiss, "Fatigue Crack Growth in SA508-Cl 2 Steel in a High Temperature, High Purity Water Environment," Trans. ASME, Ser. H., J. Eng. Mat. and Technology, Vol. 96, pp. 255-261 (1974).

22. D. Hale, C.W. Jewett, and J.N. Kass, "Fatigue Crack Growth Behavior of Four Structural Alloys in High Temperature, High Purity Oxygenated Water," ASME Paper 79-PVP-104, American Society of Mechanical Engineers, New York, NY, (1979).

23. D.A. Hale, J. Yuen, and T. Gerber, "Fatigue Crack Growth in Piping and RPV Steels in Simulated BWR Water Environment," GEAP-4098/NRC-5, General Electric Co., San Jose, CA, January 1978.

24. D.A. Hale and J.N. Kass, "Fatigue Crack Growth of Low Alloy Steel in a High Temperature, High Purity Oxygenated Water Environment," Paper #225, Corrosion 1979 Symposium, Atlanta, Georgia, March 1979.

25. W.H. Bamford and D.M. Moon, "Some Mechanistic Observations on the Crack Growth Characteristics of Pressure Vessel and Piping Steels in PWR Envioronment," Corrosion 1979, Atlanta, GA, National Association of Corrosion Engineers (1979).

26. W.H. Bamford, et al., "Effect of High-Temperature, Primary Reactor Water on the Fatigue Crack Growth of Reactor Vessel Steels" in HSST Quarterly Progress Report for April-June 1977, ORNL/NUREG/7M-147, pp. 16-28 (Dec. 1977).

27. W.H. Bamford and L.J. Ceschini, "Effects of High Temperature Primary Water on the Fatigue Crack Growth of Reactor Vessel Steels," in HSST Quarterly Progress Report for January-March 1978, ORNL/NUREG/TM-209, pp. 6-11, March 1978.

28. W.H. Bamford, D.M. Moon, and L.J. Ceschini, "Effects of High Temperature Primary Water on the Fatigue Crack Growth in Reactor Vessel Steels" in HSST Quarterly Progress Report for July-September 1978, ORNL/NUREG/TM-275, pp. 21-29 (Jan. 1979).

29. W.H. Bamford, D.M. Moon and L.J. Ceschini, "Effects of High Temperature Primary Water on the Fatigue Crack Growth of Reactor Vessel Steels," in HSST Quarterly Progress Report for October-December 1978, ORNL/NUREG/TM-298, pp. 14-232 (April 1979).

30. W.H. Bamford, D.M. Moon and L.J. Ceschini, "Effect of High-Temperature Primary Reactor Water on the Subcritical Crack Growth of Reactor Vessel Steels" in HSST Quarterly Progress Report for October-December 1977, ONRL/NUREG/TM-194, pp. 25-35 (May 1978).

31. W.H. Bamford, D.M. Moon, and L.J. Ceschini, "Effect of High-Temperature Primary Reactor Water on the Subcritical Crack Growth of Reactor Vessel Steels," in HSST Quarterly Progress Report for October-December 1977, ORNL/NUREG/TM-194, pp. 25-35 (May 1978).

32. W.H. Cullen et al., "Evaluation of Starting ΔK Phenomenon on Cyclic Crack Growth in A508 Pressure Vessel Steels," Report of NRL Progress, pp. 14-17 (July 1978).

33. M. Suzuki, et al., "The Environment Enhanced Crack Growth Effects in Structural Steels for Water Cooled Nuclear Reactors," Paper C125/77 in Proceedings, Institute of Mechanical Engineers, London, pp. 161-169 (1977).

34. T. Kondo, et al., "Fatigue Crack Propagation Behavior of ASTM A533B and A302B Steels in High Temperature Aqueous Enviornment," Paper No. 6, Heavy Section Steel Technology Progranm, 6th Annual Information Meeting, Oak Ridge National Laboratory, April 1972.

35. "Effects of Residual Elements on Predicted Radiation Damage to Reactor Vessel Materials," Regulatory Guide 1.99, U. S. Nuclear Regulatory Commission, Office of Standards Development, Washington, D.C., April 1977.

36. J. R. Hawthorne, "Notch Ductility Degradation of Low Alloy Steels with Low-to-Intermediate Neutron Fluence Exposures," in Third ASTM--EURATOM Symposium on Reactor Dosimetry, Ispra, Italy, October 1979; NRL Report 8357, October 1979.

37. S.E. Yanichko and J.N. Chirigos, "Assessment of the Validity of Trend Curves in Predicting Embrittlement of Reactor Pressure Vessels," Attachment to NS-TMA-1843, June 19, 1978.

38. J.R. Hawthorne, J.J. Koziol, and S.T. Byrne, "Evaluation of Commercial Production A533-B Steel Plates and Weld Deposits with Extra-Low Copper Content for Radiation Resistance," Symposium on Effects of Radiation on Structural Materials, ASTM STP 683, American Society for Testing and Materials (J. A. Sprague and D. Kramer, Eds.), 1979, pp. 235-251.

39. J.R. Hawthorne and E. Fortner, "Radiation and Temper Embrittlement Processes in Advanced Reactor Weld Metals," Trans. ASME, J. Engrg. for Industry,, 71WA/PVP-11, American Society of Mechanical Engineers, New York, 1971.

40. IWG RRPC-78/1, "Coordinated Research Programme on Analyses of the Behaviour of Advanced Reactor Pressure Vessel Steels Under Neutron Irradiation," Vienna, Austria, 17-18 Oct 1977.

41. J. R. Hawthorne, "Radiation Effects Information Generated on the ASTM Reference Correlation-Monitor Steels," ASTM DS 54, American Society for Testing and Materials, Philadelphia, PA, July 1974.

42. J. R. Hawthorne, "Survey of Postirradiation Heat Treatment as a Means to Mitigate Radiation Embrittlement of Reactor Vessel Steels," NUREG/CR 0486, NRL Report 8287, Naval Research Laboratory, February 14, 1979.

43. J. R. Hawthorne, H. E. Watson and F. J. Loss, "Exploratory Investigations of Cyclic Irradiation and Annealing Effects on Notch Ductility of A533-B Weld Deposits," ASTM STP 683, American Society for Testing and Materials, Philadelphia, PA, October 1979.